Engineering Library

OCT 24 '49

Journal of Research

of the

National Bureau of Standards

SEPTEMBER 1949

VOLUME 43 NUMBER 3

PERIODICALS OF THE NATIONAL BUREAU OF STANDARDS

Journal of Research

The National Bureau of Standards is the principal agency of the Federal Government for fundamental research in physics, chemistry, and engineering. It has the custody of the national standards of physical measurement in terms of which all working standards in research laboratories and industry are calibrated, and carries on necessary research leading to improvement in such standards and methods of measurement. It also has a general responsibility for basic research in physics, chemistry, and engineering, and for development of improved methods for testing materials and equipment. It determines physical constants and properties of materials, tests and calibrates standard measuring apparatus and reference standards, and studies technical processes. The results of the Bureau's research and investigations are published in the JOURNAL OF RESEARCH.

Research Papers

Reprints of individual articles appearing in the JOURNAL OF RESEARCH. They are made available to serve the needs of research workers, technical groups, and others for the separate papers relating to the special subjects in which they are interested.

Technical News Bulletin

Contains short but complete summaries of research, development, and testing in progress at the Bureau, accounts of the Bureau's national and international activities, scientific and technical announcements of new plans and programs, and a list of publications by members of the staff. It is a prompt and reliable source of official information of value to those who desire to keep in touch with the general activities of the Bureau.

Basic Radio Propagation Predictions

The CRPL-D series, Basic Radio Propagation Predictions, is issued as a monthly publication for those concerned with radio communication in determining the best sky-wave frequencies over any path at any time of day for average conditions for the month of prediction, which is made 3 months in advance. Charts of extraordinary-wave critical frequency for the F2 layer, of maximum usable frequency for a transmission distance of 4,000 km, and of percentage of time occurrence for transmission by sporadic E in excess of 15 Mc, for a distance of 2,000 km, are included.

ANNUAL SUBSCRIPTION Send order, with remittance, to Superintendent of Documents, U. S. Government Printing Office, Washington 25, D. C.	United States, Canada, Cuba, Mexico, Newfoundland, Republic of Panama	Other countries
JOURNAL OF RESEARCH of the National Bureau of Standards:		
12 monthly issues (2 volumes), paper covers	$4.50	$5.50
Bound volume (½ year, 1 volume), blue buckram	3.00	3.50
RESEARCH PAPERS	(*)	(*)
TECHNICAL NEWS BULLETIN, 12 monthly issues	1.00	1.35
BASIC RADIO PROPAGATION PREDICTIONS, 12 monthly issues	1.00	1.25

*The prices of the separate Research Papers appearing in this JOURNAL are given in the Contents. If 100 or more copies of any separate are ordered, a discount of 25 percent is allowed. Those who desire copies of separate Research Papers should send their orders and remittances without delay to the Superintendent of Documents, U. S. Government Printing Office, Washington 25, D. C. This will aid him to determine the number of copies to be printed for sale. Research Papers are not printed from electrotypes and usually no more reprints can be had when the first and only printing is exhausted.

The printing of this publication has been approved by the Director of the Bureau of the Budget, April 23, 1947

UNIVERSITY OF MICHIGAN LIBRARIES

U. S. DEPARTMENT OF COMMERCE
Charles Sawyer, Secretary
NATIONAL BUREAU OF STANDARDS
E. U. Condon, Director

SEPTEMBER 1949
VOLUME • 43
NUMBER 3

JOURNAL OF RESEARCH

of the

NATIONAL BUREAU OF STANDARDS

Contents

RP		Page
2020	Ultra-microtomy by a new method. Sanford B. Newman, Emil Borysko, and Max Swerdlow. (Price 10 cents)	183
2021	Determination of nitrogen in steel. John L. Hague, Rolf A. Paulson, and Harry A. Bright. (Price 10 cents)	201
2022	Seasonal variation of ozone at Washington, D.C. Ralph Stair. (Price 10 cents)	209
2023	Surface tension of molten zinc borates. Leo Shartsis and Rodrigo Canga. (Price 10 cents)	221
2024	A comparison of direct colorimetry of titanium pigments with their indirect colorimetry based on spectrophotometry and a standard observer. Deane B. Judd. (Price 10 cents)	227
2025	Properties of calcium-barium titanate dielectrics. Elmer N. Bunting, George R. Shelton, and Ansel S. Creamer. (Price 10 cents)	237
2026	Heats, equilibrium constants, and free energies of formation of the dimethylcyclopentanes. Morton B. Epstein, Gordon M. Barrow, Kenneth S. Pitzer, and Frederick D. Rossini. (Price 10 cents)	245
2027	Cathode heater compensation as applied to degenerative voltage-stabilized direct-current power supplies. Robert C. Ellenwood and Howard E. Sorrows. (Price 10 cents)	251
2028	Mechanical properties of laminated plastics at −70°, 77°, and 200° F. John J. Lamb, Isabelle Albrecht, and Benjamin M. Axilrod. (Price 20 cents)	257

For sale by the Superintendent of Documents, U. S. Government Printing Office, Washington 25, D. C. • Price 55 cents
$4.50 per year on subscription

UNITED STATES GOVERNMENT PRINTING OFFICE, WASHINGTON : 1949

U. S. Department of Commerce
National Bureau of Standards

Research Paper RP2020
Volume 43, September 1949

Part of the Journal of Research of the National Bureau of Standards

Ultra-Microtomy by a New Method

By Sanford B. Newman, Emil Borysko, and Max Swerdlow

Polymerization of *n*-butyl methacrylate monomer is used as a rapid and simple means for embedding fixed biological material. The solid resin provides an optically clear matrix for cutting very thin sections, one at a time, with a slightly modified conventional rotary microtome. Advance of the embedded specimen toward the knife is obtained from the thermal expansion of a brass specimen holder. These ultrathin sections have uniform thickness, large area, and integrity of tissue structure. They are suitable for producing transmission images at the higher magnifications of the conventional light, phase-contrast, and electron microscopes. Metallic shadowing of the sections provides greater contrast as well as a three-dimensional aspect to the structural details of the tissue. Micrographs and a bibliography are presented.

I. Introduction

With the development of the electron microscope as a tool of science arose the problem of preparing sections of biological materials that would give satisfactory images in the instrument. The penetrating power of the electron beam in commercial microscopes using accelerating potentials of 100 kv or less is very slight and, because of the great relative depth of field involved, the specimen structure is difficult to interpret when sections are over a fraction of a micron in thickness.

Over the years various solutions to this problem have been described in the literature, but no wholly satisfactory method for sectioning all kinds of material has appeared. It would seem that any single technique is applicable to only a selected group of materials. Cutting wedge-shaped sections and using the thinnest portions for electron microscopy is a technique described by several workers [1, 2, 4, 5].[1] The methods used, however, have been laborious and difficult to reproduce. Sjöstrand [8] produced an electron micrograph of skeletal muscle fiber from a thin section. Although details of the sectioning technique are not given, the text indicates that it was probably some variation of the wedge-section method.

[1] Figures in brackets indicate the literature references at the end of this paper.

A more successful approach to the problem was the use of the high-speed microtome [7, 12, 13, 14, 15, 19, 20, 21, 23, 24, 25], but this equipment, besides being expensive and complex, produces a low percentage of usable sections. Sections are cut so rapidly and abundantly that selection is laborious and uncertain.

The most recent effort has been that of Pease and Baker [26], who have used standard histological techniques to embed a 1-mm cube of tissue in collodion and paraffin. For sectioning, they altered a Spencer rotary microtome so that the unit of advance was reduced to approximately one-tenth of the calibrated value. The microtome was then reported to produce sections as thin as 0.1 micron [28, 29].

The need for a practical inexpensive method for cutting uniform thin sections, having adequate area and integrity of structure, is still apparent to those working with commercial transmission-type electron microscopes. The growing use of the phase-contrast method in optical microscopy has made the problem more acute. This paper describes a method for obtaining ultrathin sections involving the use of methacrylic resins as embedding media, a thermal expansion apparatus for advancing the specimen in a conventional microtome, and metallic shadow-casting for increasing observable detail in the sections.

II. Sectioning Procedure

1. Embedding Materials

It is not intended that this description of the materials to be used in producing thin sections shall include formulae of fixing solutions, components of the dehydrating series, or other information available in many histological or cytological texts.

The *n*-butyl methacrylate monomer used for embedding, as purchased,[2] contains an inhibitor (hydroquinone). This is removed by repeated washings in a separatory funnel with a dilute aqueous solution of sodium carbonate until no color is visible in the washing solution. Calcium chloride is used to remove water from the washed monomer. After the inhibitor is removed, the monomer is kept in a refrigerator to inhibit polymerization. Rubber or plastic materials should not be used for storing the monomer.

A low-temperature catalyst is necessary for use at the polymerization temperature required for this work. With its optimum activation in the temperature range from 40° to 60° C, 2,4-dichlorobenzoyl peroxide[3] has given excellent results, but other catalysts may be as satisfactory. It is best to obtain the catalyst in a pure form, since certain of the plasticizers incorporated in commercial products are insoluble in *n*-buytl methacrylate. To remove insolubles, filtration of the monomer plus catalyst may be necessary.

2. Specimen Fixation and Dehydration

Accepted cytological techniques were employed without modification for the fixation and subsequent dehydration of the tissues in an ethyl alcohol series. The tissues were then ready for embedding with the polymer. The specimens embedded did not exceed 8 mm^3 in volume. A variety of tissues were fixed in several different preparations to determine the suitability of the techniques for general use.

3. Embedding Technique

(a) Encapsulation and Polymerization

After dehydration in absolute ethyl alcohol, the tissues are transferred to a mixture of equal volumes of absolute alcohol and monomeric *n*-butyl methacrylate. After about 1 hour in the alcohol-monomer mixture, the tissue is placed in the monomer (without catalyst) for about an equal period. To ensure removal of the alcohol, the tissues are placed for at least 1 hour in each of two additional changes of monomer.

Gelatin capsules, No. 00, are used as embedding molds. The ordinary pharmaceutical colorless grade is readily available and easiest to manipulate. The main body of the capsule is set upright in a wooden block or other base (fig. 1, A). The capsule is then filled with the monomer containing 1 percent (by weight) of the catalyst, 2,4-dichlorobenzoyl peroxide. The tissue is placed in it with the desired orientation. The lid of the capsule is slipped into place to retard loss by evaporation, and the assembled capsule is placed in an oven at a temperature of 45° to 50° C (fig. 1, B). It is extremely important that the capsule be evenly heated over its entire surface. An oven with good air circulation should be used and the filled capsules suspended in it with strips of cellophane tape.

At the end of 6 to 8 hours the monomer is polymerized into a solid matrix. The tissue is, of course, embedded at the bottom of the optically clear plastic. An additional period of several hours at this temperature will ensure complete cure. After polymerization the gelatin capsule may be removed by soaking in water and peeling the softened shell from the resin.

4. Modification of the Microtome

In the beginning of this study the Spencer (Model 820) rotary microtome was modified in the manner of Pease and Baker [26]. The angle of the slide plane of the instrument was reduced to one-tenth of its original value by fastening a milled and surface-ground steel shim against the slide plane. This, in effect, reduced the cutting calibration to about one-tenth of its value.

By means of this altered instrument a number of usable sections were cut from different specimens embedded in the polymer. However, the microtome thus altered was not entirely satisfactory. Although this instrument has proved its worth in the production of thicker sections, the cutting of fractional-micron sections demands a degree of precision for which it was never designed.

[2] Obtained from Rubber Chemicals Division, Rohm and Haas Co., Philadelphia, Pa.

[3] Obtained from Lucidol Division, Novadel-Agene Corp., Buffalo, N. Y.

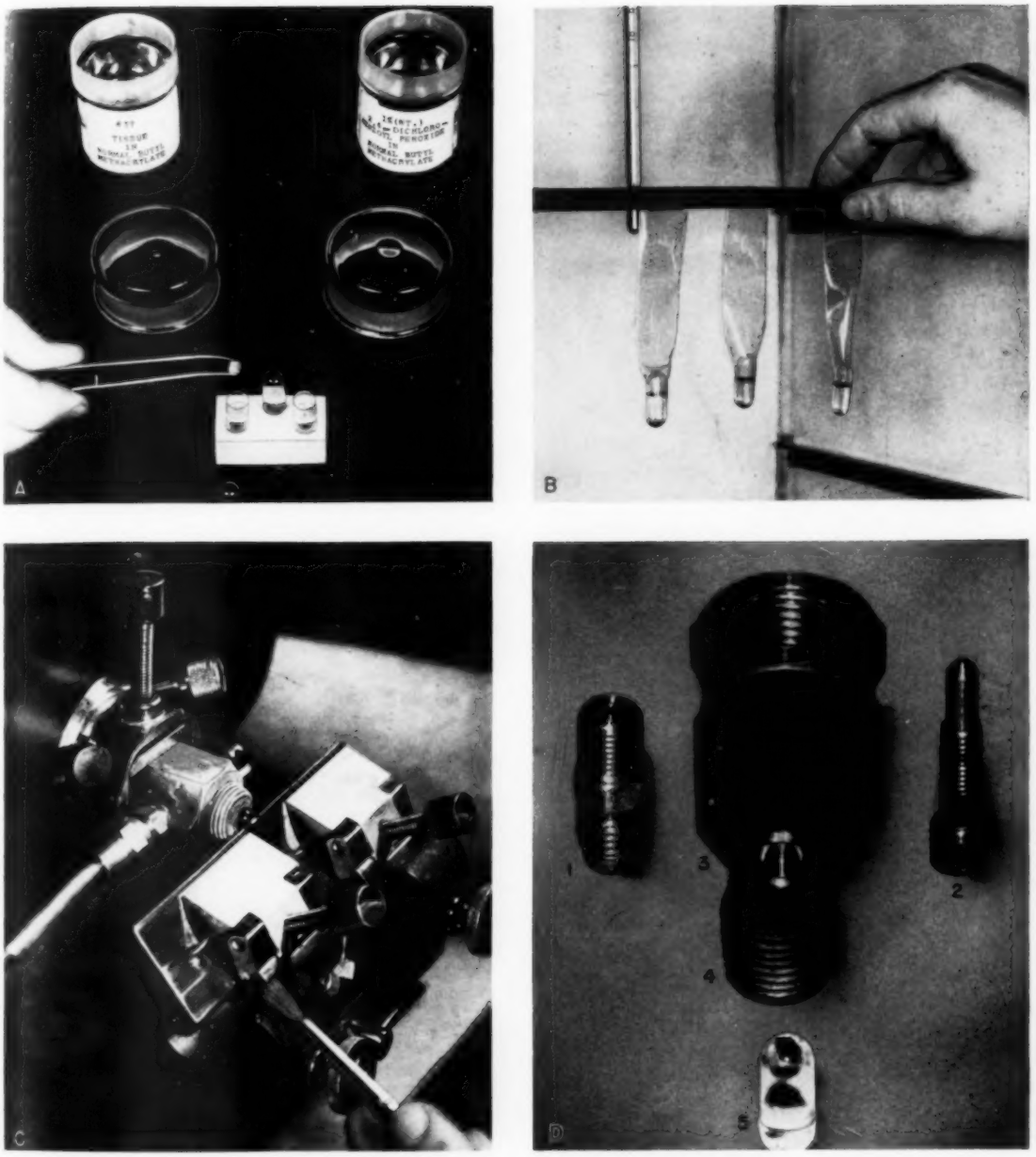

FIGURE 1. *Materials and procedures for ultra-microtomy.*

A, Encapsulation—After fixation and dehydration the tissue, impregnated with *n*-butyl methacrylate, is placed in the gelatin capsule containing the monomer to which 1 percent (by weight) of the catalyst, 2,4-dichlorobenzoyl peroxide, has been added.

B, Polymerization—The capsules containing tissue and monomer plus catalyst are closed and suspended in the circulating-air oven at 45° ± 50° C for 6 to 8 hr to polymerize the liquid.

C, Assembled thermal expansion microtome—A section is being cut with the apparatus clamped in the jaws of a commercial microtome. Compressed CO_2 gas escaping into the expansion chamber cools and contracts the specimen holder. Stopping or reducing the flow of CO_2 allows the apparatus to approach room temperature and thus advances the embedded specimen toward the knife.

D, Disassembled thermal expansion apparatus—(1) and (2) needle valve for CO_2 gas; (3) brass expansion chamber tapped for the fittings; (4) standard ⅜-in. brass pipe plug with cavity in face to seat embedded tissue; (5) tissue in the clear resin with gelatin capsule removed.

To obtain the desired precision, a metallic specimen mount was devised in which the specimen is advanced by means of thermal expansion without modifying the mechanism of the Spencer microtome. The parts for the arrangement are shown in figures 1 and 2.

The device is essentially a brass block with a hole drilled through the long axis and threaded at one end to receive a standard ⅜-in. brass pipe plug, which serves as the specimen mounting block, figure 1, D. A cavity drilled into the face of the plug provides a seat for the embedded specimen. A needle valve situated behind the plug is used to bleed in the coolant, compressed carbon dioxide gas. After cooling, specimen advance toward the knife edge is obtained by allowing the assembly to warm up again. The process involves the continuous thermal expansion of the metallic holder and specimen. This simple device can probably be adapted to any rotary or sliding microtome.

FIGURE 2. *Ultra-microtomy with the thermal expansion instrument.*

The tissue embedded in polybutyl methacrylate is seated in the brass specimen holder. Compressed CO_2 gas escaping into the expansion chamber behind the specimen cools and contracts the assembly. Stopping or reducing the flow of gas with the needle valve allows the apparatus to approach room temperature and thus provides smooth continuous advance of the embedded tissue toward the knife. The extremely thin sections are lifted from the knife with a dry camel's hair brush. A dissecting needle is used to float the section on a warm water surface.

5. Sectioning the Tissues

Before placing the mounted and embedded specimen in the microtome clamp, it is sometimes desirable to reduce the area presented to the cutting edge. Sections across the whole body of the capsule have been cut, but these present certain problems in handling; they often fold on themselves, are difficult to flatten, etc. The block containing the embedded material can be held in a lathe and the excess matrix turned down to any desired diameter, or it can simply be trimmed with a sharp knife.

In using the thermal expansion apparatus the embedded specimen is first cemented into the mounting block. To do this, a small amount of a mixture of 1 part of pure gum rubber and 20 parts of paraffin is melted in the cavity by heating the block. The embedded specimen is then pushed into the cavity, and the block is allowed to cool. With the assembled device clamped in the jaws of the microtome head, the needle valve is opened, allowing the compressed carbon dioxide gas to escape into the expansion chamber behind the mounting block. The entire assembly contracts as it is cooled below room temperature. Upon the appearance of a thin layer of frost on the metal, the knife is adjusted so that the specimen just misses it on the cutting stroke. The specimen is then mechanically advanced at 2- or 3-micron increments until the first slice is made. The mechanical advancing mechanism is then disengaged by setting it to zero and the gas flow reduced or stopped. After a few seconds the specimen, which is set above the knife edge, can be cut. Because the specimen is advancing continuously, a quick chopping stroke involving one complete revolution of the hand wheel is necessary. With a little experience one can soon judge the necessary time interval between cuts. Some control of the rate of specimen advance can be obtained by bleeding the CO_2 at various reduced rates into the expansion chamber. If, however, the temperature is not too far below surroundings, the expansion potential is small and the needle valve can be closed completely. As cutting progresses, the cooling and warming cycle is repeated as necessary.

6. Selecting and Preparing Sections

After being cut, the sections usually are somewhat folded. They are lifted from the knife with

a dry camel's hair brush, picked up with a dissecting needle, and placed on a water surface warmed on a hot plate to about 35° C, figure 2. After an interval ranging from a few minutes to an hour or more, many will flatten out on the surface and exhibit bright interference colors. A little wetting agent in the water aids in straightening the sections.

Selected sections are floated onto clean microscope slides and allowed to dry flat. Sections prepared for phase-contrast microscopy are placed in acetone or toluene for about ½ hour to remove the matrix and then mounted in Canada Balsam. For ordinary light microscopy, the matrix is dissolved and the sections stained in the usual way. Sections for these uses should be affixed to the slide by means of albumen adhesive.

In preparing material for the electron microscope, the sections are floated from the water onto clean glass slides and dried flat. No adhesive should be used. The matrix is then dissolved from the section by placing the slide in acetone, toluene, or amyl acetate. The moist tissue of the section is left adhering to the glass. A dilute solution of collodion in amyl acetate is flowed over the slide bearing the tissue. Inclining the slide permits discharge of excess collodion. It is then allowed to dry at room temperature. The collodion film containing the sections is floated from the slide onto water. The ⅛-inch, 200-mesh specimen screens are placed over the area of the film containing the section. A 250-watt drying lamp, held about a foot from the film at an angle of about 45 degrees, promotes adhesion of the screen to the film. If the film is floated on a small amount of water on a glass plate, the screens can be more accurately placed with the aid of a binocular microscope. The entire film is then floated from the plate to a larger volume of water, and the freely floating film supporting the specimen screens is removed from the water by flipping it over and out with a glass microscope slide. The screens are thereby lodged between the film and the glass as the film is dried onto the slide. The specimens are then removed for observation or metallic shadowing (fig. 3).

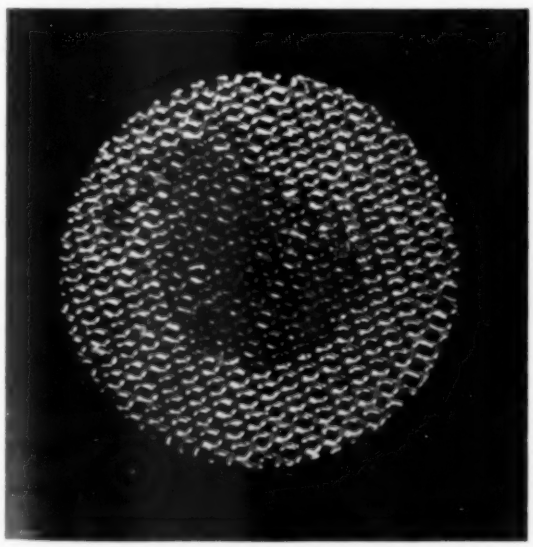

FIGURE 3. *Metal shadowed ultrathin section centered on a ⅛-inch diameter, 200-mesh specimen screen ready for electron microscopy.*

7. Metallic Shadow-Casting

Additional contrast as well as a three-dimensional aspect to certain details of the thin section can be obtained by metallic shadow-casting as described by Williams and Wyckoff [10]. Further details of the specific technique used here are given by Swerdlow and Seeman [27]. The legends under the figures give additional data for the shadowed thin sections. The shadowed sections could, of course, be used for light and phase-contrast as well as electron microscopy.

The sections are freed of the embedding medium and stripped from the glass slide with a collodion film as described previously. The sections are then mounted (tissue side up) on the screens and shadowed. This is the easier method of shadowing specimens for electron microscopy, that is, with the material lying above the substrate film. However, if the preshadowing techniques of Williams and Wyckoff [11, 16] and Williams and Backus [31] with their relative advantages and difficulties are to be used, the shadow-casting is done immediately after removal of the embedding polymer. Then the section is stripped from the glass slide along with the very thin layer of metal by the usual transfer and mounting methods.

Figures 5 to 14 illustrate the results obtained with the various techniques described. The RCA–EMU (50 kv) electron microscope was used for this work.

III. Discussion

The techniques presented here have given satisfactory results. However, a few rigid limitations in several of the steps in the procedure must be considered.

Knife sharpness is of vital importance. However, the microtome cutting edges used were maintained with two different commercial knife sharpeners. The tilt of the knife during sectioning was not particularly critical, no more so than in sectioning for optical microscopy [6, 9].

The greatest chance for failure appears to lie in the polymerization of the embedding mass. Use of low-temperature catalysts and a polymerization temperature of 45° to 50° C will usually prevent the formation of resins that are not readily soluble, cause distortion of tissue by swelling and wrinkling, and have inferior cutting qualities. Catalysts, such as benzoyl peroxide, with higher activation temperatures should be avoided. Bubbles may form in the embedding matrix, but their presence is usually not a bar to the successful sectioning of the embedding mass. Occasionally tissues are injured during the polymerization reaction, and such tissues, which are easily detected, can be promptly discarded. The mechanism of injury is not clearly understood, but delicate tissues and unhardened tissues are more often affected. For this reason, the use of fixing solutions with good hardening properties is recommended. The addition of small quantities (10 to 20% by volume) of methyl methacrylate monomer to the *n*-butyl methacrylate has been tried and yields a harder resin with somewhat better cutting properties but increases the probability of tissue injury.

Methacrylic polymers have poor resistance to electron bombardment even at low beam intensities. For this reason the matrix polymer has been dissolved out of the section. An electron micrograph of a shadowed section of the polymerized matrix (fig. 4) fails to reveal any particulate forms. Fullam and Gessler [13] showed a micrograph of a section of laboratory-polymerized methyl methacrylate containing numerous discrete bodies. Such material does not appear in the plastic used here.

FIGURE 4. *Embedding polymer, section, chromium-shadowed (4:1).*

Electron micrograph, total magnification ≈×10,400 (electronic ×5,200, optical ×2).

The materials sectioned by this method thus far have been plant and animal tissues. The ability to produce sections for study in the electron microscope in anything approaching a routine fashion would be of immense advantage to research in almost any field of biology or medicine concerned with the microstructure of such material. Although fixation artifacts remain problems for serious consideration, the new method presented here provides a practical inexpensive approach to the problem of producing extremely thin sections that have uniform thickness, large area, and integrity of tissue structure.

The authors sincerely appreciate the valuable assistance and helpful suggestions of Elmer A. Koerner, Howard F. McMurdie, and Barbara M. Sullivan in the course of this work.

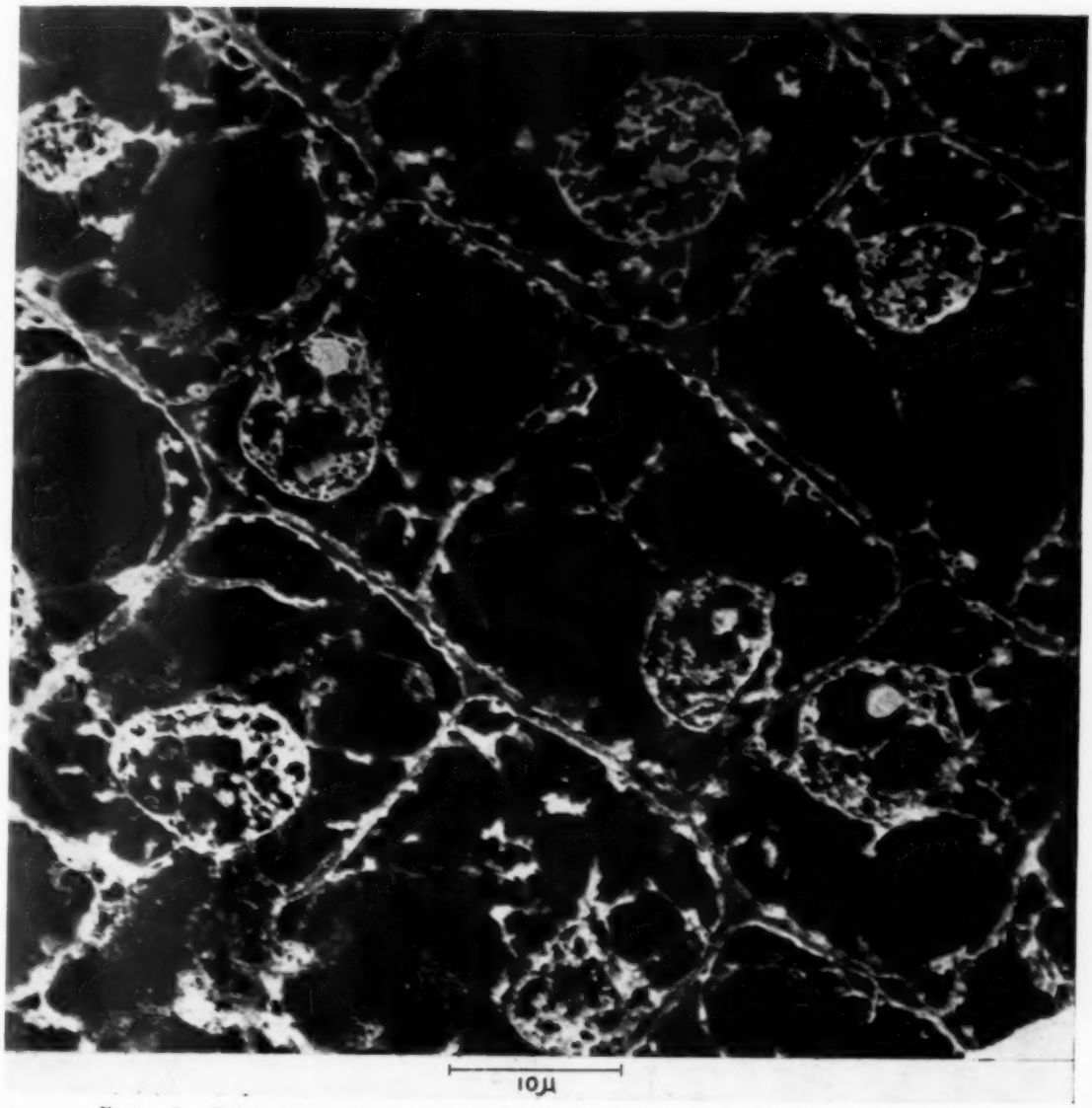

FIGURE 5. *Onion root tip, elongating cells, fixed in medium chrom-acetic, chromium-shadowed (4:1).*

Electron micrograph, total magnification ≈ ×2, 600 (electronic ×750, optical ×3.5).

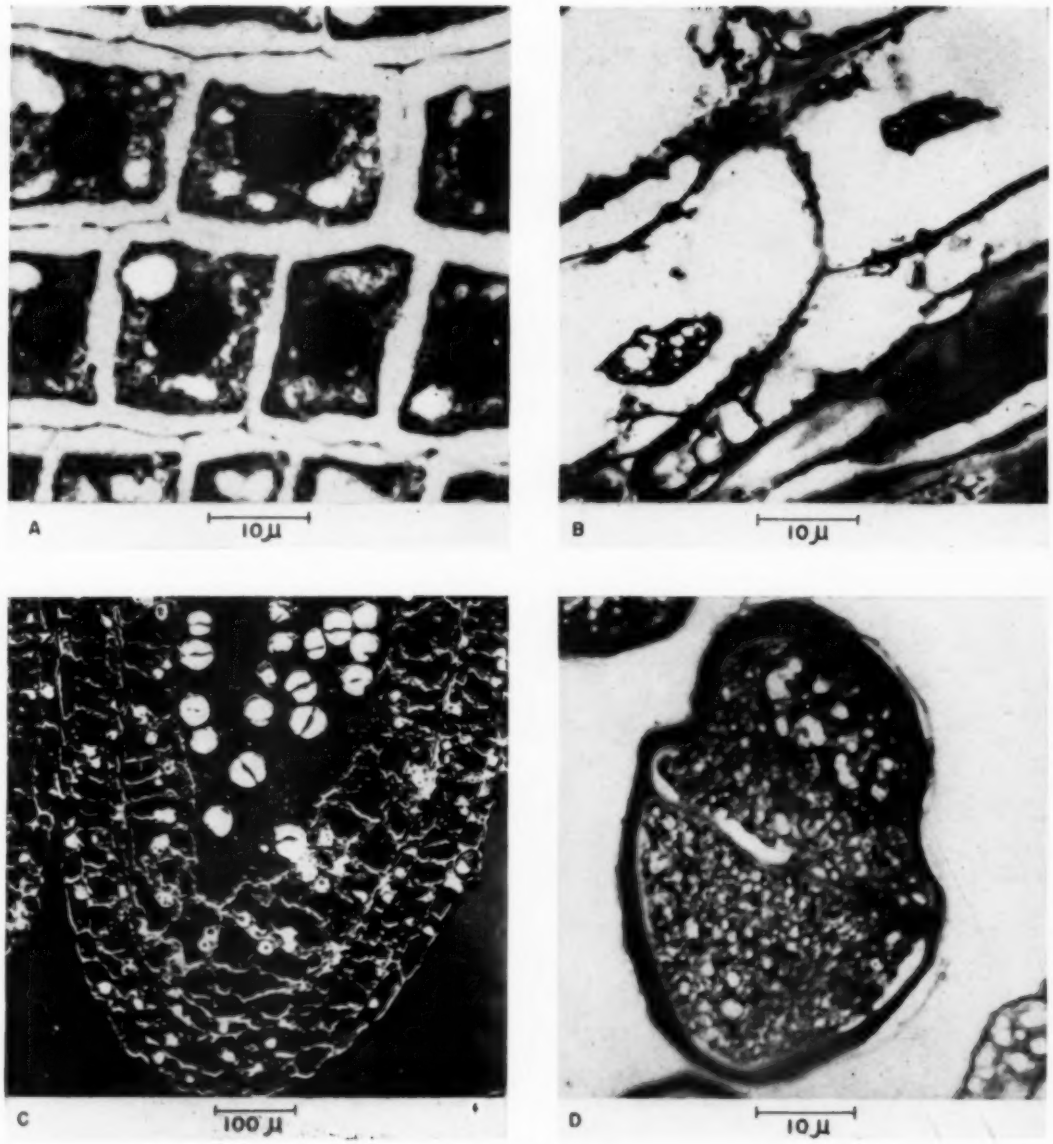

FIGURE 6.

A, Onion root tip, cells of meristem, fixed in boiling water (10 sec.). Electron micrograph, total magnification ≈ ×1, 500 (electronic ×750, optical ×2).

B, Onion root tip, zone of elongation, fixed in Zirkle-Erlikis. Electron micrograph, total magnification ≈ ×1, 500 (electronic ×750, optical ×2).

C, Lilium superbum anthers, longitudinal section through tip, fixed in acetic alcohol, stained in haematoxylin, shadowed with chromium (4:1). Photomicrograph, total magnification ≈ ×120.

D, Lilium superbum microsporocytes, two-cell stage, fixed in acetic alcohol. Electron micrograph, total magnification ≈ ×1, 500 (electronic ×750, optical ×2).

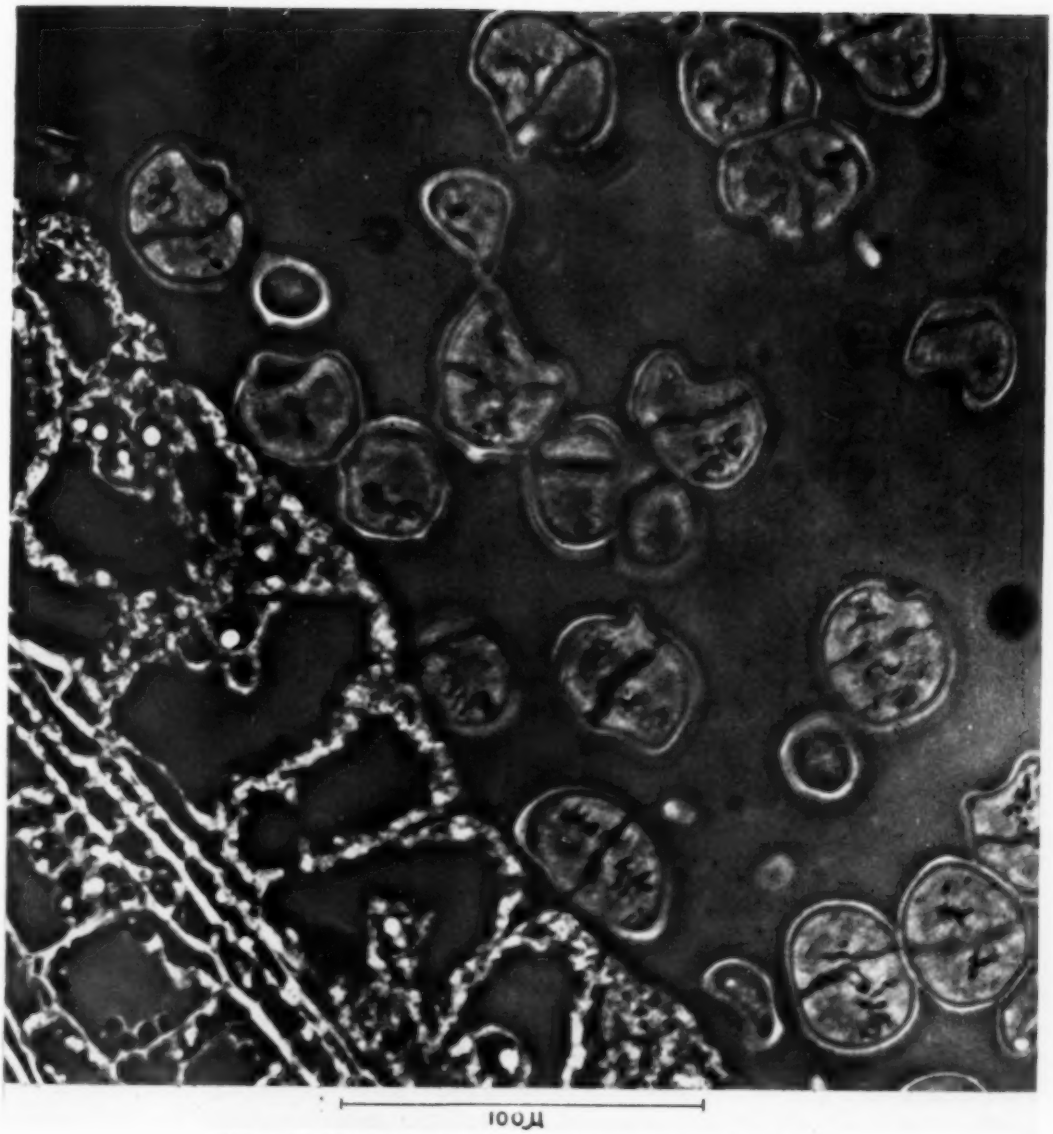

FIGURE 7. *Lilium superbum microsporocytes, fixed in acetic alcohol.*
Phase-contrast micrograph, total magnification ≈ ×550.

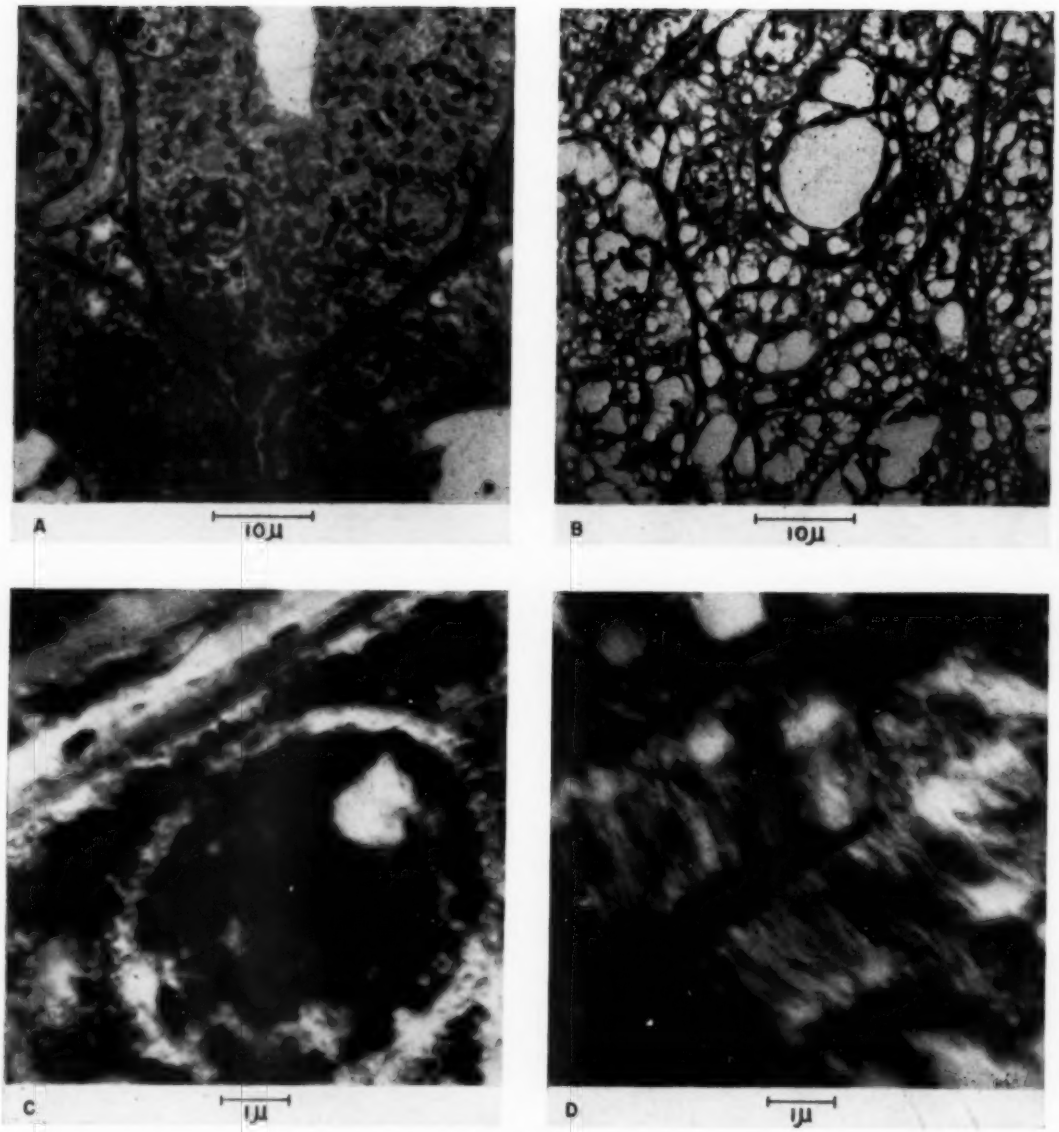

FIGURE 8.

A, Dog kidney, tubules and glomerulus, fixed in Zenker-formol. Electron micrograph, total magnification ≈×1,500 (electronic ×750, optical ×2).

B, Frog kidney, tubules, fixed in Bouin's. Electron micrograph, total magnification ≈×1,500 (electronic ×750, optical ×2).

C, Dog kidney, section through tubule nucleus and basement membrane, fixed in Zenker-formol, chromium-shadowed (5:1). Electron micrograph, total magnification ≈×10,400 (electronic ×5,200, optical ×2).

D, Dog kidney, section through brush-border cilia of tubule lumen, fixed in Zenker-formol, chromium-shadowed (5:1). Electron micrograph, total magnification ≈×10,400 (electronic ×5,200, optical ×2).

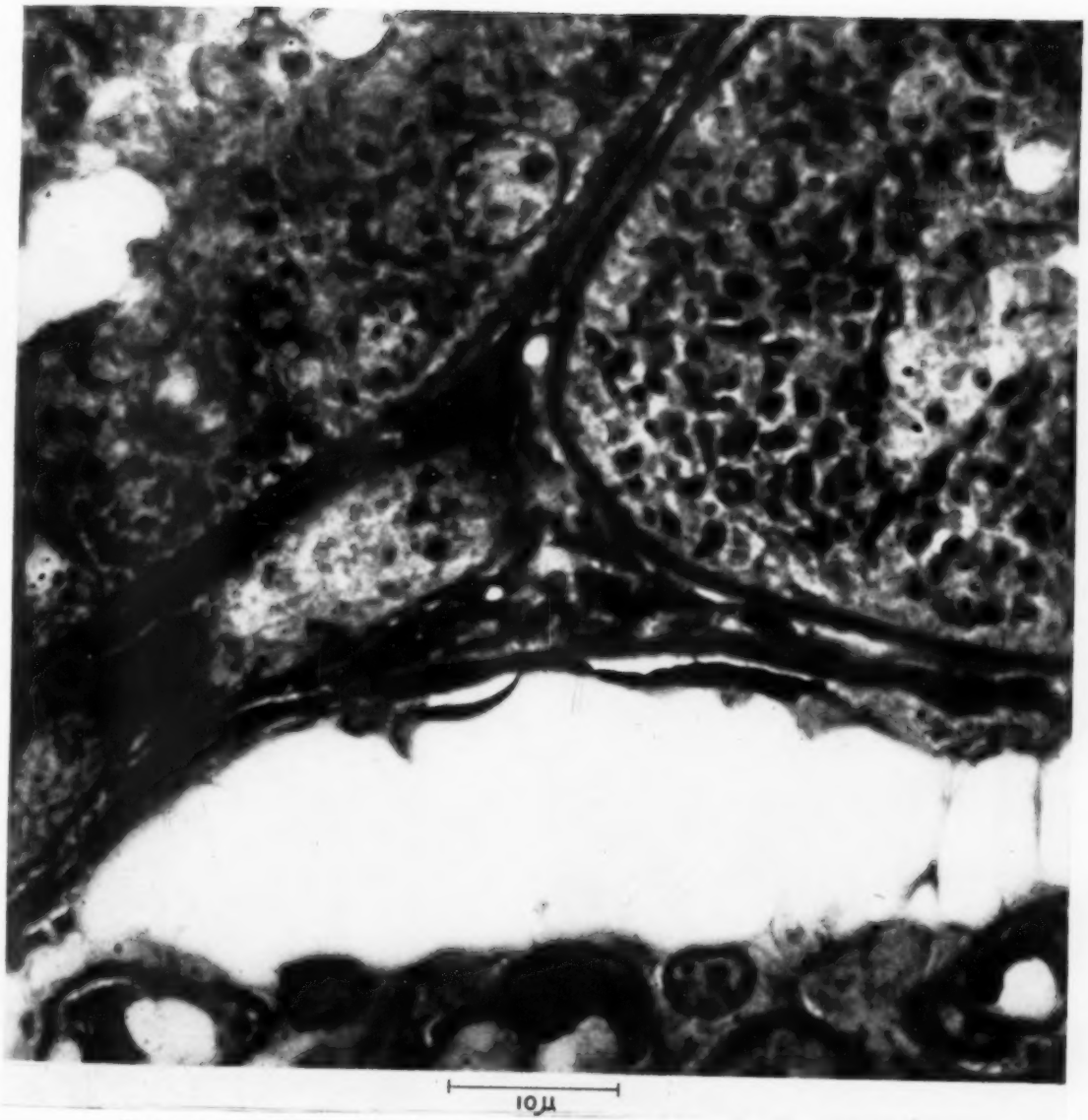

FIGURE 9. *Dog kidney, section showing tubule and part of glomerulus, fixed in Zenker-formol.*

Electron micrograph, total magnification ≈ ×2,600 (electronic ×750, optical ×3.5).

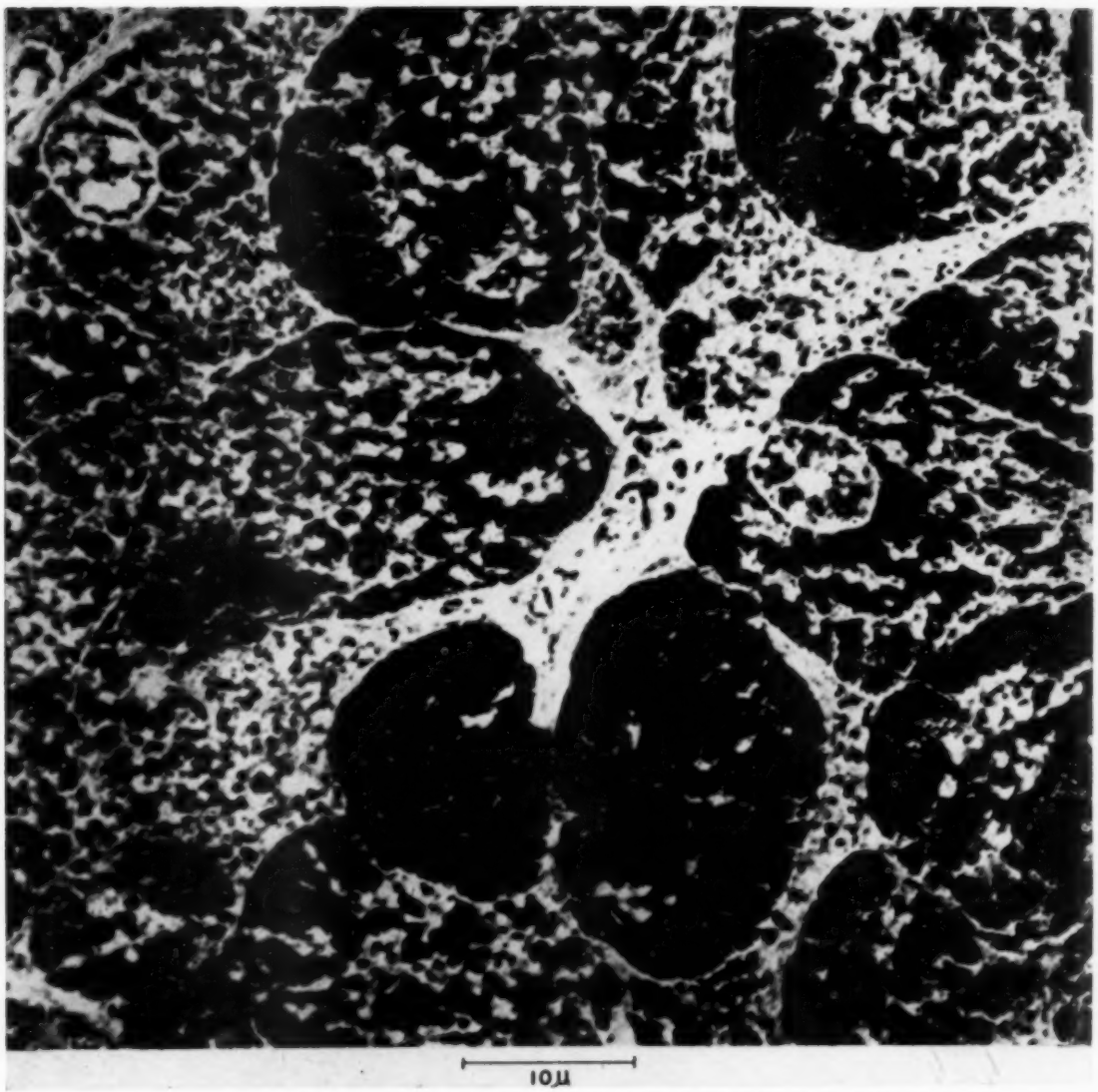

FIGURE 10. *Frog liver, fixed in Bouin's, preshadowed with chromium* (4:1).

Electron micrograph, total magnification ≈×2,600 (electronic ×750, optical ×3.5)4

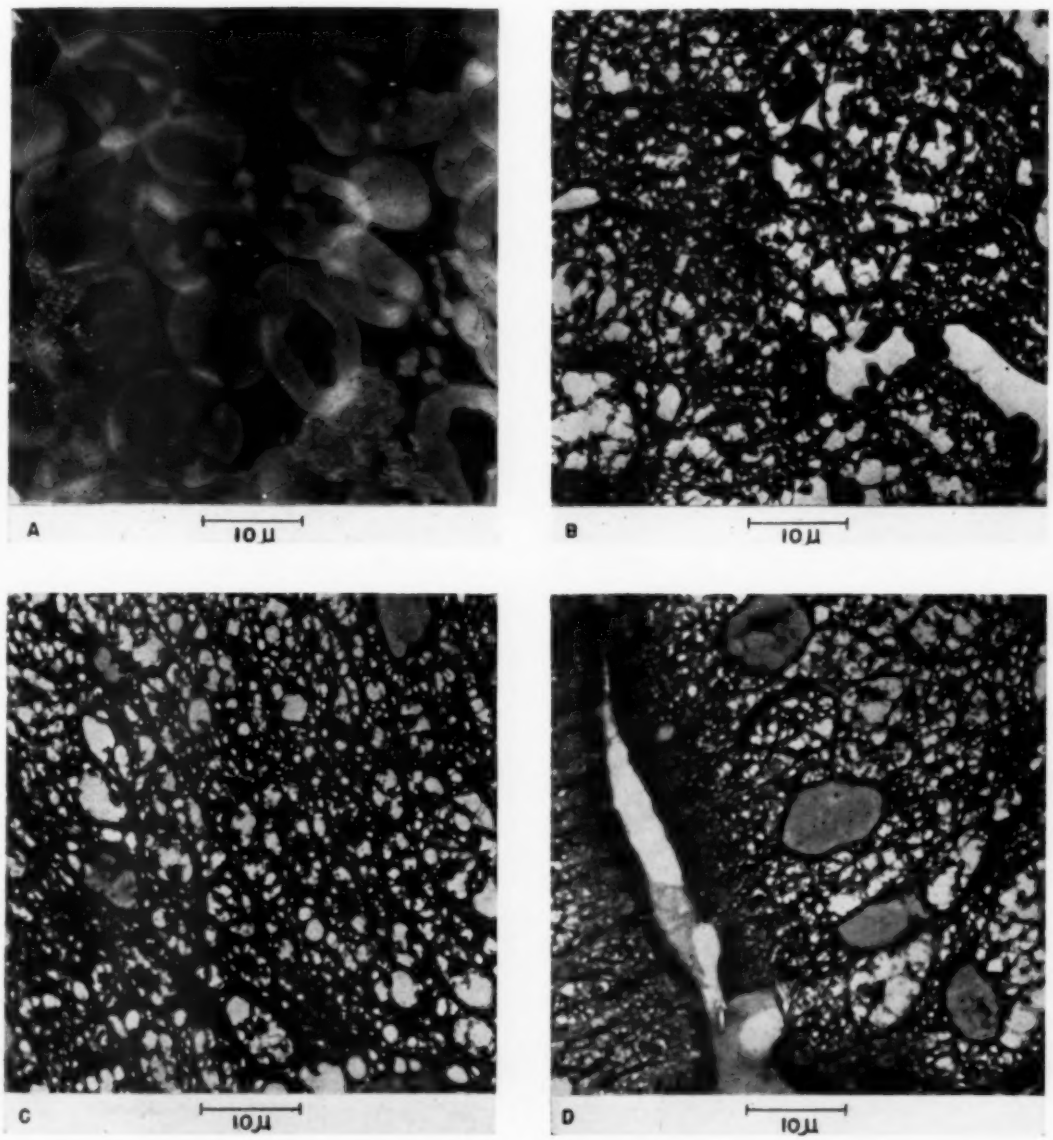

FIGURE 11.

A, Mouse red blood cells, in brain tissue, fixed in 10-percent formalin. Electron micrograph, total magnification ≈×1,500 (electronic ×750, optical ×2).

B, Mouse liver, fixed in Flemming's. Electron micrograph, total magnification ≈×1,500 (electronic ×750, optical ×2). (Tissue courtesy of National Institutes of Health).

C, Frog's small intestine, section through interior of villus, fixed in Bouin's. Electron micrograph, total magnification ≈×1,500 (electronic ×750, optical ×2).

D, Frog's small intestine, section of villus, fixed in Bouin's. Electron micrograph, total magnification ≈×1,500 (electronic ×750, optical ×2).

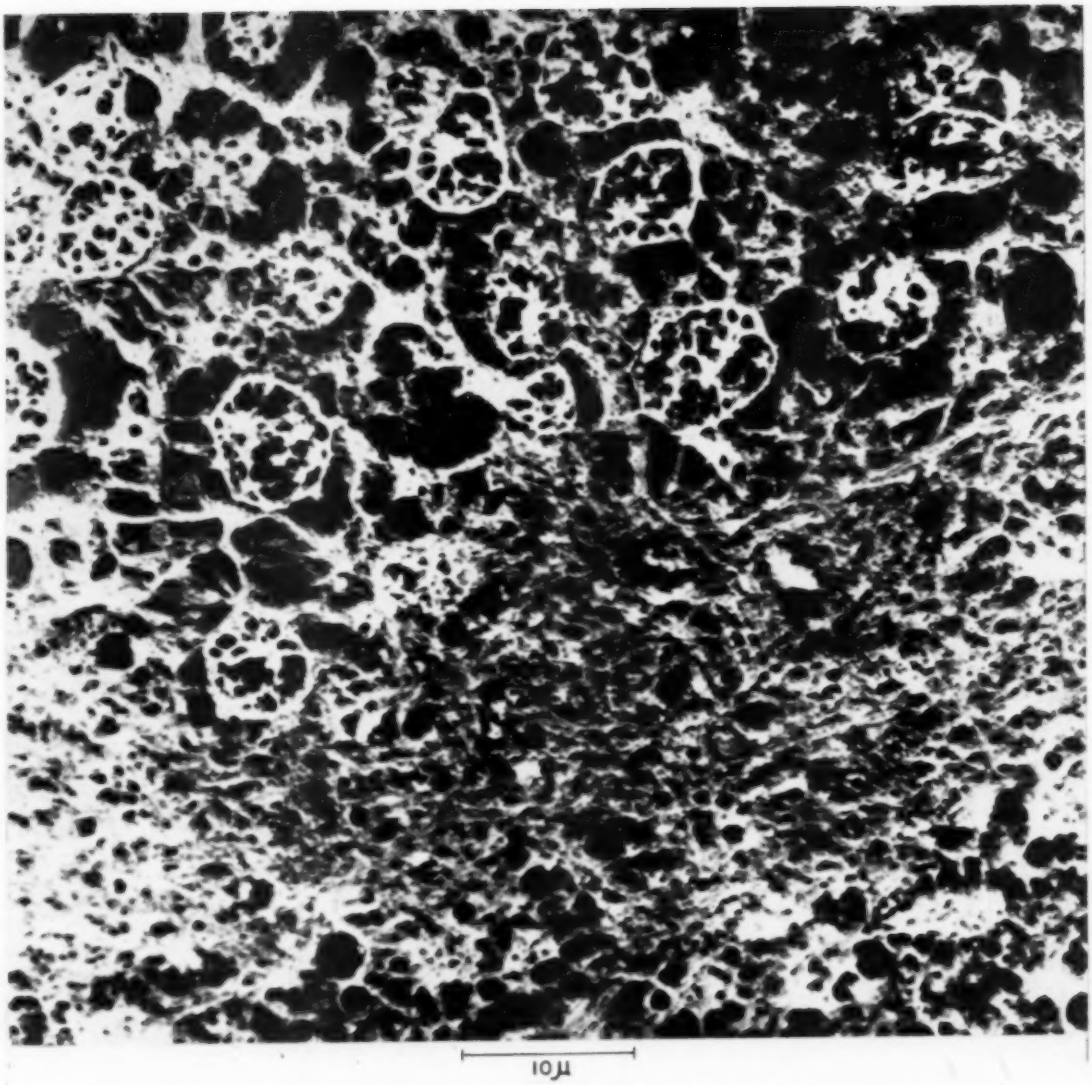

FIGURE 12. *Frog's eye, section near area of rods and cones, fixed in Bouin's, chromium shadowed (4:1)*

Electron micrograph, total magnification ≈×2,600 (electronic ×750, optical ×3.5).

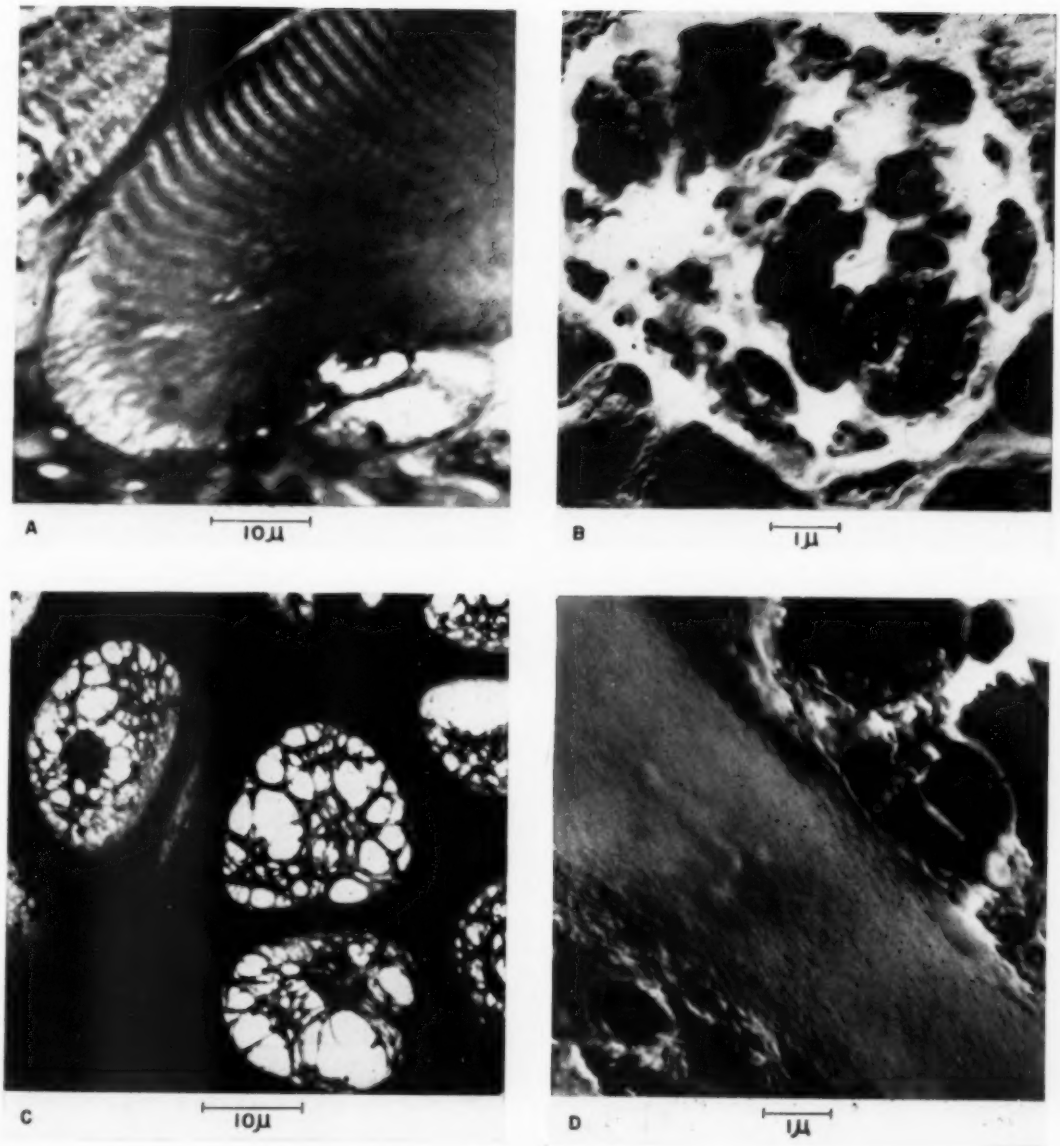

FIGURE 13.

A, Frog's eye, section through muscle fiber, fixed in Bouin's. Electron micrograph, total magnification ≈×1,500 (electronic ×750, optical ×2).

B, Frog's eye, section through nucleus of cell near rods and cones, fixed in Bouin's chromium-shadowed (4:1). Electron micrograph, total magnification ≈×10,400 (electronic ×5,200, optical ×2).

C, Frog's eye, section through cartilage, fixed in Bouin's. Electron micrograph, total magnification ≈×1,500 (electronic ×750, optical ×2).

D, Frog's eye, section through cartilage, fixed in Bouin's, chromium-shadowed (4:1). Electron micrograph, total magnification ≈×10,400 (electronic ×5,200, optical ×2).

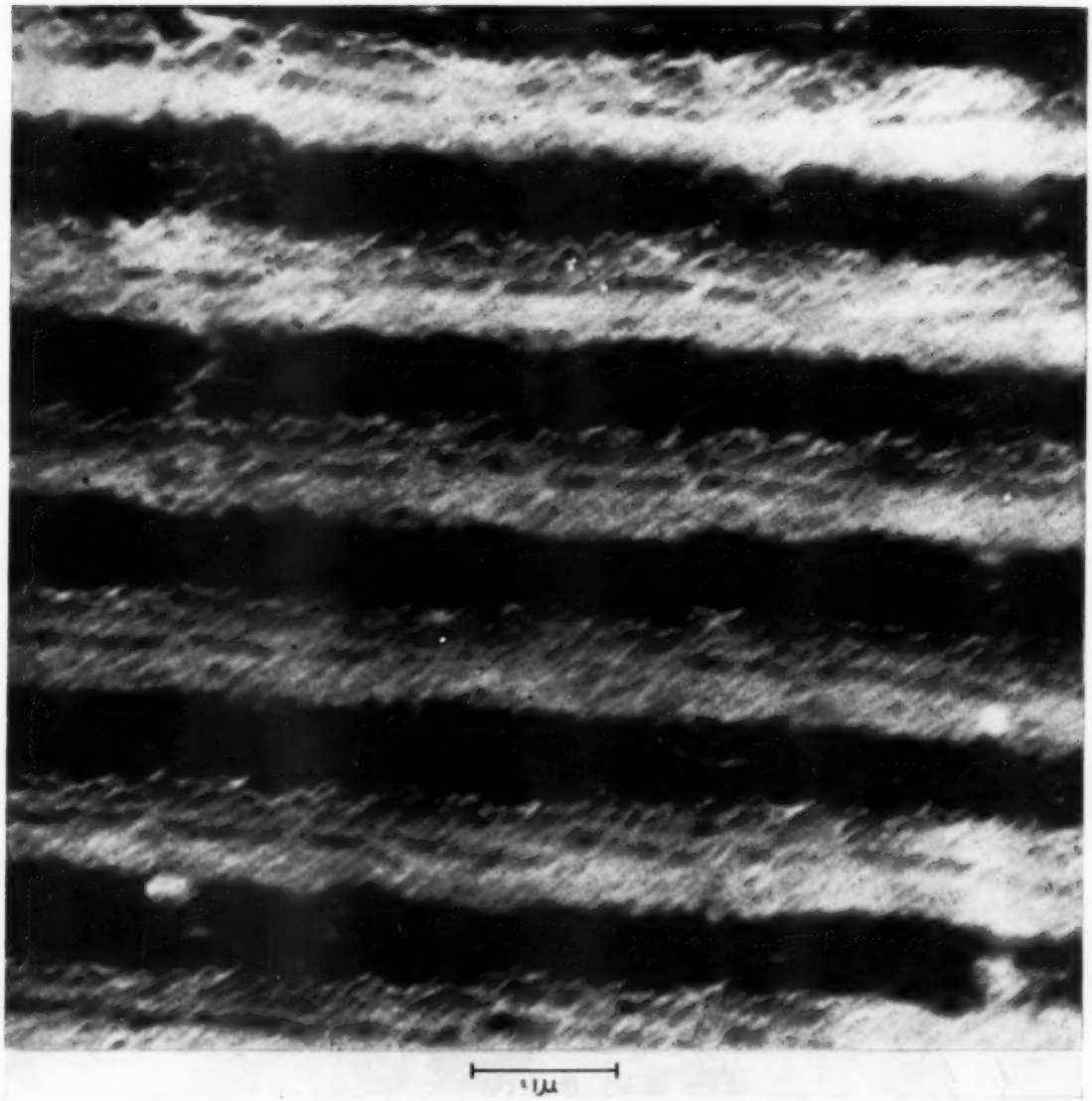

FIGURE 14. *Frog's eye, detail of striated muscle fiber, fixed in Bouin's, chromium-shadowed (4:1).*

Electron micrograph, total magnification ≈×22,000 (electronic ×5,200, optical ×4.3).

IV. References

[1] M. von Ardenne, The wedge sectioning method for producing microtome cuts of less than 10^{-3} mm thickness for purposes of electron microscopy, Z. wiss. Mikroskop. **56,** 8 (1939).

[2] M. von Ardenne, Electron microscopy of living tissue, Naturwissenschaften, **29,** 521 (1941).

[3] W. T. Dempster, The mechanics of paraffin sectioning by the microtome, Anat. Rec. **84,** 241 (1942).

[4] G. A. Richards, Jr., T. F. Anderson, and R. T. Hance, A microtome sectioning technique for electron microscopy illustrated with sections of striated muscle, Proc. Soc. Exptl. Biol. Med., **51,** 148 (1942).

[5] G. A. Richards, Jr. and T. F. Anderson, Electron microscope studies of insect cuticle with a discussion of the application of electron optics to this problem, J. Morphol. **71,** 135 (1942).

[6] O. W. Richards, The effective use and proper care of the microtome (Spencer Lens Co., Buffalo, N. Y., 1942).

[7] H. C. O'Brien, Jr. and G. M. McKinley, New microtome and sectioning method for electron microscopy, Science **98,** 455 (1943).

[8] F. Sjöstrand, Electron-microscopic examination of tissues, Nature **151,** 725 (1943).

[9] O. W. Richards, Microtomy, Medical Physics, p. 750 to 759 (1944). (Edited by O. Glasser, Year Book Publishers, Chicago, Ill.)

[10] R. C. Williams and R. W. G. Wyckoff, The thickness of electron microscope objects, J. Applied Phys. **15,** 712 (1944).

[11] R. C. Williams and R. W. G. Wyckoff, Electron shadow micrography of the tobacco mosaic virus protein, Science **101,** 594 (1945).

[12] A. Claude and E. F. Fullam, The preparation of sections of guinea pig liver for electron microscopy, J. Exptl. Med. **83,** 499 (1946).

[13] E. F. Fullam and A. E. Gessler, A high speed microtome for the electron microscope, Rev. Sci. Instruments **17,** 23 (1946).

[14] A. E. Gessler and E. F. Fullam, Sectioning for the electron microscope accomplished by the high speed microtome, Am. J. Anat. **78,** 245 (1946).

[15] M. C. Schuster, High speed microtoming, Interchem. Rev. **5,** 31 (1946).

[16] R. C. Williams and R. W. G. Wyckoff, Applications of metallic shadow-casting to microscopy, J. Applied Phys. **17,** 23 (1946).

[17] A. Claude, K. R. Porter, and E. G. Pickels, Electron microscope study of chicken tumor cells, Cancer Research **7,** 421 (1947).

[18] K. R. Porter and H. P. Thompson, Some morphological features of cultured rat sarcoma cells as revealed by the electron microscope, Cancer Research **7,** 431 (1947).

[19] A. E. Gessler and C. E. Grey, Notes on the electron microscopy of tissue sections, submicroscopic spherical bodies in carcinoma, Exptl. Med. and Surgery **V,** 307 (1947).

[20] A. E. Gessler, C. E. Grey, and K. McCarty, Notes on the electron microscopy of tissue sections: submicroscopic spherical bodies in human carcinoma II, Exptl. Med. and Surgery **VI,** 329 (1946).

[21] A. E. Gessler, C. E. Grey, M. C. Schuster, J. J. Kelsch, and M. N. Richter, Notes on the electron microscopy of tissue sections, I. Normal tissue, II. Neoplastic, Cancer Research **8,** 534 (1948).

[22] C. E. Grey, An electron microscope specimen punch, Rev. Sci. Instruments **19,** 369 (1948).

[23] C. E. Grey, Microtome for electron microscopy, Interchem. Rev. **7,** 26 (1948).

[24] C. E. Grey and J. J. Kelsch, Use of the electron microscope and high speed microtome in medicine, Exptl. Med. and Surgery **VI,** 368 (1948).

[25] B. Kisch, C. E. Grey, and J. J. Kelsch, Electron histology of the heart I, Exptl. Med. and Surgery **VI,** 346 (1948).

[26] D. C. Pease and R. F. Baker, Sectioning techniques for electron microscopy using a conventional microtome, Proc. Soc. Exptl. Biol. Med. **67,** 470 (1948).

[27] M. Swerdlow and G. S. Seeman, A method for the electron microscopy of wool, J. Research NBS **41,** 231 (1948) RP1921; Textile Res. J. **XVIII,** 536 (1948).

[28] R. F. Baker and D. C. Pease, Improved sectioning technique for electron microscopy, J. Applied Phys. **20,** 480 (1949).

[29] D. C. Pease and R. F. Baker, Preliminary investigations of chromosomes and genes with the electron microscope, Science **109,** 8 (1949).

[30] D. B. Scott and R. W. G. Wyckoff, Metal shadowing for the optical microscopy of certain tissues, Am. J. Clin. Path. **19,** 63 (1949).

[31] R. C. Williams and R. C. Backus, Electron-micrographic structure of shadow-cast films and surfaces, J. Applied Phys. **20,** 98 (1949).

WASHINGTON, June 3, 1949.

U. S. Department of Commerce
National Bureau of Standards

Research Paper RP2021
Volume 43, September 1949

Part of the Journal of Research of the National Bureau of Standards

Determination of Nitrogen in Steel

By John L. Hague, Rolf A. Paulson, and Harry A. Bright

A rapid semimicro method for the determination of nitrogen in steel is described. A 0.5- to 1.0-gram sample is usually required, and the nitrogen is put into solution as ammonium sulfate by suitable treatment of the sample with sulfuric acid. The ammonia is separated from the bulk of the sample by steam distillation from an alkaline solution. The distillate is collected in boric acid solution, and the nitrogen is determined by titration with 0.01-*N* acid. Provision is made for the solution of difficultly soluble nitrides. The effect of some of the commonly used alloying elements on the acid solubility of nitrogen compounds in steel is discussed. An accuracy of the order of 0.002 percent of nitrogen or better is indicated for samples containing up to about 0.05 percent of nitrogen and about 0.003 percent for the range of 0.05 to 0.15 percent of nitrogen. In the lower range of nitrogen contents, 0.002 percent and less, better accuracy can be obtained by attention to pertinent details and the use of a colorimetric method for the determination of the ammonia. A single determination can be completed in about 10 minutes after solution of the sample, and a group of 10 determinations can be carried out in approximately 2 hours.

I. Introduction

In connection with an investigation on the effect of nitrogen on the hardenability of boron-containing steel [8, 9] [1] it became necessary to make a large number of nitrogen determinations. The most promising process appeared to be an adaptation of the micro technique to the determination of small percentages of nitrogen involved, as it was apparent that an appreciable saving in time and reagents could be realized.

The methods commonly used for the determination of nitrogen in steel are the "vacuum-fusion" method [28] and the "solution-distillation" method. The latter, generally designated as the Allen method [1, 2, 19], depends on converting the nitrides in the test sample to an ammonium salt by solution in diluted hydrochloric or sulfuric acid. The ammonia is usually separated by distillation from an alkaline solution and determined by colorimetric or titrimetric methods. The acid-solution method then consists of two distinct parts: (1) solution of the sample and conversion of the nitrides to ammonium salts and (2) the separation and determination of the ammonia. An accurate method for the separation and determination of the ammonia is useful only if methods are available to decompose and convert the nitrides present in the sample.

Perchloric acid has been recommended [12] as a useful reagent for the decomposition of refractory nitrides. However, when solutions containing perchloric acid were used in attempts to digest the acid-insoluble portions of stainless steels, low values were sometimes obtained. If the digestions were allowed to proceed to the point of fumes and beyond, the duration of fuming markedly affected the magnitude of the nitrogen losses. Similar difficulties have been noted by others, both in the treatment of steels [6, 15, 26] and in the digestion of organic materials [29]. It was apparent that perchloric acid, at least under the conditions used, could cause erroneous results; hence the use of this acid was abandoned.

Several methods have been published in which the use of sulfuric acid as a solvent for refractory nitrides is recommended. Cunningham and Hamer [7] advocate filtration of the insoluble nitrides and fuming the filtered residue with sulfuric acid containing a mixture of potassium and copper sulfates. Kempf and Abresch [13] add a small quantity of barium chloride to the sulfuric acid solution of the steel and centrifuge the

[1] Figures in brackets indicate the literature references at the end of this paper.

barium sulfate, which has carried down any acid-insoluble residue, from the remainder of the solution. The residue is digested with H_2SO_4 and K_2SO_4, and the ammonia content of the combined solutions determined. T. Swinden [27] has proposed fuming the sulfuric acid solution of the steel for at least 15 min after the addition of potassium bisulfate. Brown [4] describes a procedure for the determination of total nitrogen in steel wherein the steel is dissolved in a mixture of diluted sulfuric and phosphoric acids, metallic selenium is added, and, after the removal of water, the mixture is digested at the point of fumes for 2 to 4 hr. Newell [21] recommends fuming the sample with sulfuric acid and potassium bisulfate, after the addition of a few drops of hydrogen peroxide, to aid in the decomposition of carbides. In the proposed method the sample is fumed for 4 hr with sulfuric acid to convert the nitrogen-containing compounds, unless it is known that a simpler process will suffice for the material at hand. Hydrogen peroxide is added, as it aids in the decomposition of some materials and does not lead to loss of nitrogen.

Steam distillation from an alkaline solution appears to be the most satisfactory method available for the separation of the ammonia. Beeghly [3] has described a semimicro procedure for the colorimetric determination of nitrogen in steel using this separation. In the procedure of Kempf and Abresch [14] the steam-distillation separation is used. The ammonia is collected in an excess of standard acid, and the excess is titrated with standard alkali.

The use of the apparatus devised by Parnas and Wagner [22, 23] for the separation of ammonia by steam distillation is recommended. The ammonia is collected in a dilute boric acid [30] solution and titrated directly with standard acid, using a methyl red-bromcresol green indicator mixture proposed by Ma and Zuazaga [20]. The volume of the ammonia distillate is kept small, approximately 15 ml of solution being collected. This small volume contributes to a small titration blank and to the sharpness of the indicator change. The particular advantages of the proposed method are rapidity and ease of operation. An individual distillation and titration may be completed in approximately 10 min. The total time required for an analysis depends principally upon the solution procedure required.

2. Reagents

Diluted sulfuric acid (1+2).

Hydrogen peroxide, (30-percent).

Boric acid solution, (20 g per l).—Dissolve 5 g of H_3BO_3 in 250 ml of water.

Sodium hydroxide solution (30-percent).—Dissolve 240 g of sodium hydroxide in 560 ml of ammonia-free water.

Indicator solution.—Dissolve 0.1 g of bromcresol green in 100 ml of 95-percent ethyl alcohol. Dissolve 0.1 g of methyl red in 100 ml of 95-percent ethyl alcohol. Mix five parts of bromcresol green solution with one part of methyl red solution for use.

Standard hydrochloric acid (0.01–N).—This solution can be prepared by accurately diluting a standardized 0.1–*N* hydrochloric acid solution with distilled water. The factor of the prepared solution can be checked against sulfamic acid through NaOH solution using the mixed indicator, or can be compared directly, using the mixed indicator, with standard borax solution [18].

II. Apparatus and Reagents

1. Apparatus

Vycor micro-Kjeldahl digestion flasks, 30-ml volume (Corning Glass Works No. 15440).

10-ml microburette.

Distillation apparatus.—Parnas and Wagner type, as illustrated in figure 1. This apparatus is standard micro-Kjeldahl equipment except for the distilling flask (D). The lower bulb of this flask is somewhat larger (175 ml instead of the usual 90 ml) in volume than ordinarily supplied and can be obtained on special order.[2] The steam generator (A) is a 1-liter round-bottomed Pyrex flask, filled two-thirds to three-quarters full of distilled water. A few chips of silicon carbide are added to insure even boiling, and 4 or 5 ml of sulfuric acid are added to fix any small amount of ammonia in the water. The steam generator is connected to the side arm of a cylindrical trap (B) of about 300-ml volume. This trap has a drain at the bottom, closed by a short length of rubber tubing and a pinchcock. A piece of glass tubing, bent at a right angle, is connected to the trap with a rubber stopper and to the steam inlet tube of the distilling

[2] Suitable flasks have been secured from A. H. Thomas Co., Philadelphia, Pa., and from Scientific Glass Apparatus Co., Bloomfield, N. J.

flask (D) with a short piece of rubber tubing. The steam inlet tube is also connected to a small funnel (C) used to introduce the sample and alkali into the flask. The flask (D) is vacuum-jacketed, and the exit end consists of an antifoaming bulb and trap. The exit end is connected by rubber tubing to a water-jacketed silver-tube condenser (E), and the distillate is caught in a 50-ml Erlenmeyer flask (F).

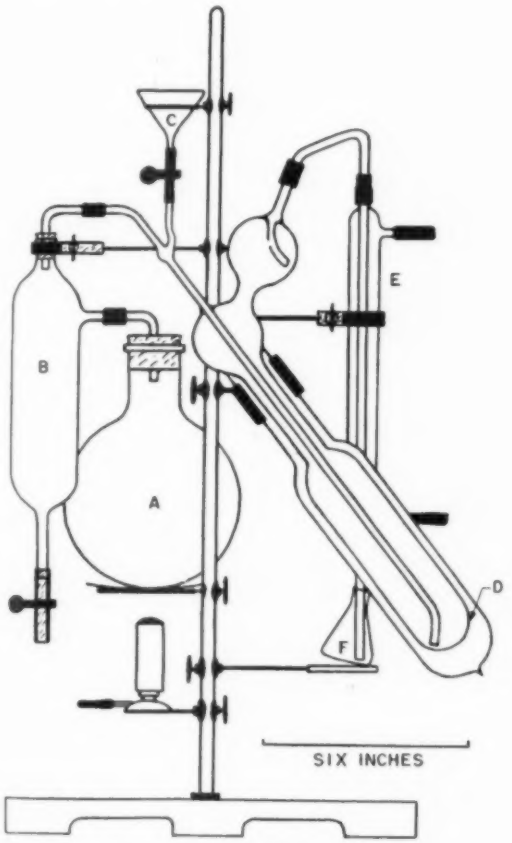

FIGURE 1. *Distillation apparatus.*

Ammonia-free water.—Satisfactory water can be prepared by distillation from a diluted sulfuric acid solution.

Nessler's reagent.—Dissolve 50 g of potassium iodide in a minimum volume of cold water (approximately 35 ml) and add slowly, with good mixing, a saturated solution of mercuric chloride until the first slight precipitate of red mercuric iodide persists. Add 400 ml of a clear 9–N NaOH solution (360 g/liter), dilute to 1 liter with ammonia-free water, and allow the reagent to stand until clear. Decant the clear supernatant liquid for use.

III. Procedure

Transfer 0.5 g of the sample to a Vycor micro-Kjeldahl flask and add 10 ml of diluted H_2SO_4 (1+2),[3] one or two drops of hydrofluoric acid (48%), and a few drops of hydrogen peroxide (30%).[4] Place the flask over a small flame on a digestion rack until solution action ceases. If the material does not contain acid-insoluble nitrides, the acid solution is now ready for the distillation of the ammonia.

Some types of steel contain acid-insoluble material that can be decomposed by a short, vigorous fuming after the addition of hydrogen peroxide. For these materials, remove the flask from the digestion rack, and while holding the neck of the flask in a test-tube holder or clamp, warm the solution with constant swirling over a low flame. When most of the water has been driven off, cool the flask under tap water, and add 1 ml of hydrogen peroxide (30%). Continue heating the solution, with a swirling motion, to the point of fumes and fume vigorously for a minute or two. Cool under tap water, add 10 ml of ammonia-free water, and warm to dissolve most of the separated salts. The solution is now ready for distillation of the ammonia.

The sulfuric acid mixtures of some materials, particularly those containing columbium and titanium, also certain other types that have been heat-treated, contain refractory nitrides that must be treated more vigorously to effect solution. After reaching the fuming point, return the flask to the digestion rack and continue the digestion for 3½ to 4 hr. The temperature should be sufficiently high to give some refluxing action with the sulfuric acid, and the flask should be rotated occasionally to prevent excessive caking. Remove the flask from the rack, cool under tap water, and add 10 ml of ammonia-free water. Warm the flask gently to loosen the salts and cool. The solution is now ready for distillation of the ammonia.

[3] Carbon and low alloy steels usually dissolve more quickly if 5 ml of water is also added. 15 ml of diluted H_2SO_4 (1+3) can be used with these types of material.

[4] Hydrogen peroxide sometimes makes high-chromium steels passive, and this addition should not be made on these types until the sample has reacted with the acid.

Transfer 5 ml of the boric acid solution (this need not be accurately measured) to a 50-ml Pyrex Erlenmeyer flask and add four drops of indicator solution. The distillation apparatus should be steamed-out thoroughly for about 30 min before the first determination is made.

Open the pinch clamps of the introductory funnel (C) and the outlet tube (B), pour the sulfuric acid solution of the sample through the funnel, and rinse the digestion flask two or three times with small portions of ammonia-free water. Light the burner under the steam generator, add 25 ml of sodium hydroxide solution (30 %) through the introductory funnel, and close the pinchcock. Suspend the flask of boric acid under the condenser. As soon as steam issues freely from the drain tube of flask (B), close the pinchcock and immediately raise the flask of boric acid to the proper level. Time the distillation by noting the time the top of the condenser (E) becomes warm, and continue the distillation for 3 min at such a rate that 3 to 5 ml per minute of condensate is collected. Lower the receiver containing the boric acid and continue the distillation for 1 min. Rinse the condenser tip with 1 or 2 ml of water and extinguish the burner. Titrate the boric acid solution with the standard 0.01-*N* HCl solution to a clear pink end point.

Correct the volume of 0.01-*N* hydrochloric acid required in titrating the boric acid solution by the volume of standard acid required in a blank run, preferably obtained by carrying a 0.5-g sample of nitrogen-free steel through all steps of the procedure. The reagents used in this procedure gave a blank of approximately 0.15 ml of 0.01-*N* hydrochloric acid. The calculation is made as follows:

$$\% \text{ nitrogen} = \frac{\text{net volume of 0.01-}N\text{ HCl} \times (0.000140) \times 100}{0.5} .$$

In the range of 0.002 percent of nitrogen and less, the determination can be conveniently completed by using a modification of the photometric procedure described by Beeghly. Collect approximately 9.5 ml of distillate in each of two Kromatrol or Klett colorimeter tubes, add 0.2 ml of Nessler's reagent, dilute to the 10-ml mark, and mix well. Measure the transmittancy or absorbency of the solution at 430 to 460 μ, after allowing the tube to stand 5 min. Determine the amount of nitrogen by use of a calibration curve prepared from data obtained from measurements of known quantities (0 to 20 μg) of nitrogen. The calibrating solutions can be prepared by aliquoting portions of a standardized solution af ammonium chloride. Correct the value obtained for a blank determined by carrying all the reagents used through all steps of the procedure [10]. With water purified by distillation from a weak sulfuric acid solution, the reagents used in testing the procedure gave a blank approximating 0.0003 percent of nitrogen on the basis of a 1-g sample.

IV. Discussion and Results

Larger amounts of hydrogen peroxide are specified in the procedure than are used ordinarily in micro-Kjeldahl digestions for the determination of nitrogen. To determine whether the use of these larger amounts of peroxide lead to the loss of nitrogen, known quantities of ammonia, added as ammonium dihydrogen phosphate, were digested at the fuming point of sulfuric acid, with and without the addition of hydrogen peroxide, and the determinations completed by distillation and titration. The results obtained indicate that the addition of 1 ml of hydrogen peroxide (30%) does not lead to the loss of nitrogen.

As the distillation of the ammonia is carried out in the presence of a relatively large precipitate of iron hydroxide, experiments were also conducted to determine whether the ammonia formed during solution could be recovered under these conditions. Known quantities of a standard solution of ammonium dihydrogen phosphate were added to the sulfuric acid solutions of 0.5-g samples of either high-purity iron (0.0005% of nitrogen) or a low-nitrogen steel (0.003% of nitrogen by the vacuum-fusion method) and the determinations completed as described in the recommended procedure. The values obtained indicate an accuracy of ± 0.001 to 0.002 percent of nitrogen for samples containing up to about 0.05 percent of nitrogen, and an accuracy of ± 0.002 to 0.003 percent of nitrogen in the range of 0.05 to 0.15 percent of nitrogen.

The accuracy actually obtained in a determination on a steel sample is somewhat more difficult to assess, since good "check" values on replicate determinations may indicate only that the samples

are decomposed to the same extent. However, a comparison of values obtained by the recommended procedure with those obtained by the vacuum-fusion process indicates that the accuracy of the method is very close to that indicated by the experiments on synthetic samples described in the preceding paragraph.

The problem of checking the accuracy of the photometric procedure for low nitrogen contents is also a difficult one. However, samples from two experimental ingots of high-purity iron gave values of 0.0007 (average deviation of 10 determinations 0.0003) and 0.0012 percent of nitrogen (average deviation of 10 determinations 0.0002). Comparison of these values with those obtained by vacuum-fusion (0.0004 and 0.0009 percent of nitrogen) indicates the accuracy to be better than 0.0005 percent of nitrogen in this low range.

A comparison of the values obtained by the recommended procedure (section III) with those obtained by the vacuum-fusion procedure over a period of several years revealed several interesting sources of error that can be encountered in the determination of nitrogen.

In one instance, a series of steels in the form of thin, flat sheets was received for analysis. The first analyses by the chemical procedure indicated a value of about 0.002 to 0.003 percent of nitrogen, whereas those obtained by the vacuum-fusion process indicated a value on the order of 0.005 to 0.006 percent of nitrogen. An exchange of the prepared samples confirmed the approximate difference, which was finally traced to the fact that the samples originally used for the vacuum-fusion analyses had been "surface cleaned" on a high-speed grinding wheel. With the large surface-to-weight ratio of this type of sample, apparently sufficient "nitriding" of the surface had occurred, due to the heating of the sample during grinding, to cause significant error, for when the determinations were repeated by both methods on "pickled" samples, concordant values in the neighborhood of 0.002 to 0.003 percent of nitrogen were obtained. Such difficulties have been encountered by others [17].

In another case, a sample that had been annealed under helium was received for confirmation of a nitrogen content of about 0.0003 percent. Using the straight acid solution technique usually employed in the "Allen-type" methods and the semimicro adaptation of the Nessler colorimetric procedure to determine the ammonia, a value closely approximating 0.0003 percent was obtained. However, when the sample was digested for 4 hrs at the fuming point with sulfuric acid, a value of 0.002-percent nitrogen resulted. Obviously, not all of the nitrogen compounds were converted to ammonia by solution in diluted acid, and similar instances can be found in the literature [5, 11, 16, 25].

A detailed study of various solution techniques was made on NBS Standard Sample 32d, a chromium-nickel (SAE 3140) steel that contains refractory nitrides, and the results are summarized in figure 2. The horizontal bar represents the maximum and minimum value obtained for the particular solution procedure specified, and the vertical bar gives the average value obtained for the number of determinations specified in parentheses.

Titanium is known to form nitrogen-containing compounds in steel that are quite insoluble in diluted acid or alkali. The behavior of NBS Standard Sample 121a, a titanium-bearing corrosion-resisting type of steel, is typical of a number of steels of this type examined [24] and is summarized in figure 3. The average value of 0.015-percent nitrogen obtained for the samples fumed 4 hrs compares favorably with the certificate value of 0.014 percent. Figure 4 illustrates the behavior of a type 347 corrosion-resisting steel containing approximately 0.8 percent of Columbium and is typical of the behavior of the samples of this type of steel examined. The loss of nitrogen by fuming solutions containing perchloric acid is also illustrated.

Figure 5 presents the behavior of NBS Standard Sample 50b, an 18W, 4Cr, 1V type of tungsten tool-steel. The short, vigorous fuming (temperature effect) and the addition of peroxide appear to aid in the decomposition of this steel, but a sufficient number of samples of this type have not been examined to allow the recommendation of the short fuming procedure for general use. The nitrogen compounds in this type of material are generally only partly soluble in diluted acid.

Many carbon and alloy steels will, for all practical purposes, yield the total nitrogen content by simple solution in diluted sulfuric acid. However, those containing even small amounts of an element such as titanium frequently do not yield all their nitrogen under these conditions. The

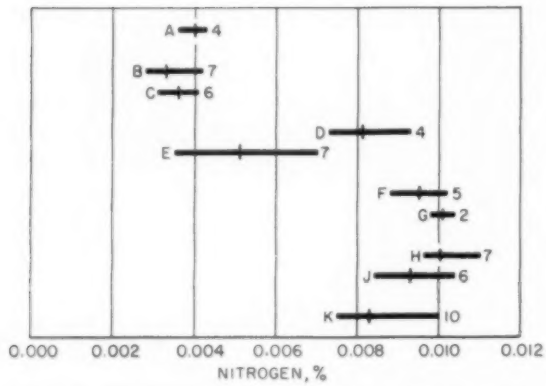

FIGURE 2. *NBS standard sample 32d* Cr–Ni *steel (SAE 3140).*

A, Allen method, HCl (1+1); *B*, H_2SO_4 solution; *C*, H_2SO_4 solution plus H_2O_2; *D*, H_2SO_4, to fumes; *E*, H_2SO_4, to fumes plus H_2O_2; *F*, H_2SO_4, fumed ½ hr; *G*, H_2SO_4, fumed ½ hr plus H_2O_2; *H*, H_2SO_4, fumed 4 hr; *J*, H_2SO_4, fumed 4 hr plus H_2O_2; K, vacuum fusion.

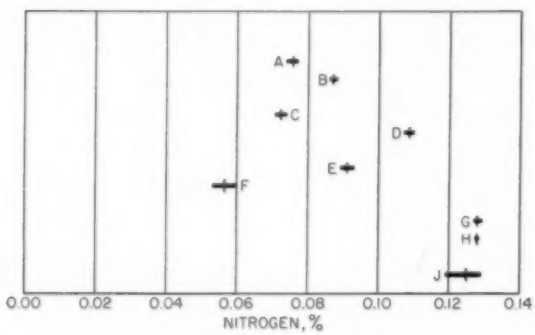

FIGURE 4. *Crucible Steel Company standard 17 (18–Cr, 11–Ni, 0.8–Cb).*

A, Solution in H_2SO_4; *B*, Solution in H_2SO_4 plus H_2O_2; *C*, H_2SO_4, fumed 2 hr; *D*, H_2SO_4 fumed 2 hr plus H_2O_2; *E*, H_2SO_4, H_3PO_4, $HClO_4$, fumed 15 min; *F*, H_2SO_4, H_3PO_4, $HClO_4$, fumed 3 hr; *G*, H_2SO_4, fumed 4 hr; *H*, H_2SO_4, fumed 4 hr plus H_2O_2; *J*, vacuum fusion.

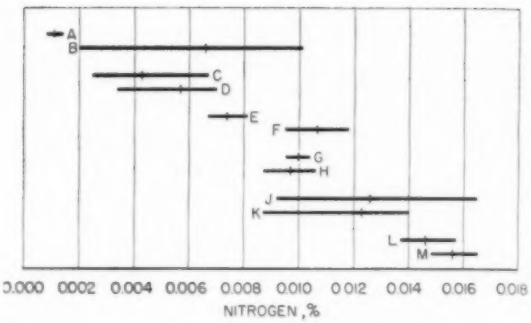

FIGURE 3. *NBS standard sample 121A (18–Cr, 10–Ni, 0.4* Ti *steel).*

A, H_2SO_4 solution; *B*, H_2SO_4 solution plus H_2O_2; *C*, H_2SO_4, to fumes; *D*, H_2SO_4, to fumes plus H_2O_2; *E*, H_2SO_4, to strong fumes; *F*, H_2SO_4, to strong fumes plus H_2O_2; *G*, H_2SO_4, fumed strongly 5 min; *H*, H_2SO_4, fumed strongly 5 min plus H_2O_2; *J*, H_2SO_4, fumed ½ hr; K, H_2SO_4, fumed ½ hr plus H_2O_2; *L*, H_2SO_4, fumed 4 hr; *M*, H_2SO_4, fumed 4 hr plus H_2O_2.

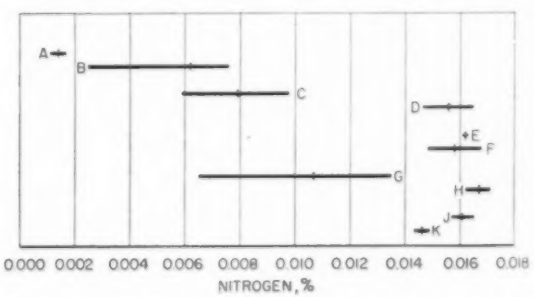

FIGURE 5. *NBS standard sample 50B (18–W, 4–Cr, 1–V steel).*

A, H_2SO_4 solution; *B*, H_2SO_4 solution plus H_2O_2; *C*, H_2SO_4, to strong fumes; *D*, H_2SO_4, to strong fumes plus H_2O_2; *E*, H_2SO_4, fumed strongly 5 min; *F*, H_2SO_4, fumed strongly 5 min plus H_2O_2; *G*, H_2SO_4, fumed ½ hr; *H*, H_2SO_4, fumed ½ hr plus H_2O_2; *J*, H_2SO_4, fumed 4 hr; K, H_2SO_4, fumed 4 hr plus H_2O_2.

short, vigorous fuming with sulfuric acid and peroxide appears to aid in the decomposition of this type of material. These rapid solution procedures should prove useful where they can be shown by experiment to be applicable, especially in plant laboratories where the elapsed time of analysis is important.

The authors are especially indebted to H. E. Cleaves, Chief of the Chemical Metallurgy Section, whose staff determined, by the vacuum-fusion method, the nitrogen content of many of the samples used in testing the procedure; and to K. D. Fleischer, formerly of the Chemistry Division, for valuable assistance in the early stages of the development of the method.

V. References

[1] A. H. Allen, J. Iron Steel Inst. **7,** 480 (1879).
[2] A. H. Allen, J. Iron Steel Inst. **8,** 181 (1880).
[3] H. F. Beeghly, Ind. Eng. Chem., Anal. Ed. **14,** 137 (1942).
[4] W. D. Brown, Proc. Conf. Natl. Open Hearth Comm., Iron and Steel Div., Am. Inst. Mining Met. Engrs. **27,** 166 (1944).
[5] W. D. Brown, Proc. Conf. Natl. Open Hearth Comm., Iron and Steel Div., Am. Inst. Mining Met. Engrs. **27,** 168 (1944).
[6] Chemists of U. S. Steel Corp., Sampling and analysis of carbon and alloy steels, p. 288 (Reinhold Publishing Corp., New York, N. Y., 1938).
[7] T. R. Cunningham and H. L. Hamer, Ind. Eng. Chem., Anal. Ed. **11,** 303 (1939).
[8] T. G. Digges, Influence of nitrogen on some properties of steels with and without boron and titanium additions, OSRD No. 1506, Serial No. M–84 (June 3, 1943).
[9] T. G. Digges and F. M. Reinhart, Trans. Am. Soc. Metals **40,** 1124 (1948).
[10] J. L. Hague, Proc. Am. Soc. Testing Materials **44,** 715 (1944).
[11] C. Holthaus and W. Holtmann, Arch. Eisenhüttenw. **17,** 247 (1944).
[12] C. M. Johnson, Iron Age **134,** No. 4, 10 (1934).
[13] H. Kempf and K. Abresch, Arch. Eisenhüttenw. **14,** 255 (1940).
[14] H. Kempf and K. Abresch, Arch. Eisenhüttenw. **14,** 258 (1940).
[15] H. Kempf and K. Abresch, Arch. Eisenhüttenw. **17,** 121 (1943).
[16] H. Kempf and K. Abresch, Arch. Eisenhüttenw. **17,** 261 (1944).
[17] H. Kempf and A. Neuberger, Arch. Eisenhüttenw. **17,** 5 (1943).
[18] I. M. Kolthoff and N. H. Furman, Volumetric analysis **2,** 94 to 96 (John Wiley & Sons, Inc., New York, N. Y., 1929).
[19] G. C. Lloyd, Sixth report on the heterogenity of steel ingots, Iron and Steel Inst. (1935). Speical Report No. 9, Section 7, p. 121.
[20] T. S. Ma and G. Zuazaga, Ind. Eng. Chem., Anal. Ed. **14,** 280 (1942).
[21] W. C. Newell, J. Iron Steel Inst. **152,** 333 (1945).
[22] J. K. Parnas, Z. anal. Chem. **114,** 261 (1938).
[23] J. K. Parnas and R. Wagner, Biochem. Z. **125,** 253 (1921).
[24] S. J. Rosenberg and J. H. Darr, J. Research NBS **40,** 324 (1948).
[25] T. Swinden, J. Iron Steel Inst. **148,** No. 2, 306 (1943).
[26] T. Swinden, J. Iron Steel Inst. **148,** No. 2, 312 (1943).
[27] T. Swinden, J. Iron Steel Inst. **148,** No. 2, 316 (1943).
[28] H. C. Vacher and L. Jordan, BS J. Research **1,** 375 (1931).
[29] L. F. Wicks and H. I. Firminger, Ind. Eng. Chem., Anal. Ed. **14,** 760 (1942).
[30] L. W. Winkler, Z. angew. Chem. **26,** 231 (1913).

Washington, May 10, 1949.

U. S. Department of Commerce
National Bureau of Standards

Research Paper RP2022
Volume 43, September 1949

Part of the Journal of Research of the National Bureau of Standards

Seasonal Variation of Ozone at Washington, D. C.

By Ralph Stair

This paper gives data on the variation in the total amount of ozone in the atmosphere above Washington, D. C., covering a 9-year period extending from 1934 to 1943. The amount of ozone was determined from solar ultraviolet measurements made by means of a phototube and filter method on direct sunlight.

The ozone determinations indicate a seasonal variation having a maximum value during late winter and early spring (range 0.20 to 0.30 centimeters normal-temperature pressure) with a minimum value in late summer or early fall (range 0.16 to 0.20 centimeters normal-temperature pressure).

No correlation appears to exist between total ozone value and surface pressure pattern or between ozone value and sunspot number. A close correlation does, however, exist between total ozone and air temperatures at altitudes near 8 kilometers, that is, within the upper part of the troposphere. A slight opposite correlation appears to hold for altitudes within the stratosphere, with the change-over occurring near the level of the tropopause.

I. Introduction

The data on the variation in the total amount of ozone above Washington, D. C., recorded in this paper are based upon measurements of direct ultraviolet solar radiant energy made on clear days at the National Bureau of Standards. The original data were obtained in collaboration with W. W. Coblentz, formerly Chief of the radiometry laboratory of this Bureau, and represent 244 days within a 9-year period extending from 1934 to 1943. Ordinarily measurements were made only on days when there was little smoke or haze and the sky was relatively free from clouds. During most of the days on which measurements were made, the wind was from a westerly direction which, coupled with the fact that the observing station is in the northwest edge of the city, resulted in essentially "country air" conditions. Except during the winter months when the solar altitudes were low, even at noon, most of the measurements employed in this work were obtained through an air mass not exceeding 1.5 atmospheres, so that most of the data are based on measurements of high-intensity ultraviolet solar radiant flux densities.

The method employed in this work involves the use of titanium phototubes sensitive to solar radiant energy between about 3,000 and 3,400 A, together with glass filters having transmittances beginning at 2,900 to 3,100 A and increasing with wavelength. Since ozone is strongly absorbing within this region of the spectrum, any change in its value is immediately reflected as a change in the observed transmittance of the filters. Likewise, a change in the relative spectral emission of the sun would produce a similar change in the observed filter transmittance. Although it is known that there are large fluctuations in the short ultraviolet emission from the sun [1, 2, 3],[1] which appear to be associated with sunspots and other solar activity, no extensive study has been made either of variation of solar radiant energy at these wavelengths or of ozone changes accompanying them. It is assumed, however, and the present work seems to bear this out, that any change in the relative spectral energy within the range of 3,000 to 3,400 A is small or nonexistant. Hence, it is believed that changes in solar emission may be neglected without introducing a serious error in the determinaton of the total amount of ozone at any particular time.

[1] Figures in brackets indicate the literature references at the end of this paper.

II. Instruments and Methods

In this work the two Westinghouse type 767 titanium phototubes (No. 1 and No. 4) and four filters, together with the sensitive d-c amplifier, were employed, as described in previous papers [4, 5], in connection with the determination of ultraviolet solar radiant-energy intensities. As a matter of fact, some of the solar data employed in the present determinations were included in the earlier reports. In the present case, however, attention is given only to their use in ozone determinations.

The general method employed in the reduction of the data in the present work is the same as that previously used and described in detail elsewhere [6, 7, 8]. The relative spectral response curves of the two phototubes, the spectral transmittances of the four filters, spectral transmittance curves for selected amounts of ozone, and Rayleigh scattering transmittance factors for various air masses are given in figures 1 and 2 to illustrate the general region of the spectrum involved in the measurements and calculations. For detailed information regarding the method, reference should be made to the previous publications. In general, measurements were made alternately with two phototubes

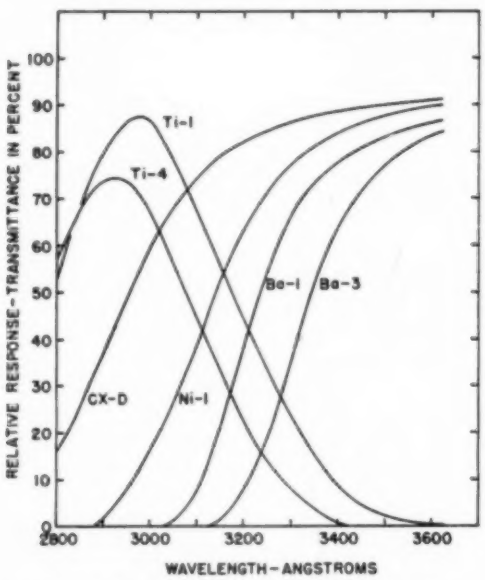

FIGURE 1. *Relative spectral response curves for the two titanium phototubes, also the spectral transmittances of the four filters.*

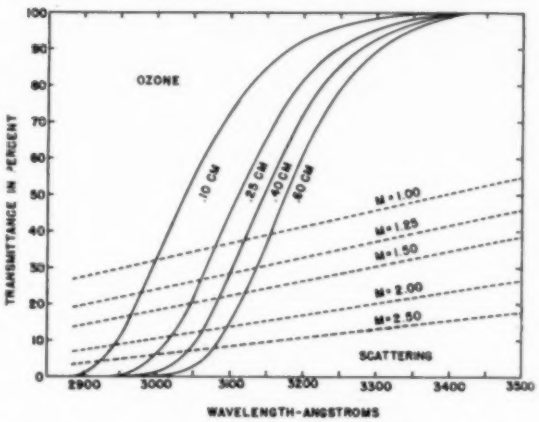

FIGURE 2. *Spectral transmittance of the atmosphere in terms of molecular (Rayleigh) scattering and ozone absorption.*

Scattering data are given for several air masses, M; ozone transmission data are given for varying thicknesses of ozone, normal temperature pressure.

and four filters. However, on many days when only a few measurements were possible, especially during the winter months, because of changing weather conditions, only one phototube was employed. As the two phototubes and the separate filters were calibrated independently, it is to be expected that the eight determinations (using 2 phototubes and 4 filters) of ozone from any one complete set of measurements would be scattered over a limited range. Hence, to reduce this scattering to a minimum, a mean is taken for the four filter measurements and plotted (see fig. 4) in the illustration as a single ozone determination. A second adjustment, amounting to 0.01 cm of ozone, was made to bring the data for the two phototubes into agreement, so that on days when a single phototube was employed the values obtained would be representative of the mean for the two tubes. The data shown in figure 4 are representative of individual determinations on 4 days having high, medium, and low amounts of ozone. From each daily curve a weighted mean value was obtained for use in figures 5 to 10, inclusive (values from 10:00 a. m. to 2:00 p. m. were given greater weight).

III. Solar Energy Curve

The determination of ozone by this method is based upon an energy curve of the sun outside the earth's atmosphere. Measurements have been

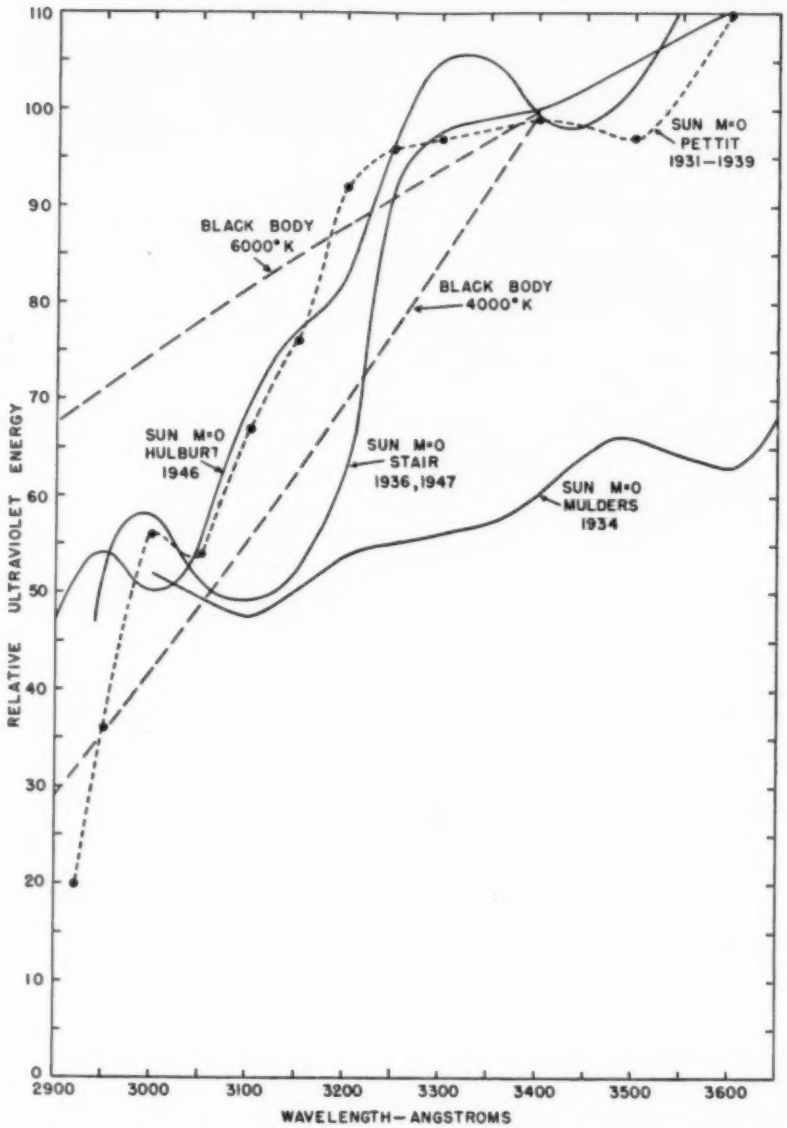

FIGURE 3. *Distribution of energy in the extreme ultraviolet of the solar spectrum.*

The ordinates for the Pettit and Stair curves are given in terms of microwatts per square centimeter per 10 angstroms. For the other solar curves and for the two black body temperatures the ordinates are arbitrary.

made by many observers, but in most cases the data either do not include the region of 3,000 to 3,400 A, or else they are insufficiently accurate for the purpose. Some of the best data extending to even below 3,000 A were obtained at Mt. Wilson Observatory by Pettit [9]. However, the use of wide slits (about 100 A) by Pettit, together with the low sensitivity of the equipment, as well as the fact that in many of the measurements only a segment of the solar disk was employed, render the short wavelength ultraviolet data much less useful. Data published by Mulders [10] extend to 3,000 A, but they likewise lack sufficient wavelength dispersion to show more than a rough

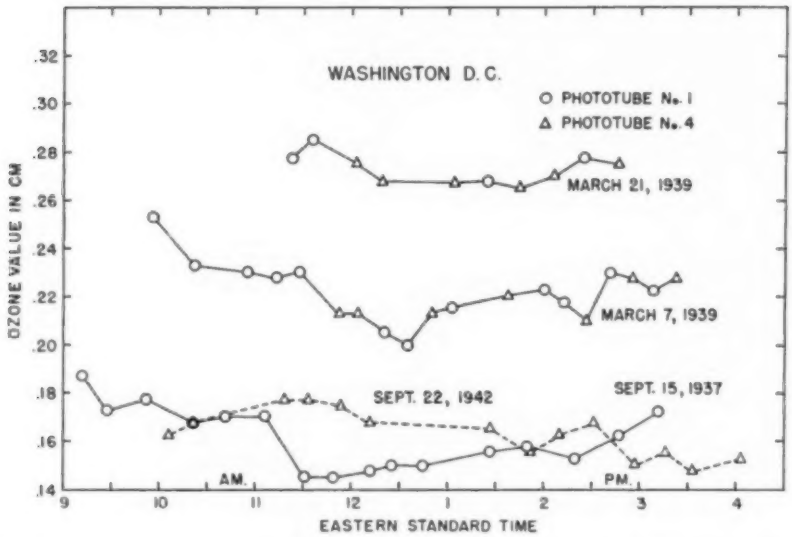

FIGURE 4. *Individual ozone determinations with the two phototubes for days on which there were large, medium, or small amounts of ozone.*

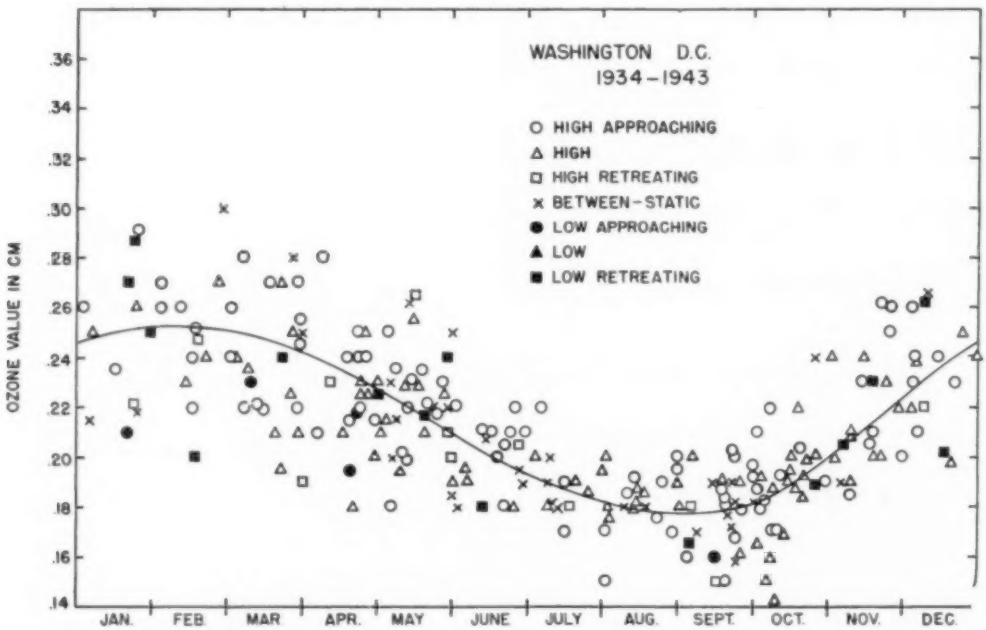

FIGURE 5. *Seasonal variation of ozone at Washington, D. C.*

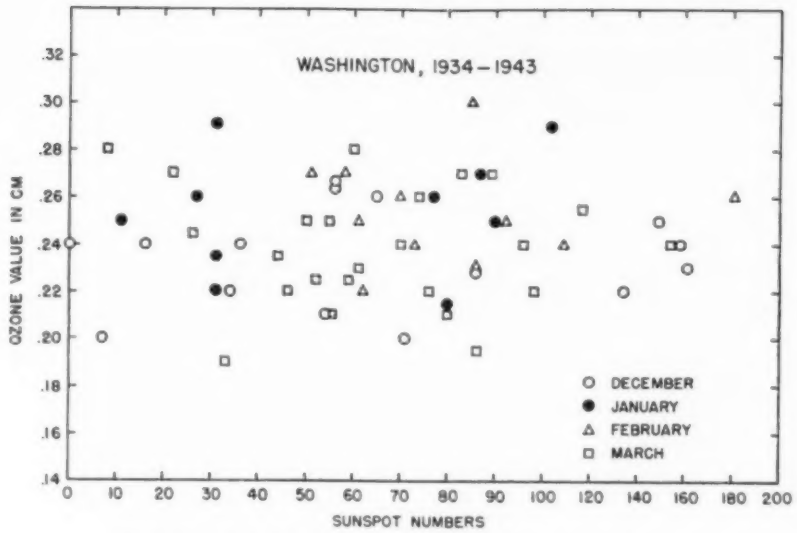

FIGURE 6. *Plot of amount of ozone and sunspot number.*

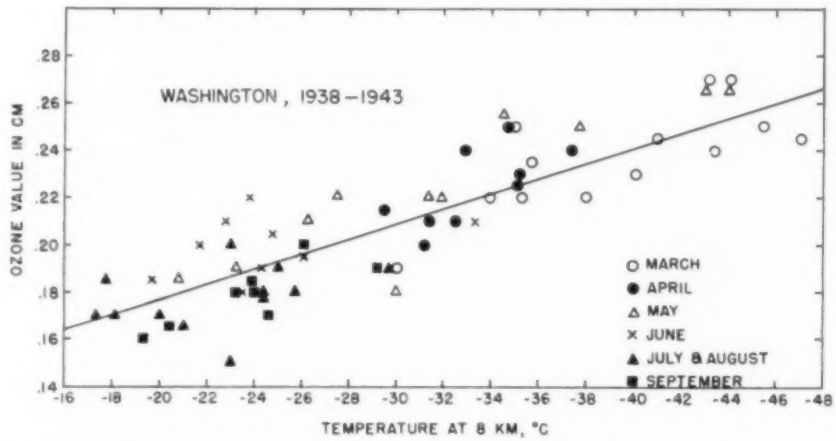

FIGURE 7. *Positive correlation in the spring, summer, and fall between the amount of ozone and air temperatures at an altitude of 8 km.*

Fraunhofer structure. In general, measurements by Abbot [11], Götz [12], Reiner [13], Hess [14], Fabry and Buisson [15], and others give few or no useful data within the spectral region from 3,000 to about 3,400 A, that is, within the spectral region employed in this investigation.

Instruments transported aloft by rockets offer great promise, as exemplified by a single preliminary set of data recently reported by Hulburt [16]. Although obtained under adverse conditions, these data are no doubt the best available for the spectral region of 3,000 to 3,400 A. The published curve is, however, the upper envelope of the solar intensity curve and does not include the dips due to Fraunhofer lines. When additional data of this type have been obtained and proper corrections made for Fraunhofer and other line and band absorption, the measurement of ozone concentration will have been established on a much firmer basis. Meanwhile it becomes necessary either to assume or calculate a solar energy curve applicable to the measurements

847618—49——3

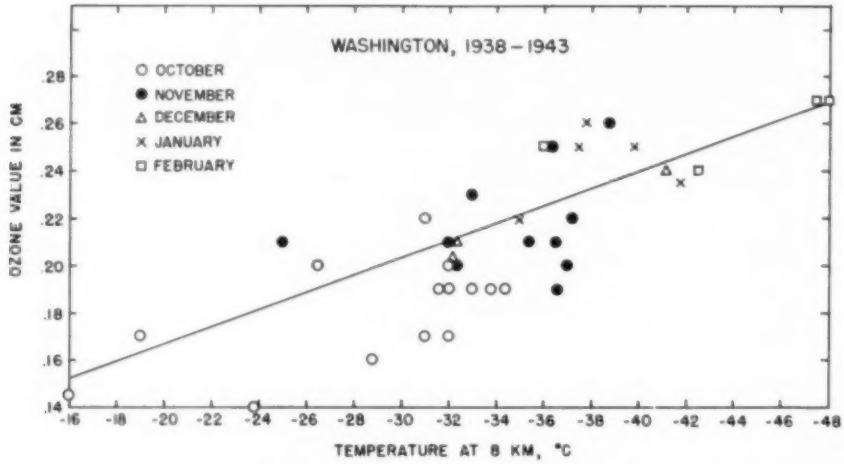

FIGURE 8. *Positive correlation in the winter between the amount of ozone and air temperatures at an altitude of 8 km.*

being made. For the present work, the relative energy curve obtained and employed in previous work [6, 7, 8] has been used. This calculated curve, together with some of those observed by others, is shown in figure 3. It is to be noted that this curve was obtained by a phototube and filter integration method and may not be precise with regard to specific features, as the curve obtained is simply a smooth curve, which appears to represent best the experimental data on which it was based. On the other hand, the curves obtained by Pettit or by the Naval Research Laboratory in the rocket experiment are not fully corrected for Fraunhofer absorption lines and bands. The calculated curve is preferred and used in this work because its use results in closer agreement with the experimental data for high air masses relative to low air masses, as pointed out in a previous report [8]. The broad minimum located near 3,100 A is not substantiated by the NRL data [16], which show a lesser minimum located at about 3,000 A. In some of Pettit's [9] data a marked minimum appears about midway between 3,000 and 3,100 A, whereas Mulders [10] shows it located at 3,100 A. Hence it is not possible at the present time to set up any solar energy curve between 3,000 and 3,400 A with certainty.

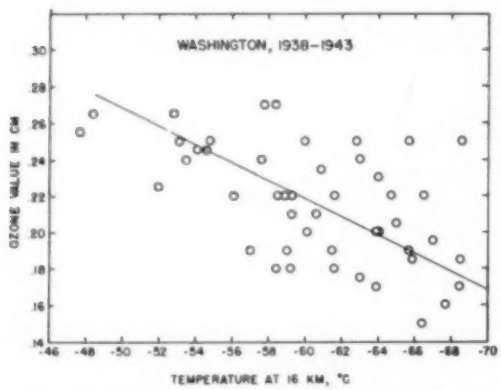

FIGURE 9. *Negative correlation during the year between the amount of ozone and air temperatures at an altitude of 16 km.*

It is, of course, further recognized that the use of a fixed solar energy curve within the spectral region of 3,000 to 3,400 A allows no liberty for actual variations in its shape from day to day as the result of solar activity. If the short wavelength ultraviolet should increase relative to the longer wavelengths, the effect would be equivalent to an indicated decrease in ozone. Then if more ozone is produced by the more intense ultraviolet, the over-all effect reduces, apparently, to the case of constant ozone and constant spectral quality of solar radiant energy. This explanation is fairly well contradicted, however, by the fact that large short-time fluctuations in ozone amount are not observed, as would be expected if the spectral quality changed and ozone measurements were made before an equilibrium condition could be reached.

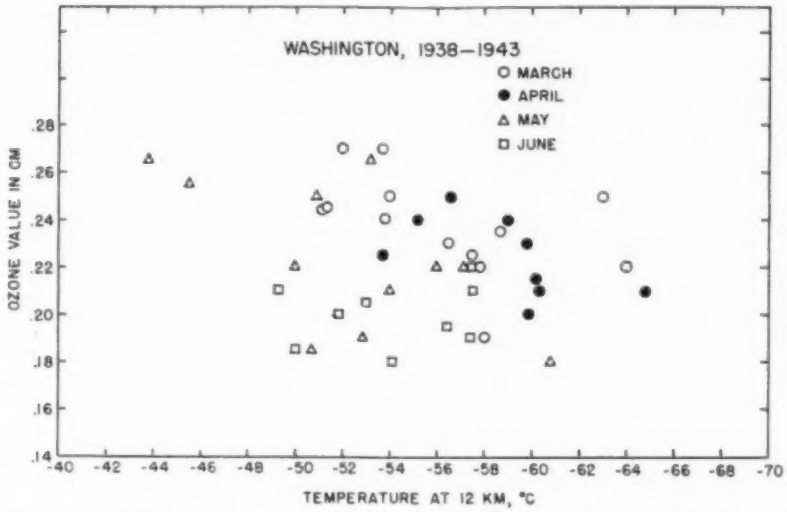

FIGURE 10. *Low correlation in the spring and early summer between the amount of ozone and air temperatures at an altitude of 12 km.*

IV. Amount of Atmospheric Ozone

The mean amount of ozone, based on the calculated solar energy curve of figure 3, is displayed in figure 5 for each day on which observations were made during the 9-year period extending from May 1934 to April 1943. Each point shown on the diagram is displayed in terms of the general pressure condition existing on that particular day, so that any obvious relationship between pressure pattern and amount of ozone should be revealed. The pressure patterns were obtained from U. S. Weather Bureau surface maps. The smooth curve representing the seasonal variation in ozone was simply located, without resort to mathematical calculation, in such a manner that an approximately equal number of observed points fell on each side of the line. (The same simple procedure was applied to the other illustrations.)

Several things are worthy of note in this illustration other than the fact that the observed seasonal variation agrees in both magnitude and time with that obtained by other observers [17, 18, 19, 20] for similar latitudes. Although there appears to be no observable relationship between pressure pattern and total amount of ozone, it is during those periods of the year, namely the late fall, winter, and spring, when pressure pattern changes are pronounced, that both high values and erratic changes in ozone are observed, whereas during the summer "quiescent" period the ozone value remains low and relatively constant.

Although it does not seem possible to establish any definite connection between the pressure pattern and ozone value, there is a relationship between air movements and ozone concentration. The seeming noncorrelation between cyclonic areas and ozone can be accounted for by the multiple types of synoptic air masses reaching the Washington Area. For example, Dobson and his collaborators [17] found the highest ozone values above the rear of cyclones in western Europe, while Lejay [21, 22] found the highest ozone during anticyclonic weather in eastern China. This apparent discrepancy has been analyzed by Haurwitz [23] on the basis of the height of the synoptic air mass, that is, in both cases the ozone would be highest in cyclones at high levels and lowest in anticyclones at high levels. If the present data could be analyzed after this fashion, a similar relationship would probably result, judging from the temperature relationships given in a later section of this paper.

An attempt was made in figure 6 to reveal any simple relation between total ozone and solar disturbances. For this purpose, use was made of the sunspot numbers [24] recorded for the days on which observations were made. No correlation appears to exist. In a similar manner, when the ozone values were plotted as a function of the total

sunspot number for a period of 10 days preceding the ozone measurements, the correlation was again essentially zero. Hence, it appears that if there is any change in short wavelength ultraviolet solar radiant energy associated with excess solar sunspot activity, it has little effect upon the total ozone over a particular locality.

According to the investigations of Wulf and Deming and others [20, 25, 26], excess accumulation of ozone would be reduced greatly because of two facts. First, the photochemical production of ozone occurs principally at altitudes exceeding 30 km, below which level is 90 percent of the ozone present at any time within the atmosphere; and secondly, an equilibrium condition in the amount of ozone above the level of maximum concentration is quickly restored once it has been disturbed. According to their views, we should probably not expect to find a definite correlation between amount of ozone and the magnitude of solar activity as indicated by the number of sunspots [42].

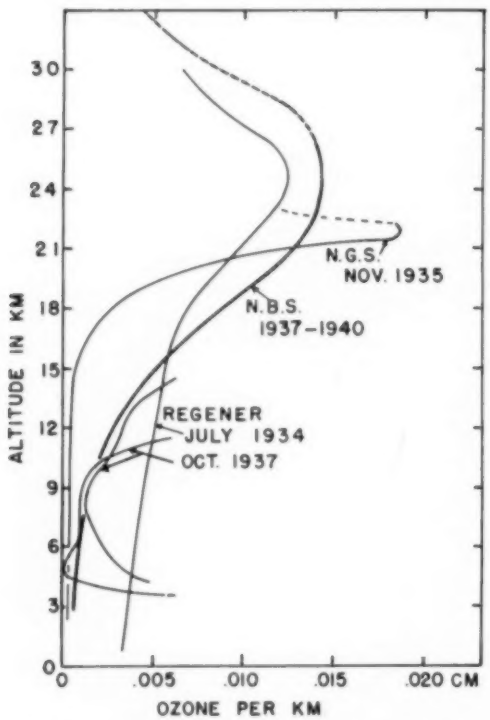

FIGURE 11.—*Vertical distribution of ozone in the stratosphere.*

The NBS curve is the mean of June and early July measurements obtained in 18 unmanned balloon flights during the four years, 1937 to 1940.

In figures 7 to 10 some of the data on total amount of ozone are plotted as a function of upper-air temperatures measured at Washington, D. C., by the United States Weather Bureau through the use of the radiosonde [27]; the temperature data were obtained from Weather Bureau files. Most of the temperature measurements were made near noon on the days on which the ozone measurements were made. In some cases the data were taken in the early morning hours, and in some others it was necessary to use midnight values because of failure of midday radiosonde flights. For the greater part of the work, the upper air temperatures correspond in both time and place with the ozone measurements. This is an important factor, since radical changes in upper-air conditions often occur within 12 hr.

In the work of Meetham [28, 29], many of the radiosonde measurements were made at points 50 to 120 miles distant, so that entirely different upper-air conditions could easily have prevailed between the two stations. Nevertheless, his work shows a certain amount of correlation between ozone and upper-air temperatures, pressures, height of tropopause, etc., but not of the magnitude existing in the present work and most beautifully displayed (in fig. 7) by the spring-summer-fall values for an altitude of 8 km. The winter values for the same altitude shown in figure 8 scatter more for a number of reasons, such as instrumental errors as a result of low solar intensity, small uncorrected temperature coefficients of the glass filters, and greater dust and smoke scattering, which, spectrally, may not be entirely nonselective.

If the ozone values are plotted as a function of the upper-air temperature at some point well within the stratosphere, for example at 16 km (see fig. 9), there is a much lower correlation between the two, and it is opposite to that existing in the region of 8 km. At 12 km, just above the tropopause (see fig. 10), the correlation is still lower—in fact it is near zero, as is to be expected, at or near the tropopause. Inasmuch as the mean altitude of the tropopause shifts with the season of the year, one might expect a seasonal shift in the ozone-temperature correlation curves.

If the correlation had been made in terms of the amount of ozone as a function of the altitude of

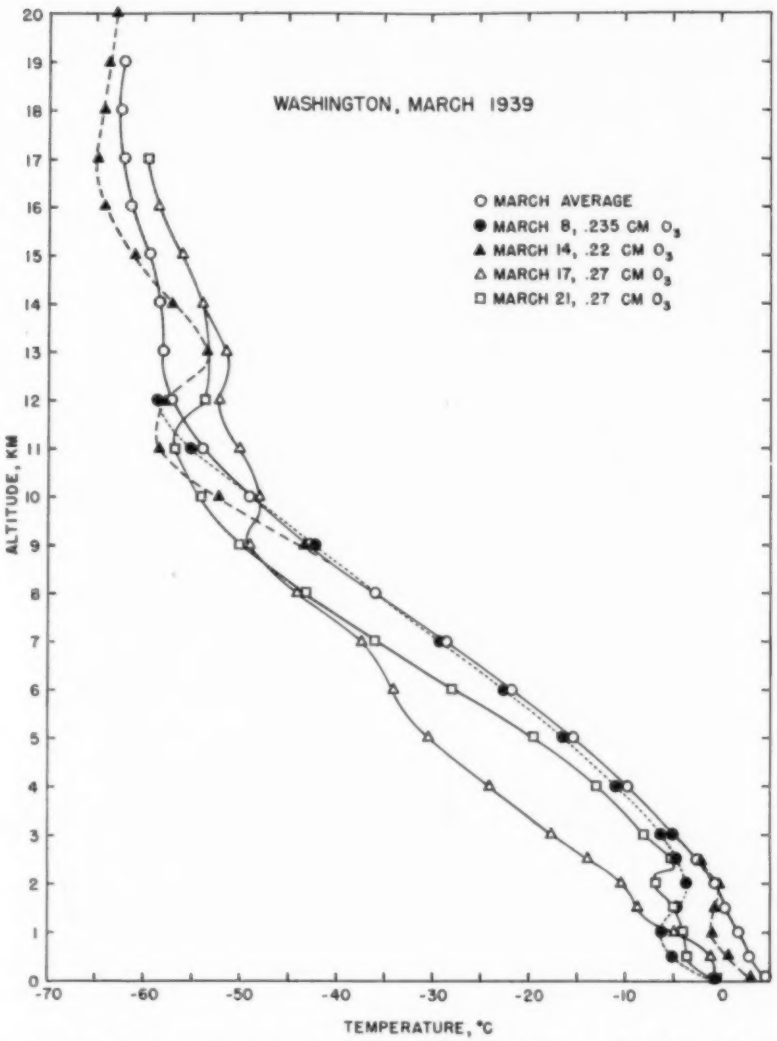

FIGURE 12. *Some March 1939 air temperatures as a function of the altitude on days of high and of low amounts of ozone.*

These data were obtained by the U. S. Weather Bureau through the use of the radiosonde.

the tropopause, the agreement would probably be as good as in the case when correlated with the temperature at 8 km, since the tropopause shifts with temperature changes below that level. In other words, high ozone values are associated with low tropopause altitudes as previously found by Meetham [29].

V. Discussion of the Ozone Data

The ozone data recorded herein show, in agreement with other investigations [17, 18, 19, 20, 30, 31, 39], in particular that of Dobson and Götz, a marked seasonal variation. They also show significant changes that are in some way connected with air mass movements, but which cannot be tied down to surface conditions of pressure, temperature, etc. The curves reproduced in figures 11 and 12, relative to the vertical distribution of ozone [33 to 40], and those for measured air temperatures as a function of altitude for several days on which measurements were made indicate a very close relationship between the position of

the ozone band and normal atmospheric characteristics. Very little ozone normally exists within the troposphere as the result of air currents that rapidly bring it into conditions of pressure, temperature, etc., that accelerate its degeneration. This fact is illustrated by the experimental data reproduced in the curves of figure 11, which show but little ozone until altitudes above the tropopause are reached. Hence, the irregularities in the temperature curves in the lower part of the atmosphere (see fig. 12) would not be expected to affect directly the amount of ozone in any way. It is only when something happens at a much higher level, in general, to change effectively the position of the tropopause, that fluctuations in the ozone value would be expected. An analysis of the curves of figure 12, taking into account the vertical distribution of ozone (see fig. 11) and the observed relationship between the amount of ozone and the temperature at various altitudes (see figs. 7 to 10), indicates that ozone changes are directly associated with air movements above about 6 or 8 km. A vertical motion of the air at these levels would change the temperature below and above the tropopause, as well as change the tropopause level. Similar changes in atmospheric characterics would result with lateral movements of air from other latitudes. Both of these movements occur, as can be determined by cloud movements. As a matter of fact, rapid vertical motions at altitudes as high as 25 km have been observed by Stormer [41]. Both high-vertical and lateral-air movements are sometimes observed in trails left by meteors. The relative importance of these two types of air movements in increasing or decreasing the amount of ozone at a particular station is unknown.

A combination of air motions wherein a significant part of the ozone layer moves downward, together with a lateral inward motion of air of high ozone content, could be expected to result in a very high ozone value. Similarly, an opposite type of air motion should produce a very low ozone value. In either case, any disturbance within the upper 10 percent of the ozone layer would rapidly be brought to equilibrium as the result of normal photochemical reactions.

If the measurement of ozone should be placed on a routine basis and correlated with other upper-air measurements at a number of stations within a continental area, for example, much information on this subject should soon become available.

The existence of a noon "dip" in the daily ozone curve (see fig. 4) continuing into the afternoon may be subject to some question, as it is not found in any early published investigation available to the author. A noon dip has, however, been observed and described in recent papers by Ramanathan [43] and by Karandikar [44]. The noon dip is not large but nearly always occurs not only in the data for Washington, but also in measurements made in both mountain and desert [5, 6, 7, 8] locations using the same or similar instruments. If the noon dip is real, its magnitude may be even larger than indicated in figure 4, as its existence is very much dependent upon the solar energy curve employed in the calculations. If one of the curves as observed by Pettit [9], or that obtained by the NRL [16] group, be employed in the calculations, the noon dip is appreciably greater. The total ozone value is also greater. To remove effectively the noon dip would require the use of a solar energy curve even steeper within the spectral range of 3,100 to 3,400 A than that now employed. This procedure seems unjustified at the present time. It is rather to be expected that the noon dip is real, and that we should credit its existence to either a diurnal decrease in ozone or to some other variable atmospheric condition that affects the relative spectral transmittance of the atmosphere. Changes in size of water particles or amount of dust have been suggested, but neither existed in appreciable quantity in the case of some of the mountain and desert measurements. Furthermore, there seems to be no obvious relationship between local humidity and observable dustiness and apparent ozone value from measurements made on days when they are high. Recent extensive measurements made by the author at a high altitude station in southern New Mexico, where haze and humidity are extremely low, should, when reduced, do much toward clearing up the question of a noon dip in ozone value.

In conclusion, a question may be raised about possible errors in all past ozone work resulting from unknown or uncorrected temperature coefficients [45]. The high correlation between zonal air temperatures and ozone amount observed in this work may be significant in this respect.

VI. References

[1] C. G. Abbot, Solar variation and forecasting, Smithsonian Misc. Collections **77,** No. 5 (1925).

[2] Edison Pettit and S. B. Nicholson, Radiation measurements on the corona. Pubs. Astron. Soc. Pacific **37,** 152 (1925).

[3] G. M. B. Dobson, Measurements of the sun's ultraviolet radiation and its absorption in the earth's atmosphere, Proc. Roy. Soc. London [A], **104,** 252 (1923).

[4] W. W. Coblentz and R. Stair, Factors affecting ultraviolet solar-radiation intensities, J. Research NBS **15,** 123 (1935) RP816.

[5] W. W. Coblentz and R. Stair, Evaluation of ultraviolet solar radiation of short wave lengths, J. Research NBS **16,** 315 (1936) RP877.

[6] R. Stair and I. F. Hand, Methods and Results of Ozone Measurements over Mount Evans, Colo., Monthly Weather Rev. **67,** 331 (1939).

[7] Ralph Stair, Measurements of Ozone over the Organ Mountains, New Mexico, J. Research NBS **40,** 9 (1948) RP1851.

[8] Ralph Stair, Winter Measurements of Ozone over the Organ Mountains, New Mexico, J. Research NBS **42,** 145 (1949) RP1958.

[9] Edison Pettit, Spectral Energy-curve of the Sun in the Ultraviolet, Astrophys. J. **91,** 159 (1940).

[10] G. F. W. Mulders, Aequivalente Breedten Van Fraunhoferlijnen in Het Zonnespektrum, Dissertation, Nijmegen (1934).

[11] C. G. Abbot, F. E. Fowle, and L. B. Aldrich, The Distribution of Energy in the Spectra of the Sun and Stars, Smithsonian Misc. Collections **74,** No. 7 (1923).

[12] F. W. Paul Götz and Ernst Schönmann, Die spectrale Energieverteilung von Himmels- und Sonnenstrahlung, Helv. Phys. Acta **21,** 151 (1948).

[13] Heinz Reiner, Die Struktur des Sonnen Spektrums Zwischen 400 und 600 mμ, Gerlands Beitr. Geophys., **55,** Heft 2, 234 (1939).

[14] Paul Hess, Untersuchungen über die spektrale Energie-verteilung im Sonnenspektrum von 350 mμ bis 500 mμ, Inaugural-Dissertation, Universität Frankfurt a. M. (1938).

[15] C. Fabry and M. Buisson, Etude de l'éxtremité ultraviolete du Spectre solaire, J. phys. radium **2,** 197 (1921).

[16] E. O. Hulburt, The Upper Atmosphere of the Earth, J. Opt. Soc. Am. **37,** 405 (1947).

[17] G. M. B. Dobson, D. N. Harrison, and J. Lawrence, Proc. Roy. Soc. London [A] **114,** 521 (1927); [A] **122,** 456, (1928).

[18] F. W. P. Götz, Ergeb. Kosmichen Phys. **III,** 253 (1938).

[19] F. W. P. Götz, Der Stand des Ozonproblems, Vierteljahrsschr. naturforsch. Ges. Zürich **89,** 250 (1944).

[20] Richard Ansel Craig, The observations and photochemistry of atmospheric ozone and their meteorological significance. (Thesis, Mass. Inst. of Tech., 1948).

[21] Rev. Pierre Lejay, Quart. J. Roy. Meteorol. Soc., Atm. Ozone, Suppl. to Vol. **62** (1936).

[22] Rev. Pierre Lejay, Ozone Measurements and Currents in the Stratosphere, Bul. Am. Meteorol. Soc. **20,** 298 (1939.)

[23] B. Haurwitz, Atmospheric Ozone as a Constituent of the Atmosphere, Bul. Am. Meteorol. Soc. **19,** 417 (1938).

[24] W. Brunner, Sunspot Numbers for 1934—1943, Terr. Mag. and Atmos Elec. **40** to **49** (1935–44).

[25] O. R. Wulf and L. S. Deming, Terr. Mag. and Atmos. Elec. **41,** 299, 375 (1936); **42,** 195 (1937).

[26] Oliver Reynolds Wulf, Proc. Eighth Am. Sci. Congr. **VII,** 439 (1940).

[27] H. Diamond, W. S. Hinman, and F. W. Dunmore, The Development of a Radio Meteoragraph System for the Navy Department, Bul. Am. Meteorol. Soc. **18,** 95 (1937).

[28] A. R. Meetham, Correlation of Atmospheric Ozone with other Geophysical Phenomena, Quart. J. Roy. Meteorol. Soc. Suppl. to vol. **62,** p. 59 (1936).

[29] A. R. Meetham, The Correlation of the Amount of Ozone with other Characteristics of the Atmosphere, Quart. J. Roy. Meterolog. Soc. **63,** 289 (1937).

[30] G. M. B. Dobson and A. R. Meetham, Quart. J. Roy. Meteorol. Soc. (London) **60,** 265 (1934).

[31] G. M. B. Dobson, Proc. Roy. Soc. London [A] **129,** 411 (1930).

[32] G. M. B. Dobson, A. W. Brewer, and B. M. Cwilong, Proc. Roy. Soc. London [A] **185,** 144 (1946).

[33] R. Stair and W. W. Coblentz, Radiometric Measurements of Ultraviolet Solar Intensities in the Stratosphere, J. Research NBS **20,** 185 (1938) RP1075.

[34] W. W. Coblentz and R. Stair, Distribution of Ozone in the Stratosphere, J. Research NBS **22,** 573 (1939) RP1207.

[35] W. W. Coblentz and R. Stair, Distribution of Ozone in the Stratosphere: Measurements of 1939 and 1940, J. Research NBS **26,** 161 (1941) RP1367.

[36] E. Regner and V. H. Regner, Aufnahmen des ultravioletten Sonnenspektrums in der Stratosphäre und die vertikale Ozonverteilung, Phys. Z. **35,** 788 (1934).

[37] Brian O'Brien, H. S. Stewart, and F. L. Mohler, Vertical Distribution of Ozone in the Atmosphere, Nat. Geogr. Soc. Contrib. Tech. Papers, Stratosphere Series No. 2, page 49, 1936.

[38] V. H. Regner, Neue Messungen der vertikalen Verteilung des Ozons in der Atmosphäre, Phys. Z. **109,** 642 (1938).

[39] E. Tonsberg and K. L. Olsen, Investigations on Atmospheric Ozone at Nordlysobservatoriet, Tromso, Geof. Pub. **13,** No. 12 (1944).

[40] A. R. Meetham and G. M. B. Dobson, The Vertical Distribution of Atmospheric Ozone in High Latitudes, Proc. Roy. Soc. London **148,** 598 (1935).
[41] C. Stormer, Höhe und Farbenverteilung der Perlmutterwolken. Geophys. Pub. **IX,** No. 4 (1932).
[42] B. Haurwitz, Relations Between Solar Activity and the Lower Atmosphere, Trans. Am. Geophys. Union, **27,** 161 (1946).
[43] K. R. Ramanathan, Assemblée UGGI, Oslo (1946).
[44] R. V. Karandikar, Studies in Atmospheric Ozone. Proc. Indian Acad. Sci. **28,** 63 (1948).
[45] Vassy and Vassy, Variation diurne de la température moyenne de l'ozone atmosphérique, Compt. rend. **228,** 764 (1949).

WASHINGTON, June 8, 1949.

U. S. Department of Commerce
National Bureau of Standards

Research Paper RP2023
Volume 43, September 1949

Part of the Journal of Research of the National Bureau of Standards

Surface Tension of Molten Zinc Borates

By Leo Shartsis and Rodrigo Canga [1]

The surface tension of melts in the system ZnO-B_2O_3, ranging from 0 to 79.5 percent of ZnO, were measured with a maximum pull-on-cylinder method. In the two-liquid region, which extends from approximately 0 to 53 percent of ZnO, the value of surface tension was that of B_2O_3 within the limits of experimental error. With percentages of ZnO beyond the two-liquid region, the surface tension value increased rapidly. Melts containing approximately 55 to 65 percent of ZnO showed minima in the curves of surface tension versus temperature. Melts containing approximately 65 to 75 percent of ZnO had positive temperature coefficients of surface tension. The melt containing 79.5 percent of ZnO had a negative temperature coefficient of surface tension. The densities at room temperature were also measured.

I. Introduction

Zinc oxide and boric oxide are used extensively in glasses, glazes, and enamels. It was considered, therefore, that a study of surface tension in this system of oxides might be of interest in several fields of ceramics. Furthermore, studies of simple systems are not only interpreted more easily but also may be of use in the study of more complex systems.

A further consideration in the selection of the system zinc oxide-boric oxide for study was the expectation of obtaining additional data for the positive temperature coefficients of surface tension. Previous studies [1] [2] had indicated that the phenomenon would probably occur in the present study.

The normal process tending to lower the surface tension as the temperature is raised is generally considered to be associated with the decrease in the force of attraction between adjacent molecules as their average distance of separation increase with rising temperature. The mechanism leading to negative-temperature coefficients of surface tension should always be operative in liquids that have a positive thermal expansion. Any mechanism that operates to give a positive coefficient must then be considered as superimposed upon the normal tendency.

Two mechanisms have been proposed for explaining the increase in surface tension with increasing temperature. W. A. Weyl [2] postulated that this phenomenon is caused by the presence of asymmetrical groups in the surface of the melt as based upon the observed positive temperature coefficients of surface tension of some glasses high in PbO and of fused B_2O_3. These groups tend to orient themselves so that the surface energy is a minimum. As the temperature is increased, the increase in the thermal agitation of the asymmetrical groups produces a decrease in the effective asymmetry, thus raising the surface tension.

Another mechanism, first proposed by Worley [3], depends upon the concentration changes taking place in the surface of a liquid as its temperature is raised. If the surface concentration of a component that depresses the surface tension of the liquid decreases with increasing temperature, the effect is to counteract the normal decrease in surface tension. This counteraction, depending on the magnitude of the effect, may cause the coefficient to become less negative, attain a zero value, or even to become positive. On the other hand, an increase in the surface concentration of the capillary active component with rise in temperature should result in an intensification of the negativity of the coefficient of the test liquid.

[1] Instituto de Optica. Consejo Superior de Investigaciones Cientificas, Madrid, Spain. Guest worker at the National Bureau of Standards 1948-49.

[2] Figures in brackets indicate the literature references at the end of this paper.

847618—49——4

An important point to note is that, according to this mechanism, the coefficient of the pure capillary active substance does not determine the coefficient of the solution. Thus, although phenol and water each have negative coefficients, some of their mixtures have positive ones, and molten PbO and molten B_2O_3 have positive coefficients, whereas some of their molten mixtures have negative ones. Pure substances such as B_2O_3 and PbO, which have positive coefficients, are molecularly complex according to this theory.

Worley's concepts were applied to the data obtained with the systems PbO-B_2O_3 and PbO-SiO_2 [1]. The slope of the curve for surface tension versus concentration of PbO, $[\Delta\sigma/\Delta c]_t$, was estimated at several temperatures from the data on the surface tension of the system PbO-B_2O_3 for a composition containing 85 percent of PbO (table 1). It will be noted that for this liquid the slope is negative. This implies that the surface contains more PbO than the interior of the liquid according to the Gibbs adsorbtion isotherm [4]. The absolute value of the concentration coefficient is a measure of excess PbO that decreases as the temperature is raised and becomes zero at 900° C, at which temperature the concentration of PbO in the surface is the same as in the interior of the liquid. Since an increase in the PbO content lowers the surface tension of this liquid, the decrease in PbO concentration in the surface resulting from increase in its temperature raises the surface tension, therefore, this liquid has a positive temperature coefficient of surface tension.

TABLE 1. *Change of concentration coefficient of surface tension* ($[\Delta\sigma/\Delta c]_T$, *dynes/cm/percent of* PbO) *with temperature for some melts in the systems* PbO-B_2O_3 and PbO-SiO_2 [1].

Percentage of PbO	PbO-B_2O_3			
	600° C	700° C	800° C	900° C
85	−1.3	−0.8	−0.3	−0
71	+0	+ .7	+1.3	+1.8

Percentage of SiO_2	PbO-SiO_2				
	900° C	1,000° C	1,100° C	1,200° C	1,300° C
6.3	−6.4	−5.6	−5.5	−4.5	−4.1
16.8	−2.9	−2.9	−2.8	−2.8	−2.7

It is interesting to apply the same type of reasoning to the melt that contains approximately 71 percent of PbO (table 1). The concentration coefficient of surface tension is positive, implying that there is less PbO in the surface than in the interior, and the value of the coefficient is a measure of the amount of this deficiency. Since the coefficient rises with increasing temperature, the concentration of PbO must decrease as the temperature rises. In this concentration region, however, PbO raises the surface tension and, therefore, decrease of PbO in the surface must result in a lowering of the surface tension and a resultant negative temperature coefficient of surface tension, even though both components of this solution themselves have positive coefficients. Thus, both negative and positive temperature coefficients in this system are accompanied by appropriate concentration changes in the surface of the liquid.

In the system PbO-SiO_2 [1], the temperature coefficients of surface tension are positive in the low silica range and become smaller as the silica content is increased until they approach zero at about 30 to 35 percent of silica. Increasing the amount of PbO lowers the surface tension in this composition range and, therefore, there must be an excess of PbO in the surface. Judging by the decrease in the magnitude of the concentration coefficients with increasing temperature (table 1), the concentration of PbO in the surface decreases as the temperature is raised.

II. Phase Equilibrium Relations

Figure 1 shows the phase-equilibrium diagram [5] of the system ZnO-B_2O_3. A region of liquid immiscibility extends from almost zero to about 53 percent of ZnO.[3] Previous experience [1] has shown that in this region the value of surface tension obtained is that of the upper liquid. In this investigation the upper liquid is almost pure B_2O_3. From the two-liquid region to about 68 percent of ZnO the liquidus curve, 1,000±3° C, is very flat even though a compound exists in this region. It was expected that in this region clear glasses could be obtained. Above 68 percent of ZnO the liquidus temperature rises rapidly with increasing amounts of ZnO, and it is to be expected that the glass-forming tendency would be restrained because of the rapid crystallization of the melts.

[3] All compositions are expressed as weight percent.

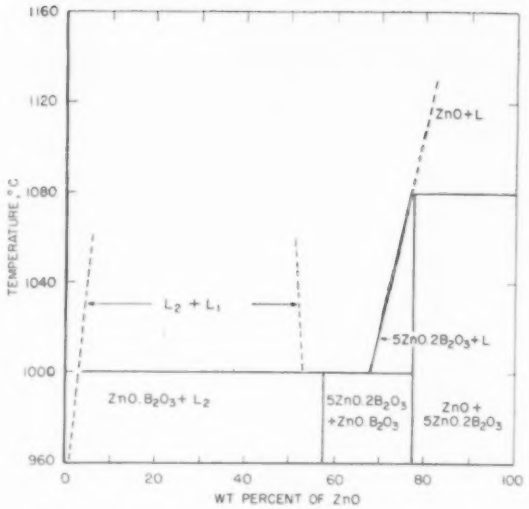

FIGURE 1. *Phase equilibrium diagram of the system* ZnO-B_2O_3 [5].

III. Preparation of Melts and Methods of Test

1. Preparation of Melts

The liquids investigated were made by melting in platinum crucibles the requisite amounts of chemically pure zinc oxide and boric acid. The melts, weighing from 300 to 500 g, were stirred with a motorized propellor-type platinum stirrer and, when they seemed homogeneous, were poured into iron molds. Melts containing more than 65 percent of ZnO crystallized while cooling, and even that containing 65 percent showed traces of devitrification.

In order to obtain a clear glass containing the smallest amount of ZnO possible in this system, a preparation containing about 52.5 percent of ZnO was prepared. When cooled, the product had an opalescent coating representing the upper layer that was removed readily by immersing in hot distilled water for a few minutes.

2. Chemical Analysis

Samples from each melt were analyzed for ZnO by a triple evaporation with HF and H_2SO_4. Analyses were made also of many of the samples remaining from the individual determinations of surface tension.

3. Measurement of Surface Tension

The method [6] of measuring surface tension was that of determining the maximum pull exerted on a thin-walled platinum cylinder when its lower edge was in contact with the test liquid. In general, the first determination of surface tension of any melt was made at 1,300° C. Subsequent measurements were made at 100-deg C intervals of decreasing temperature until the glass was too viscous to yield in a reasonable time or until crystallization had occurred. In several instances, however, this schedule was altered in order to determine the effect of such a change on the character of the temperature coefficient of surface tension. Tests on the same melt at different temperature schedules are often not comparable, a phenomenon that has been noted before [6].

4. Measurement of Density

In order to obtain accurate values of surface tension with the method adopted, it is necessary to know the density of the liquid at the temperature of test. Great accuracy, however, is not necessary, as an error of 10 percent would, in general, cause an error of about 0.5 percent in the values of surface tension. The densities of the solid compositions were measured by determining the buoyant effect of distilled water. To convert the densities at room temperature to those at 1,000° C, 0.2 was subtracted from each value, because experience has shown that with many glasses the average decrease in density from room temperature to 1,000° C is about 0.2.

IV. Results and Discussion

1. Analytical Results

The analytical results are given in the last two columns of table 2. With two exceptions, the percentages of ZnO obtained after surface tension determinations were a little higher than those corresponding to the original preparations. The differences in no case, however, exceed 0.3 percent.

2. Reproducibility of Surface Tension Data

The values of surface tension are given in table 2. Inspection of this data shows that the agreement between the surface tension results of duplicate melts was poor when the schedules of tem-

TABLE 2. *Surface tension, density, and chemical analysis of some compositions in the system* ZnO-B_2O_3

Accepted percentage of ZnO	Determination number	Surface tension, dynes/cm, at —							Percentage of ZnO by analysis		
		1,400° C	1,300 °C	1,200° C	1,100° C	1,000° C	900° C	800° C	Density at approximately 25° C	Before surface-tension measurement	After surface-tension measurement
0		97.2	93.6	90.1	86.5	83.0	79.5	75.9			
10	1		95.2	91.1	86.5	82.0	78.4				
50	1			90.9							
	2				87.9	83.2	79.7				
55.0	1		153.8	143.6	137.4	138.2			3.37	55.0	
	[a] 2				133.5	135.0	141.8				
56.1	1		162.7	157.0	150.2	151.0	159.9		3.42	56.1	56.4
	[a] 2				144.2	147.9	156.5				56.1
58.6	1		184.4	181.8	179.4	180.0	185.2	[b] [195.5]	3.48	58.6	58.8
	2		185.8	180.2	177.9	178.9	183.5	[191.3]			58.9
	[a] 3				174.5	175.9	178.7	[189.5]			
60.8	1		208.0	203.6	201.3	201.0	203.2		3.56	60.8	
	2		205.6	204.5	201.6	201.0	203.8				
64.6	1		237.8	235.2	232.5	232.1	234.7		3.68	64.6	
	[a] 2			236.6	234.1	234.5	235.4				64.6
65.6	1		250.0	246.6	244.2	242.0	[239.7]		3.70	65.6	65.7
	2		250.5	245.8	243.8	242.5					
70.6	1		286.8	285.2	281.5	277.0				70.5	70.7
	2		287.1	285.7	283.4	280.3					70.2
	3		289.7	286.5	283.4	278.7					
74.6	1		321.6	318.9	314.7				[c] 4.02	74.6	
	2		321.8	319.3	315.6						
79.5	1	355.3	355.9	360.3					[c] 4.22	79.6	79.5
	2	353.3	354.2								

[a] Not on regular temperature versus time schedule.
[b] Figures in brackets are extrapolated values.
[c] Crystallized.

perature were varied. However, the magnitude only, and not the algebraic sign of the temperature coefficient of surface tension, was dependent on the schedule.

The dependence of the surface-tension results obtained upon the thermal treatment of the melt can be traced to several factors, among which are:

(1) The slowness with which the equilibrium between the surface layer and the interior of the liquid is adjusted,

(2) The presence of bubbles in the melt, and the

(3) Volatilization, which affects the equilibrium between the surface and the interior and, in addition, may cause some material to condense on the upper portion of the cylinder and its supporting wire.

3. Surface Tension Minima

Figure 2 shows, in graphical form, the surface-tension results obtained when the previously described schedules of making observations was maintained. A point of interest is the appearance of minima in the curves for liquids that contain between 55 and 65 percent of zinc oxide. The behavior of solutions of phenol and water [3], with regard to the change of surface tension with increase in temperature, is similar to that of the system ZnO-B_2O_3. The more concentrated solutions also exhibit minima in the surface tension versus temperature curves. This phenomenon points to two competing mechanisms; one tends to decrease the surface tension and the other to increase it with an increase in temperature.

4. Region Above 65 Percent of ZnO

The measurements of surface tension below the liquidus temperature of these liquids was impossible because of the strong tendency of the melts in this region of composition to crystallize. This onset of crystallization was observed by the decrease in the values of surface tension as the melt was maintained at a constant temperature. The crystalline material, apparently denser than the melt, sank and there remained a liquid with a surface tension value lower than that of the original melt.

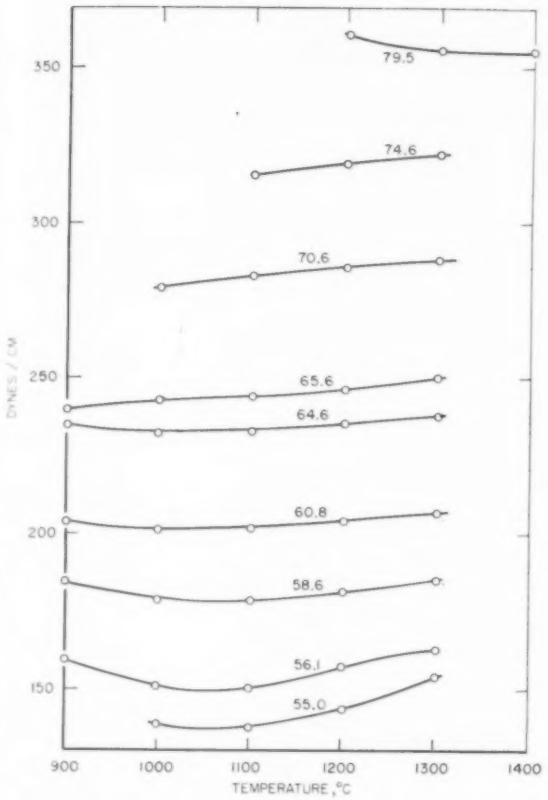

FIGURE 2. *Surface tension of melts in the system* ZnO-B_2O_3 *as a function of temperature.*

The percentage of ZnO is shown just above each curve.

With the exception of the liquid containing 79.5 percent of ZnO, the temperature coefficient of surface tension of melts in this region was positive.

5. Effect of Composition

A plot of surface tension values at 1,200° C against the percentages of ZnO is shown in figure 3. in the two liquid region extending from almost pure B_2O_3 to about 53 percent of ZnO the surface tension is that of the upper liquid, which is known to be practically pure B_2O_3. The first measurements, determined for a melt containing 50 percent of zinc oxide, were very erratic, and successive measurements at the same temperature resulted in unexpected differences in surface tension values of about 20 dynes/cm. Further investigation revealed that this erratic behavior was due to an extremely thin upper layer and, because of this, the bottom edge of the cylinder sometimes contacted the lower layer and gave relatively high values. If great care was exercised in contacting only the upper layer, correct results could be obtained.

Above the two-liquid region, the values of surface tension rise rapidly with increasing amounts of ZnO. According to the Gibbs adsorption isotherm, this indicates that the concentration of ZnO in the surface is less than that in the body of the liquid. This is one factor that would operate to cause a greater loss of B_2O_3 than of ZnO in melts heated at high temperatures as indicated by the analytical results (table 2). In addition, the greater volatility of B_2O_3 as compared to ZnO should also result in an increase in the ZnO content of melts heated at high temperatures.

V. Summary

The surface tension values of zinc borate melts were practically constant within the two-liquid region extending from about zero to 53 percent of ZnO and that of B_2O_3. With percentages of ZnO beyond the two-liquid region, the surface-tension values increased rapidly with increasing ZnO content. With one exception, melts of all composi-

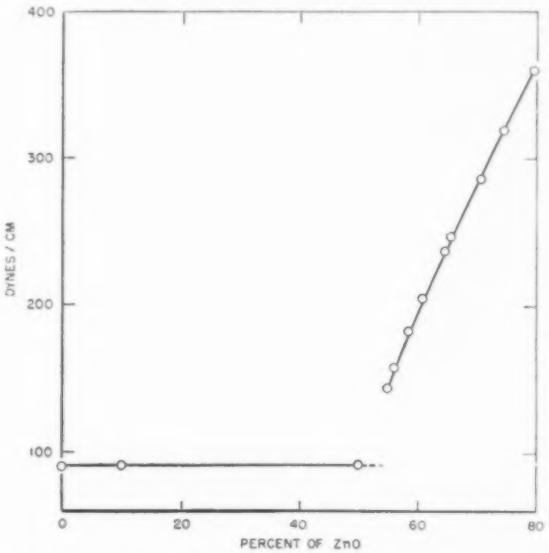

FIGURE 3. *Surface tension of melts in the system* ZnO-B_2O_3 *at 1,200° C as a function of the percentage of* ZnO.

tions had positive temperature coefficients of surface tension, and those containing 55 to 65 percent of ZnO showed minima in the curves of surface tension versus temperature. Two theories regarding the cause of positive temperature coefficients of surface tension were reviewed.

VI. References

[1] L. Shartsis, S. Spinner, and A. W. Smock, J. Research NBS **40,** 61 (1948) RP1855.

[2] W. A. Weyl, Glass Industry **25,** 264 (1948).

[3] R. P. Worley, J. Chem. Soc. **105,** 260 (1914).

[4] H. Freundlich, Colloid and Capillary Chemistry, p. 46 (E. P. Dutton & Co., Inc., New York, N. Y., 1922).

[5] E. Ingerson, G. W. Morey, and O. F. Tuttle, Am. J. Sci. **246,** 31 (1948).

[6] L. Shartsis and A. W. Smock, J. Research NBS **38,** 41 (1947) RP1771

Washington, May 2, 1949.

U. S. Department of Commerce
National Bureau of Standards

Research Paper RP2024
Volume 43, September 1949

Part of the Journal of Research of the National Bureau of Standards

A Comparison of Direct Colorimetry of Titanium Pigments With Their Indirect Colorimetry Based on Spectrophotometry and a Standard Observer

By Deane B. Judd

Recent work by Jacobsen in the colorimetry of titanium pigments has indicated that the ICI standard observer weights too lightly the spectral region below 430 millimicrons to accord with visual perception by average observers. This paper presents a repetition of this work for a single pair of titanium-pigment paints whose difference was measured by spectrophotometric means and then by seven observers by means of a visual colorimeter. Four of the seven observers corroborated Jacobsen's conclusion; three checked closely the standard observer. A modified standard observer based upon the spectral luminosity determinations of Gibson and Tyndall and Wald has been derived and is shown to account closely for the settings of the group of four observers that disagreed with the standard observer.

I. Introduction

It has recently been reported by Jacobsen [1][1] that the ICI standard observer [2] apparently does not weight the far blue region of the spectrum in accordance with visual perception. This report is based upon an attempt to apply the spectrophotometer to the colorimetry of certain of the well-known near-white anatase and rutile titanium dioxide pigments when incorporated in a paint vehicle. The ICI (x,y)-chromaticity coordinates of these two paints were found to be essentially identical, although the spectrophotometric curves show marked differences in the spectral region below 430 mμ, and the paints exhibited visual color differences. It is suggested by Jacobsen that the ICI standard observer weights too lightly the spectral region below 430 mμ.

This suggestion agrees with two previous reports. It was pointed out by Judd [3] that an empirical formulation for chromaticity sensibility (the uniform-chromaticity-scale triangle) broke down badly for two observers unless the standard luminosity function be replaced for these observers (Priest, Brickwedde) by the Gibson-Tyndall experimental mean [4] between 400 and 440 mμ. This experimental mean is higher than the ICI standard luminosity function by factors of 1.9 and 2.8 at 440 and 430 mμ, respectively, and the extrapolated values are increasingly higher toward 400 mμ at which wavelength the ratio is more than 10. It was reported later by Wald [5] that the reciprocals of the absolute foveal thresholds, although agreeing fairly well in other parts of the spectrum, depart widely in the short-wave end of the spectrum from the ICI luminosity function. He states, "At 436 mμ they reveal an average sensitivity of about 2.4 times, and at 405 mμ about 9 times as high as the ICI factors indicate."*

Table 1 gives the relative spectral luminosities read from the curve published by Wald and compares them with the Gibson-Tyndall experimental mean and with the standard luminosity function.

It may be seen from this table that the indirect evidence by Judd and the direct determinations by Wald (both referring to fields of 2° or less) combine to indicate that the Gibson-Tyndall experimental mean was given too little weight in adopting values for the standard luminosity function [6]. Thus these two reports are in qualitative agreement with Jacobsen's more recent suggestion.

[1] Figures in brackets indicate the literature references at the end of this paper.

*A recent paper by Weaver (J. Opt. Soc. Am. **39**, 278; 1949) likewise reports spectral luminosities considerably higher, between 400 and 450 mμ, than the standard luminosity function.

TABLE 1. *Relative spectral luminosity*

Wavelength	ICI	Wald	Gibson-Tyndall
mμ			
370		0.00005	
380	0.0000	.0004	
390	.0001	.0014	
400	.0004	.004	[a]0.005
410	.0012	.009	[a].012
420	.0040	.018	[a].022
430	.0116	.032	.033
440	.023	.045	.043
450	.038	.050	.051

[a] Extrapolated by Gibson and Tyndall.

It is the purpose of this paper to determine whether Jacobsen's conclusion is in quantitative, as well as qualitative, agreement with Wald's, and to report on the results of a repetition, by somewhat more refined methods, of Jacobsen's study of titanium-pigment paints.

II. Colorimetric and Spectrophotometric Study of Two Samples of Titanium-Pigment Paints

1. Preparation of Specimens

The samples of rutile and anatase forms of titanium dioxide pigment [2] were rubbed up with linseed oil in accord with standard procedures.[3] The resulting pastes were used to fill a cylindrical cavity, 1 mm deep, in aluminum holders, and were placed in optical contact with clear cover glasses cut from nearby parts of the same sheet.

2. Spectrophotometric Measurements

The spectral reflectances of these two specimens relative to freshly prepared magnesium oxide were measured between 400 and 750 mμ on an automatic recording spectrophotometer,[4] the specularly reflected energy from the cover glass being eliminated from measurement by insertion of a black velvet plug in the porthole of the sphere corresponding to the direction of mirror reflection. Corrections for zero, 100-percent, and wavelength-scale errors were applied [7]. Spectral directional (45°0°) reflectances relative to magnesium oxide were also measured for similar specimens prepared from the same pastes on the Beckman spectrophotometer [8] over the wavelength range 350 to 400 mμ.[5] These reflectances were multiplied by a constant (nearly equal to one) so that the product agreed with the spectral reflectances found on the recording spectrophotometer at 400 mμ, and the corresponding products were adopted for the spectral range 350 to 400 mμ. Table 2 and figure 1 give the results of these measurements.

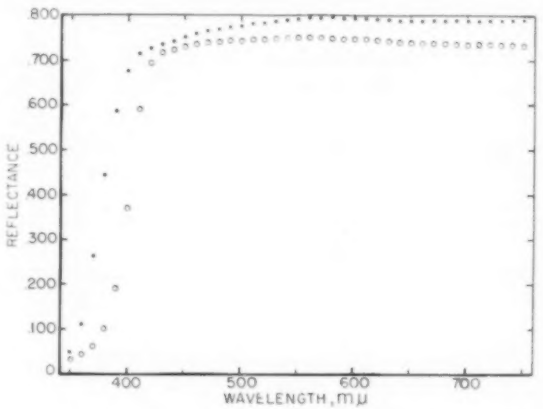

FIGURE 1. *Spectral reflectance of pastes made by rubbing up in linseed oil two forms of titanium dioxide pigment.*

●, Anatase+cover glass; ○, rutile+cover glass.
Both pastes were in contact with idential cover glasses during measurement. Note that the rutile form yields much lower spectral reflectance in the neighborhood of 400 mμ.

Figure 1 shows that our measurements duplicate the essential features of the spectrophotometric curves published by Jacobsen, but differ in two respects; first, the curve for rutile is everywhere lower than that for anatase, particularly in the long-wave end; second, both curves decline slightly toward the long-wave end. The first difference suggests that the standard procedure of rubbing up the pigment in linseed oil with a glass muller has darkened the rutile paste more than the procedures used by Jacobsen. The second difference is ascribable to the cover glasses. Because of multiple reflections between the pigment-oil paste and the under side of the front face of the cover glass, any slight absorption of energy by the cover glass increasing with wavelength may produce an appreciable effect.

[2] Supplied from the Research Laboratory, Titanium Division, National Lead Company, by Jacobsen.
[3] Under the direction of E. F. Hickson of this Bureau.
[4] Measurements made by H. J. Keegan of this Bureau.
[5] Measurements made by Marion A. Belknap of this Bureau.

TABLE 2. *Spectral directional reflectances of rutile and anatase titanium dioxide pigments in oil behind a cover glass.*

Wavelength	Spectral directional reflectance	
	Rutile	Anatase
mμ		
350	0.033	0.049
360	.045	.111
370	.063	.262
380	.101	.444
390	.191	.586
400	.371	.676
410	.591	.714
420	.694	.726
430	.717	.735
440	.724	.742
450	.730	.751
460	.736	.758
470	.739	.765
480	.741	.769
490	.743	.773
500	.744	.776
510	.745	.780
520	.746	.783
530	.748	.786
540	.749	.789
550	.750	.792
560	.751	.794
570	.750	.794
580	.748	.794
590	.747	.793
600	.746	.792
610	.746	.792
620	.744	.791
630	.742	.790
640	.740	.788
650	.739	.788
660	.738	.788
670	.738	.788
680	.737	.788
690	.737	.789
700	.735	.788
710	.736	.788
720	.735	.788
730	.734	.788
740	.734	.788
750	.734	.789

3. Colorimetric Measurements

The same specimens (pigment-oil behind cover glass) that were measured on the recording spectrophotometer were compared on a chromaticity-difference colorimeter [9] on the same and following day by seven observers. The luminator used consists of an incandescent-filament projection lamp combined with Corning daylite glass of such thickness as to produce closely a correlated color temperature of 6,800° K. The relative energy distribution of this source is given in the Report of the OSA Committee on Colorimetry [10]. The observing field has a double trapezoid pattern and subtends 13° vertically and 9° horizontally at the eye of the observer. The difference in the settings of the wedges of the colorimeter, corresponding for each observer to the chromaticity differences between the rutile and anatase specimen, were converted to differences in the chromaticity coordinates (x,y) of the ICI system by calibration graphs based on the luminator used (Macbeth 6,800° K). These (x,y)-differences (rutile minus anatase) have been applied to the (x,y)-chromaticity coordinates of the anatase computed in the usual way from the ICI standard observer, thus yielding experimental determinations for the chromaticity coordinates (x,y) of the rutile specimen. Figure 2 compares these results

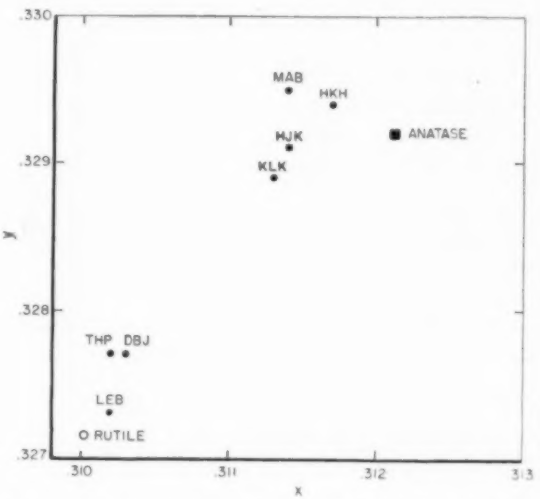

FIGURE 2. *Chromaticity of specimens of titanium pigment in oil under cover glass.*

Observer: ICI Standard; luminator: Macbeth 6,800° K; ○, ■, computed from spectral reflectance via 10_4 observer; ●, observed relative to anatase.

Note that three of the observers (THP, DBJ, LEB) find the chromaticity difference between the anatase and rutile forms to be closely in accord with that computed by means of the ICI standard observer; but the other four observers (MAB, HKH, HJK, KLK) do not.

with the chromaticity coordinates found for the rutile specimen from its spectral reflectance by the usual computation based on the ICI standard observer. On this extended scale the chromaticity of the luminator ($x=0.3082$, $y=0.3228$) would be

represented rather far off the graph, the specimens being yellowish whites.

It will be noted immediately from figure 2 that there is a considerable individual observer difference in this determination. The chief differences lie along the straight line passing through the short-wave portion of the spectrum. This difference is to be expected among observers having varying amounts of (yellowish) ocular pigmentation. It may be noted also that the observers divide into two groups. This division into two groups was unexpected, and may be statistically nonsignificant because of the small number of observers. One group of three observers, however, yields a fairly good check of the result computed by the ICI standard observer, the maximum discrepancy being a y-difference of 0.0005, only slightly higher than the estimated uncertainty (0.0003) of the determination of the difference on the chromaticity-difference colorimeter. The other group of four observers yields a very poor check, the maximum discrepancy being a y-difference of 0.0023, which is seven or eight times the uncertainty of the determination of the difference. It is assumed that the observers used to obtain Jacobsen's result of nonadaptability of the ICI standard observer would correspond to this group. The result of this check, therefore, is a qualified corroboration of Jacobsen's finding. Our average experimental result deviates from the result computed from the ICI observer by indicating a higher short-wave sensitivity than that of the ICI observer, and no one of our observers made a setting corresponding to a lower sensitivity. But some of our observers checked the result of the ICI standard observer to a degree that would be considered satisfactory even to the color graders of commercial materials.

III. Modification of the ICI Standard Observer

There remains yet to discover whether the experimental result of Wald based on 22 observers of the average age of 20, which agrees qualitatively with Jacobsen's finding, also agrees quantitatively. The qualitative check suggests that the standard luminosity function is nonrepresentative in the sense that it corresponds to an observer having too heavy an ocular pigmentation (yellowish) to correspond to the average. It is proposed, therefore, to derive the tristimulus values of the spectrum for an observer differing from the ICI standard by having such ocular pigmentation as would change his luminosity function from the standard so as to agree with the Wald-Gibson-Tyndall experimental average (see table 1). These distribution functions are then to be applied to the spectral reflectances of table 2, in place of the distribution functions of the standard observer, to see whether they will result in a check of the second group of observers in the same way as the standard observer has checked the first group.

If $\bar{y}'$ be the modified luminosity function, this check could be obtained by computing modified $\bar{x}$- and $\bar{z}$-functions defined as:

$$\bar{x}'=\bar{y}'\ (x/y),\ \text{and}\ \bar{z}'=\bar{y}'\ (z/y), \tag{1}$$

where $x\equiv\bar{x}/(\bar{x}+\bar{y}+\bar{z})$, $y\equiv\bar{y}/(\bar{x}+\bar{y}+\bar{z})$, and $z\equiv\bar{z}/(\bar{x}+\bar{y}+\bar{z})$.

The chromaticity diagram generated by this $(\bar{x}', \bar{y}', \bar{z}')$-system, however, would differ grossly from the (x,y)-chromaticity diagram, the equienergy point, for example, being displaced far from the center of the Maxwell triangle. This gross difference would make difficult the interpretation of any computed results. It has seemed worthwhile, therefore, to define the modified distribution functions $(\bar{x}_g, \bar{y}_g, \bar{z}_g)$ by a further linear, homogeneous transformation so as to make the functions and the chromaticity diagram as similar as possible to the ICI functions and diagram. Define, then:

$$\left.\begin{aligned}\bar{x}_g&=k_1\bar{x}'+k_2\bar{y}'+k_3\bar{z}'\\ \bar{y}_g&=k_4\bar{x}'+k_5\bar{y}'+k_6\bar{z}'\\ \bar{z}_g&=k_7\bar{x}'+k_8\bar{y}'+k_9\bar{z}'\end{aligned}\right\} \tag{2}$$

where k_1 to k_9 are constants independent of wavelength satisfying the following conditions:

(a) $\bar{y}_g$ shall be as closely like $\bar{y}$ as possible. There is no reason why $\bar{y}_g$ should depart from $\bar{y}$ at all except in the spectral range 460 mμ and below. Set, therefore, $k_4=k_6=0$ and $k_5=1$. This makes $\bar{y}_g=\bar{y}'$.

(b) $\bar{z}_g$ shall be as closely like $\bar{z}$ as possible. This condition is met by setting $k_7=k_8=0$, making $\bar{z}_g=k_9\bar{z}'$.

(c) $\bar{x}_g$ shall be as closely like $\bar{x}$ as possible. This condition is closely met by setting the chromaticity coordinate $x_g = \bar{x}_g/(\bar{x}_g + \bar{y}_g + \bar{z}_g) = 0.0070$ at 500 mμ, that is, by making the modified $\bar{x}$-function be nearly zero at 500 mμ like the original $\bar{x}$-function, but still large enough to prevent the modified x-function from being anywhere less than zero.

(d) The equienergy point on the modified system shall be at $x_g = y_g = z_g = 1/3$, like that of the modified system.

(e) The $\bar{x}_g$ and $\bar{y}_g$ functions shall have the same long-wave crossing point (about 578.1 mμ) as the $\bar{x}$ and $\bar{y}$ functions.

The constants, k_1 to k_9, meeting these requirements have been found by solution of simultaneous equations, and we may write the definitions of $\bar{x}_g$, $\bar{y}_g$ from eq1 and 2 as follows:

$$\left.\begin{aligned} \bar{x}_g &\equiv 0.9310\ \bar{y}'(x/y) + 0.0688\ \bar{y}' - 0.0866\ \bar{y}'(z/y) \\ \bar{y}_g &\equiv +1.0000\ \bar{y}' \\ \bar{z}_g &\equiv +0.5273\ \bar{y}'\ (z/y) \end{aligned}\right\}, \quad (3)$$

which is in terms simply of the revised luminosity function, $\bar{y}'$, and the chromaticity coordinates (x, y) of the ICI system.

Table 3 gives the tristimulus values of the spectrum $(\bar{x}_g, \bar{y}_g, \bar{z}_g)$ computed from eq 3 and also the chromaticity coordinates (x_g, y_g). It shows, of course, the revised values of the luminosity function $(\bar{y}_g)$ on which the other two distribution functions are based. Comparison with table 1 will show that the revised luminosity function agrees well both with the Gibson-Tyndall and with the Wald experimental mean for the spectral region of 450 mμ and below. For 470 mμ and above it is identical with the standard luminosity function. Figure 3 compares the modified distribution functions with the standard functions, and figure 4 compares the spectrum locus of the modified chromaticity diagram with that of the standard (x,y)-diagram. The equienergy points of the two diagrams are, of course, coincidental, and it may be seen that, as intended, $x_g = 0.007$ for 500 mμ, and the two loci also coincide at the long-wave crossing point of x and y. Elsewhere there is considerable change in the spacing of the spectrum chromaticities, and Macbeth 6,800° K has been shifted from $x = 0.3082$, $y = 0.3228$ to $x_g = 0.3113$, $y_g = 0.3276$. These changes are caused by the temporary adoption of the revised luminosity function. Figure 3 shows that the comparatively minor change in this function (difference between $\bar{y}_g$ and $\bar{y}$) has generated a considerably larger change in the x-function and a rather drastic change in the z-function, making it, of course, considerably higher in the spectral region 430 mμ and below as suggested by Jacobsen.

TABLE 3. *Tristimulus values and chromaticity coordinates of the spectrum in the modified ICI system*

Wavelength	Tristimulus values			Chromaticity coordinates		
	$\bar{x}_g$	$\bar{y}_g$	$\bar{z}_g$	x_g	y_g	z_g
mμ						
360	0.0001	0.000005	0.0004	.....	.....	.....
370	.0009	.00005	.0042	.....	.....	.....
380	.0072	.0004	.0346	.....	.....	.....
390	.0261	.0014	.1237	.....	.....	.....
400	.0754	.0040	.3611	0.171	0.009	0.820
410	.1870	.0100	.9036	.170	.009	.821
420	.3474	.0200	1.7028	.168	.010	.822
430	.4903	.0320	2.0154	.164	.013	.823
440	.3250	.0430	1.7154	.156	.021	.823
450	.2175	.0510	1.2545	.143	.034	.824
460	.1478	.0680	0.9975	.122	.056	.822
470	.0766	.0910	.6789	.090	.108	.802
480	.0282	.1390	.4287	.047	.233	.719
490	.0038	.2080	.2453	.008	.455	.537
500	.0032	.3230	.1434	.007	.688	.305
510	.0296	.5030	.0834	.048	.817	.135
520	.1009	.7100	.0412	.118	.833	.048
530	.2097	.8620	.0223	.192	.788	.020
540	.3342	.9540	.0107	.257	.734	.008
550	.4711	.9950	.0046	.320	.676	.003
560	.6216	.9950	.0021	.384	.615	.001
570	.7748	.9520	.0011	.448	.551	.001
580	.9128	.8700	.0009	.512	.488	.000
590	1.0075	.7570	.0006	.571	.429	.000
600	1.0322	.6310	.....	.621	.379	.000
610	0.9681	.5030	.....	.658	.342	.000
620	.8217	.3810	.....	.683	.317	.000
630	.6163	.2650	.....	.699	.301	.000
640	.4290	.1750	.....	.710	.290	.000
650	.2713	.1070	.....	.717	.283	.000
660	.1577	.0610	.....	.....	.....	.....
670	.0836	.0320	.....	.....	.....	.....
680	.0448	.0170	.....	.....	.....	.....
690	.0217	.0082	.....	.....	.....	.....
700	.0109	.0041	.....	.....	.....	.....
710	.0055	.0021	.....	.....	.....	.....
720	.0028	.00105	.....	.....	.....	.....
730	.0013	.00052	.....	.....	.....	.....
740	.0007	.00025	.....	.....	.....	.....
750	.0003	.00012	.....	.....	.....	.....
760	.0002	.00006	.....	.....	.....	.....
770	.0001	.00003	.....	.....	.....	.....

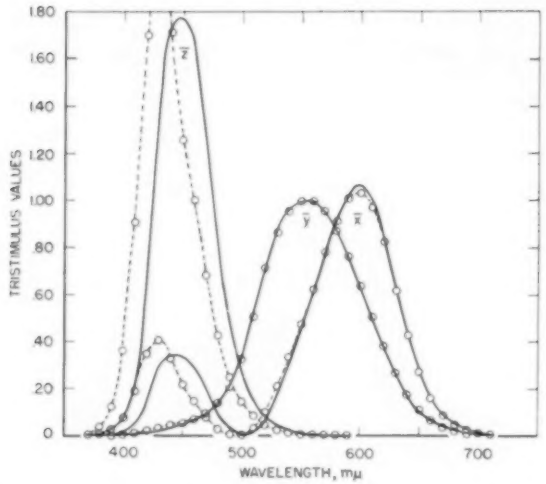

FIGURE 3. *Comparison of the tristimulus values of the spectrum according to the ICI standard observer (solid lines) with those (dotted lines) according to an observer modified to agree with the Wald-Gibson-Tyndall data on spectral luminosity below 470 mμ.*

Note that the small changes introduced into the spectral luminosity ($\bar{y}$) function near the short-wave extreme require changes to be made in the other ($\bar{x}$ and $\bar{z}$) functions that are relatively large; for example, the peak of the $\bar{z}$-function is shifted by about 15 mμ in the short-wave direction.

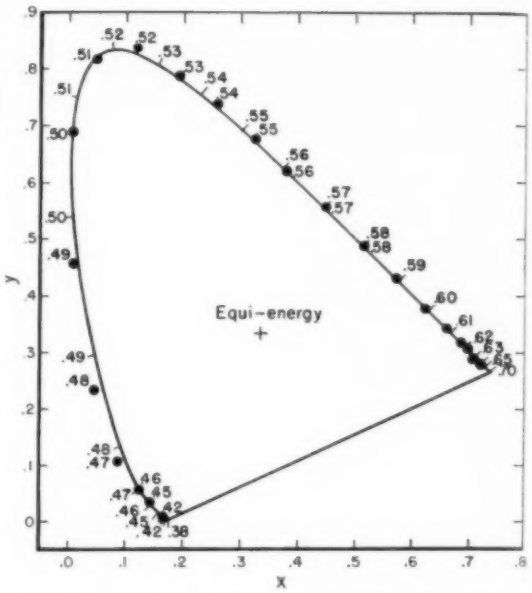

FIGURE 4. *Comparison of the spectrum locus on the (x, y)-chromaticity plot of the ICI system with that (dots) on the corresponding plot of the modified ICI system.*

The equienergy point is set at $x=y=1/3$ in both systems. Note that the chromaticity region near the short-wave extreme of the spectrum has been expanded relative to other regions in the modified system.

IV. Check of Modified Distribution Functions Against Experimental Results on Anatase and Rutile

The first check of the modified distribution functions is to apply them in the same way as the standard distribution functions were applied to obtain the comparison given in figure 2. The wedges of the chromaticity-difference colorimeter were recalibrated by means of the modified functions, the experimental results recomputed on that basis, and the chromaticity coordinates of the specimens (pigment in oil plus cover glass) recomputed in the ($\bar{x}_g$, $\bar{y}_g$, $\bar{z}_g$) system. Figure 5 compares the computed chromaticity of the rutile specimen with experimental determinations of chromaticity of the rutile specimen found relative to the anatase specimen as standard. Table 4 gives the chromaticity coordinates from which figures 2 and 5 have been plotted. It will be seen that the modified distribution functions do indeed check the results by the second group of observers (KLK, HJK, MAB and HKH) much as the standard ICI observer checks the results by the first group of observers (LEB, DBJ, THP).

The second check of the modified distribution functions against the experimental results on anatase and rutile was carried out in such a way as to avoid even the presumably negligible uncertainties of applying the calibration of the wedges of the chromaticity-difference colorimeter. It is based simply on the average experimental result. This result may be summarized by saying that, if the rutile specimen be viewed through thicknesses of the yellow and green wedges corresponding to 90 and 36 wedge units, respectively, then the average of the seven observers will find that it has the same chromaticity as the anatase specimen viewed through thicknesses corresponding to 82 yellow- and 43 green-wedge units. The spectral transmittances of the pairs of wedges of these thicknesses have been computed from the known spectral transmittances of the yellow wedge at a thickness corresponding to 164 units and those of the green wedge at a thickness corresponding to 98 units [9]. These spectral transmittances have been multiplied by the spectral reflectances of the

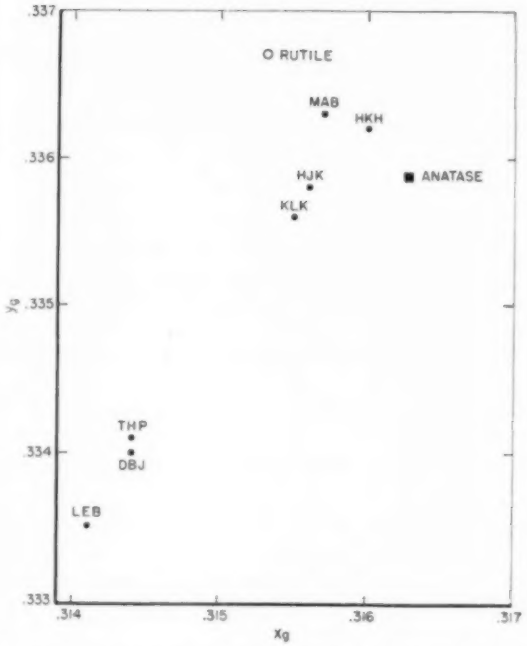

FIGURE 5. *Chromaticity of specimens of titanium pigments in oil under cover glass.*

Observer: modified ICI standard; luminator: Macbeth 6,800° K; ○ ■, computed from spectral reflectance via modified ICI observer; ●, observed relative to anatase.

Note that the spectrophotometric result by the modified observer agrees well with visual observations by the second group of observers (MAB, HKH, HJK, KLK) much in the same way as the ICI observer agreed with the first group (THP, DBJ, LEB).

titanium pigment specimens (see table 2) and by the relative spectral distribution of the luminator (Macbeth, 6,800° K) that was used. These triple products give the spectral distributions of radiant flux that the seven observers on the average found to have identical chromaticities. These two spectral distributions of radiant flux, if adjusted by a constant factor to correspond to the same luminance, form for the average of these seven observers, therefore, what is known as a metameric pair. They are shown in figure 6 together with the spectral distribution of the luminator used (Macbeth 6,800° K).

If a standard observer truly represented the average of the seven observers used in this study, use of that standard observer to compute chromaticity coordinates for these two spectral distributions should yield identical results. Both the standard observer and the modified standard observer have been subjected to this test. Figure

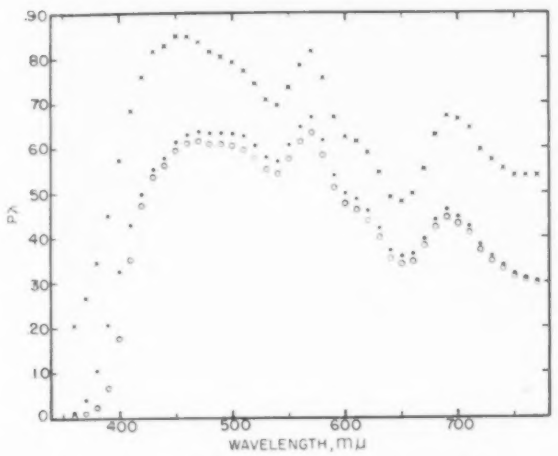

FIGURE 6. *Spectral distributions of radiant flux.*

x, Macbeth daylight, color temperature 6,800° K used as source; ●, reflected from anatase plus cover glass, transmitted by thicknesses of yellowish and greenish glass, 90Y plus 36G; ○, reflected from rutile plus cover glass, transmitted by thicknesses of yellowish and greenish glass, 82Y plus 43G. The latter two distributions correspond to the same chromaticity according to the average of our seven observers.

TABLE 4. *Chromaticity coordinates for titanium pigments in oil behind a cover glass*

Method of evaluation	Form of titanium pigment	Chromaticity difference		Chromaticity coordinates	
		Δx	Δy	x	y
Spectrophotometric.	Rutile	0.0021	0.0020	0.3100	0.3272
	Anatase			.3121	.3292
Colorimetric:					
LEB	Rutile	.0019	.0019	.3102	.3272
DBJ	do	.0018	.0015	.3103	.3277
THP	do	.0019	.0015	.3102	.3277
KLK	do	.0008	.0003	.3113	.3289
HJK	do	.0007	.0001	.3114	.3291
MAB	do	.0007	−.0003	.3114	.3295
HKH	do	.0004	−.0002	.3117	.3294
		Δx_ϕ	Δy_ϕ	x_ϕ	y_ϕ
Spectrophotometric.	Rutile	0.0010	−0.0008	0.3153	0.3367
	Anatase			.3163	.3359
Colorimetric:					
LEB	Rutile	.0022	.0024	.3141	.3335
DBJ	do	.0019	.0019	.3144	.3340
THP	do	.0019	.0018	.3144	.3341
KLK	do	.0008	.0003	.3155	.3356
HJK	do	.0007	.0001	.3156	.3358
MAB	do	.0006	−.0004	.3157	.3363
HKH	do	.0003	−.0003	.3160	.3362

7 shows the result. It will be seen that both fail to meet this test by an x-difference of about 0.001. It will be seen that, relative to our seven observers, the standard observer underweights the short-wave extreme of the spectrum, and the modified standard observer overweights it by about the same amount. It is evident that a modification based on an average between the standard luminosity function and the Gibson-Tyndall-Wald experimental mean would successfully meet this test within experimental uncertainty (an x- or y-difference of 0.0003).

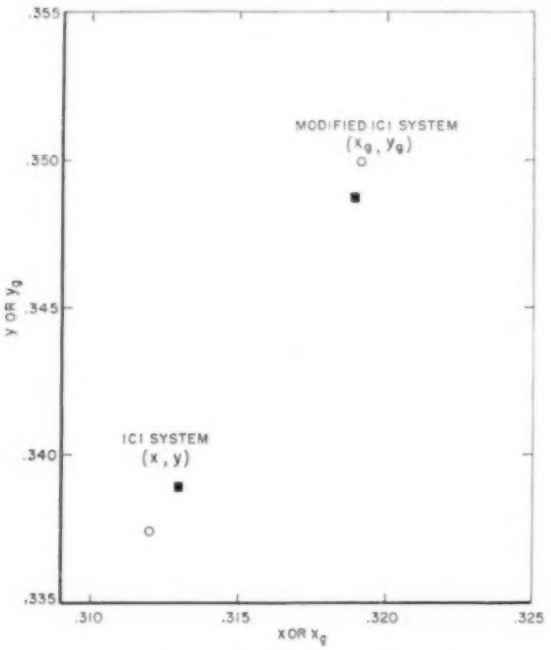

FIGURE 7. *Comparison of the chromaticities computed from the spectral distributions of radiant flux shown in figure 6.*

Luminator: Macbeth 6,800° K; ■, anatase (82Y, 43G); ○, rutile (90Y, 36G).

The rather small size of this average discrepancy (0.001) between observed and computed chromaticity coordinates serves to emphasize the concern of the pigment industry with small color differences. This discrepancy is scarcely more than twice the least chromaticity difference that is perceptible with certainty, yet, since all observers deviate from the standard observer in the same direction, it is likely that industrial laboratories having to interpret spectrophotometric measurements of titanium pigments will set the standard observer aside and substitute some other more or less arbitrary functions for this purpose unless steps are taken to make a suitable revision of the standard observer.

Note that the ICI (x, y)-diagram fails to indicate the same chromaticities for these two distributions, and that the modified (x_g, y_g)-diagram likewise fails, but in the opposite sense by about the same amount. This shows that an average of the ICI standard observer with the modified observer would closely account for the average result obtained by the seven observers on the chromaticity-difference colorimeter.

V. Summary and Conclusions

1. Jacobsen's study of the adaptability of the ICI standard observer to the indirect colorimetry of titanium dioxide pigments in linseed oil has been repeated for a single pair of specimens, one rutile, the other anatase.

2. The result of this repetition is a qualified corroboration of Jacobsen's conclusion that the ICI standard observer weights the short-wave extreme of the spectrum too lightly. Not all of our observers made settings significantly contrary to the standard observer, however. Three out of the seven obtained results in reasonable agreement with the ICI standard.

3. A modified standard observer based upon the spectral luminosity determinations of Gibson and Tyndall and of Wald has been derived. This modification is shown to account for the settings of the second group (four out of seven) much as the ICI standard accounts for those of the first group. It is presumed that the settings of Jacobsen's observers would likewise be accounted for by the modified standard observer.

4. It is suspected that if the ICI standard observer is to be maintained in its present status of general acceptability for commercial colorimetry, it may have to be modified so as to weight more heavily the short-wave extreme of the spectrum.

5. Further data relating to the luminosity of the spectrum in the wavelength region below 430mμ should be gathered to form an adequate basis for this modification.

VI. References

[1] A. E. Jacobsen, Non-adaptability of the ICI system to some near-whites which show absorption in the far-blue region of the spectrum, J. Opt. Soc. Am. **38,** 442 (1948).

[2] Proceedings of the 8th Session, Commission Internationale de l'Éclairage, Cambridge, England, pp. 19 to 29 (1931).

[3] D. B. Judd, A Maxwell triangle yielding uniform chromaticity scales, J. Research NBS **14,** 41 (1935) RP756; J. Opt. Soc. Am. **25,** 31 (1935).

[4] K. S. Gibson and E. P. T. Tyndall, Visibility of radiant energy, BS Sci. Pap. **19,** 131 (1923) S 475.

[5] G. Wald, Human vision and the spectrum, Science, **101,** 653 (1945).

[6] Proceedings of the 6th Session, Commission Internationale de l'Éclairage, Geneva, (1924).

[7] K. S. Gibson and H. J. Keegan, Calibration and operation of the General Electric recording spectrophotometer of the National Bureau of Standards, J. Opt. Soc. Am. **28,** 372 (1928).

[8] K. S. Gibson and M. M. Balcom, Transmission measurements with the Beckman quartz spectrophotometer, J. Research NBS **38,** 601 (1947) RP 1798.

[9] D. B. Judd, Specification of uniform color tolerances for textiles, Textile Research **9,** 253 (1939).

[10] Committee on Colorimetry, Quantitative data and methods for colorimetry, J. Opt. Soc. Am. **34,** 639 (1944); table IV.

WASHINGTON, April 28, 1949.

U. S. Department of Commerce
National Bureau of Standards

Research Paper RP2025
Volume 43, September 1949

Part of the Journal of Research of the National Bureau of Standards

Properties of Calcium-Barium Titanate Dielectrics

By Elmer N. Bunting, George R. Shelton, and Ansel S. Creamer

Dielectrics having compositions in the system $3CaO:TiO_2$-$BaTiO_3$-TiO_2 were matured at 1,260° to 1,500° C. Data are given for the compositions, heat-treatments, absorption, shrinkage, and for K, the dielectric constant, and Q, the reciprocal of the power factor, at 25° C for frequencies of 50, 1,000 and 20,000 kilocycles per second and for 3,000 megacycles per second when K is not greater than 50. Values of K were also determined at 1 megacycle per second for various temperatures from −60° to +85° C. Lowest values of Q (and highest of K) were associated with specimens of high baria content. Linear thermal expansion (25° to 700° C) ranged from 0.65 to 0.87 percent. The specimens of some compositions were unstable and changed in K and Q values with time.

I. Introduction

This paper is the third of a series dealing with ceramic dielectrics composed of titanium dioxide and the oxides of the alkaline earth elements. A study of these titanate systems previously reported [1, 2] [1] revealed dielectrics of diverse properties that find application in the fields of electronic instrumentation, particularly where the space factor is important, as in hearing aids and other special circuits. These dielectrics are also valuable for the production of capacitors for use at temperatures above 150° C, where paper and electrolytic capacitors do not function satisfactorily.

A rather limited amount of information has been published by others [3, 4] on the electrical properties of the calcium-barium titanates. However, it is desirable to investigate these materials for a wide range in composition so that a more complete knowledge of their properties will be available. Because the temperature coefficient of the dielectric constant for calcium titanate was known to be negative, it was expected that many of the calcium-barium titanate dielectrics might have a negative coefficient. Also, the low electrical-loss character of calcium titanate indicated that a large portion of the field in this system would probably behave similarly.

[1] Figures in brackets indicate the literature references at the end of this paper.

II. Preparation of Dielectrics and Methods of Test

Dielectrics having the compositions shown in figure 1 were prepared from reagent quality carbonates of calcium and barium and the commercial grade of titania (grade TMO) used in the preparation of the other alkaline earth titanate dielectrics [1, 2]. A chemically pure grade of titania (99.9%) was used in the preparation of a few specimens for comparison purposes. The methods of preparing these dielectrics and of determining

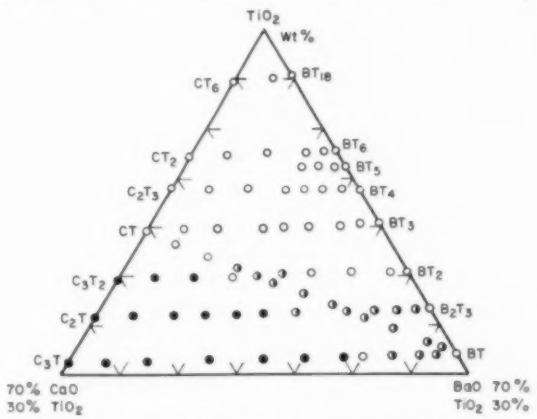

FIGURE 1. *Ternary diagram for system* CaO-BaO-TiO_2 *showing compositions studied.*

B = BaO; C = CaO; T = TiO_2; thus, $B_2T_3 = 2BaO:3TiO_2$. ●, Decrease in K and Q with time; ◑, decrease in K and increase in Q with time; ○, stable.

their properties have been previously described [1, 2].

III. Results and Discussion

In table 1, data are given for the composition, heat-treatment, absorption, shrinkage, dielectric constant K, and reciprocal of the power factor, Q, of the matured specimens. The data for a given composition are considered to be the most representative among those obtained from measurements of 3 to 11 test specimens.

TABLE 1. *Composition, heat treatment, absorption, shrinkage, dielectric constant K, and Q of bodies in the system* $3CaO:TiO_2$-$BaTiO_3$-TiO_2

Specimen designation	Proportion of end members of join, weight percent		Composition weight			Heat treatment				Absorption	Shrinkage	Dielectric constant K at 25° C and—				Reciprocal, Q, of power factor at 25° C and—			
						No. 1		No. 2											
			BaO	CaO	TiO_2	Temperature	Time	Temperature	Time			50 kc/s	1,000 kc/s	20 mc/s	3,000 mc/s	50 kc/s	1,000 kc/s	20 mc/s	3,000 mc/s
	$CaO·6TiO_2$-$BaO·18TiO_2$																		
			%	%	%	°C	hr	°C	hr	%	%								
CT6	100			10.5	89.5	1,100	1	1,275	1	0.00	16.5	117	117	117	.....	1,700	1,900	2,400	.....
18BC6	33	67	6.5	3.5	90	1,100	1	1,275	1	.00	15.4	86	86	86	.....	600	1,000	1,800	.....
BT18	.....	100	9.6	.....	90.4	1,100	1	1,275	1	.00	15.0	75	74	74	.....	200	1,000	7,000	.....
	$CaO·2TiO_2$-$BaO·6TiO_2$																		
CT2	100		.....	26.0	74.0	1,100	1	1,310	1	.00	18.0	142	141	141	.....	1,900	1,200	1,800	.....
6BC2	73	27	6.5	19.0	74.5	1,100	1	1,300	1	.01	15.6	107	107	107	.....	700	500	1,000	.....
6BC5	43	57	13.0	12.0	75.0	1,100	1	1,310	1	.00	17.1	84	83	83	.....	3,000	1,400	2,700	.....
6BC8	20	80	19.5	5.5	75.0	1,100	1	1,275	1	.00	16.4	60	60	60	.....	3,000	4,000	10,000	.....
6BC9	5	95	23.0	1.5	75.5	1,100	1	1,275	1	.00	15.9	49	49	49	48	2,000	10,000	10,000	960
BT6	.....	100	24.3	.....	75.7	1,100	1	1,275	1	.00	13.7	46	45	44	39	85	400	2,200	490
	$2CaO·3TiO_2$-$BaO·4TiO_2$																		
C2T3	100		.....	31.9	68.1	1,100	1	1,310	1	.00	17.9	151	151	151	.....	2,000	1,000	1,600	.....
BC22	80	20	6.5	25.5	68.0	1,100	1	1,300	1	.06	15.8	115	114	114	.....	700	300	700	.....
BC24	60	40	13.0	19.1	67.9	1,100	1	1,295	1	.01	18.3	88	87	87	.....	1,000	1,000	1,500	.....
BC26	40	60	19.5	12.7	67.8	1,100	1	1,290	1	.00	16.8	68	68	68	.....	2,000	1,600	4,000	.....
BC27	30	70	22.7	9.6	67.7	1,100	1	1,290	1	.00	17.2	60	60	60	.....	2,700	1,800	10,000	.....
BC28	20	80	25.9	6.4	67.7	1,100	1	1,290	1	.00	17.2	51	51	50	47	2,600	4,000	10,000	940
BC29	10	90	29.2	3.2	67.6	1,100	1	1,290	1	.00	16.9	44	44	43	42	2,700	1,900	5,000	2,100
BT4	.....	100	32.4	.....	67.6	1,100	1	1,330	1	.00	15.1	34	34	35	34	1,600	2,000	3,700	2,600
	$CaO·1.8TiO_2$-$BaO·5TiO_2$																		
5BC8	18	82	22.7	5.0	72.3	1,100	1	1,285	1	.00	17.0	56	56	56	.....	560	600	1,000	.....
5BC9	9	91	25.2	2.5	72.3	1,100	1	1,285	1	.00	16.0	49	49	49	.....	700	550	850	.....
5BC95	5	95	26.5	1.2	72.3	1,100	1	1,285	1	.00	15.1	45	45	45	.....	750	770	1,000	.....
BT5	.....	100	27.7	.....	72.3	1,100	1	1,325	1	.04	12.0	39	37	37	.....	1,500	2,300	1,300	.....
	$CaO·TiO_2$-$BaO·3TiO_2$																		
CT	100		.....	41.2	58.8	1,100	1	1,400	1	0.01	16.7	143	143	143	.....	2,000	3,500	800	.....
BC2	83	17	6.5	34.4	59.1	1,000	1	1,320	5	*2.65	18.3	115	112	109	.....	20	59	225	.....
BC3	70	30	11.7	28.9	59.4	1,000	1	1,320	5	*1.62	19.4	112	110	107	.....	25	98	570	.....
BC5	50	50	19.5	20.6	59.9	1,000	1	1,275	2	0.00	19.0	94	94	94	.....	1,300	1,200	1,100	.....
BC6	40	60	23.4	16.5	60.1	1,100	1	1,290	1	.04	16.6	82	82	81	.....	600	1,400	2,800	.....
BC7	30	70	27.3	12.4	60.3	1,100	1	1,290	1	.00	17.0	72	72	71	.....	1,600	2,400	4,000	.....
BC8	17	83	32.4	7.0	60.6	1,100	1	1,290	1	.00	17.0	57	57	56	.....	3,800	3,400	10,000	.....
BC9	10	90	35.1	4.1	60.8	1,100	1	1,290	1	.00	17.7	52	52	51	50	2,400	3,600	10,000	1,200
BT3	.....	100	39.0	.....	61.0	1,100	1	1,290	1	.03	17.4	44	44	43	42	650	720	800	440

TABLE 1. *Composition, heat treatment, absorption, shrinkage, dielectric constant K, and Q of bodies in the system* $3CaO:TiO_2$-$BaTiO_3$-TiO_2—Continued

Specimen designation	Proportion of end members of join, weight percent		Composition weight			Heat treatment				Absorption	Shrinkage	Dielectric constant K at 25° C and—				Reciprocal, Q, of power factor at 25° C and—			
						No. 1		No. 2				50 kc/s	1,000 kc/s	20 mc/s	3,000 mc/s	50 kc/s	1,000 kc/s	20 mc/s	3,000 mc/s
	$CaTiO_3$-$BaTiO_3$		BaO	CaO	TiO_2	Temperature	Time	Temperature	Time										
			%	%	%	°C	hr	°C	hr	%	%								
CT	100			41.2	58.8	1,100	1	1,400	1	.01	16.7	143	143	143		2,000	3,500	800	
CB1	90	10	6.6	37.1	56.3	1,100	3	1,430	1	.01	16.3	155	155	155		6,400	3,800	1,900	
CB2	80	20	13.1	33.0	53.9	1,100	3	1,430	1	.01	15.7	185	185	185		2,300	2,100	1,200	
CB3 [b]	70	30	19.7	28.9	51.4	1,100	3	1,430	1	.00	14.3	220	220	220		1,000	680	470	
CB35 [b]	65	35	23.2	26.8	50.0	1,245	1	1,400	1	.05	13.1	240	240	240		1,000	700	520	
CB4 [b]	60	40	26.3	24.7	49.0	1,100	3	1,430	1	.01	14.3	265	265	265		780	480	280	
CB5 [b]	50	50	32.8	20.6	46.5	1,100	3	1,430	1	.03	13.8	315	315	315		600	390	190	
CB6 [b]	40	60	39.4	16.5	44.1	1,100	3	1,430	1	.03	13.7	380	380	380		440	310	175	
CB64 [b]	36	64	42.0	15.0	43.0	1,100	3	1,430	1	.00	13.4	400	400	400		460	270	130	
CB7 [b]	30	70	46.0	12.4	41.6	1,100	3	1,430	1	.00	15.6	440	440	430		400	290	120	
CB8 [b]	20	80	52.5	8.3	39.2	1,100	3	1,430	1	.00	14.6	540	540	530		570	325	175	
CB9 [b]	10	90	59.1	4.1	36.8	1,100	3	1,430	1	.00	14.6	600	600	580		240	160	95	
CB95 [b]	5	95	62.4	2.1	35.5	1,100	3	1,430	1	.02	14.3	840	840	830		130	120	80	
BT		100	65.7		34.3	1,245	1	1,385	2	.05	10.6	1,400	1,400	1,400		100	130	70	
	$3CaO:2TiO_2$-$BaO:2TiO_2$																		
C3T2	100			51.3	48.7	1,245	1	1,500	1	.02	15.1	55	55	55		2,000	10,000	2,400	
BC321	87	13	6.5	44.5	49.0	1,100	1	1,470	1	.00	14.1	67	67	67		2,000	3,000	2,000	
BC323	74	26	13.0	37.5	49.5	1,245	1	1,500	1	.01	16.9	83	83	83		1,500	1,600	1,900	
BC324	60	40	19.5	31.0	49.5	1,245	1	1,500	1	.01	17.0	150	150	150		1,600	1,600	1,700	
BC325	53	47	23.2	26.8	50.0	1,100	1	1,420	1	.01	15.0	235	233	231		500	350	200	
BC326	43	57	28.0	22.0	50.0	1,000	1	1,275	5	* .48	18.6	265	260	258		61	65	60	
BC327	33	67	32.8	17.2	50.0	1,000	1	1,275	2	* .48	19.1	270	265	265		60	65	45	
BC328	20	80	39.4	10.0	50.6	1,100	1	1,265	1	.04	17.3	215	210	209		80	65	43	
BC329	6	94	46.0	3.0	51.0	1,100	1	1,265	1	.00	15.5	185	180	175		60	50	38	
BT2		100	49.0		51.0	1,100	1	1,280	1	.02	16.4	204	200	197		100	70	35	
	$2CaO:TiO_2$-$2BaO:3TiO_2$																		
C2T	100			58.4	41.6	1,100	1	1,500	*1	.01	18.3	40	40	40	40	2,700	5,000	1,700	360
B2C21	89	11	6.2	52.0	41.8	1,100	1	1,500	1	.00	19.8	46	46	46	44	1,400	2,700	1,200	470
B2C22	76	24	13.2	44.6	42.1	1,100	1	1,500	1	.06	18.0	46	46	46	45	1,800	3,300	1,200	520
B2C23	68	32	18.1	39.5	42.3	1,100	1	1,450	1	.00	16.0	49	49	49		1,400	2,100	2,000	
B2C24	58	42	23.7	33.7	42.6	1,100	1	1,300	1	.00	14.5	56	56	56		900	1,400	1,800	
B2C25	50	50	28.1	29.2	42.7	1,100	1	1,430	1	.00	15.4	73	73	73		700	2,000	2,000	
B2C26 [b]	40	60	33.7	23.3	43.0	1,100	1	1,500	1	.01	14.5	210	210	210		1,000	1,000	1,000	
B2C28 [b]	17	83	46.6	9.9	43.5	1,100	1	1,280	3	* .23	14.6	480	480	470		67	55	35	
B2C29 [b]	10	90	50.5	5.8	43.7	1,100	1	1,265	1	.00	14.6	520	515	500		50	33	25	
B2C295 [b]	5	95	53.3	2.9	43.8	1,100	1	1,265	1	.00	15.5	580	570	550		40	27	20	
B2T3		100	56.1		43.9	1,250	1	1,300	1	.01	10.8	910	900	890		70	50	25	
	$3CaO:TiO_2$-$BaTiO_3$																		
C3T	100			67.8	32.2	1,100	1	1,500	1	.01	22.0	34	34	34	33	2,000	5,000	3,000	300
BC31	90	10	6.6	61.0	32.4	1,100	1	1,500	1	.00	24.0	40	40	40	38	1,200	2,600	2,400	580
BC32	80	20	13.1	54.2	32.6	1,100	1	1,500	1	.00	22.8	39	39	39	38	2,000	3,000	3,000	680
BC33	64	36	23.6	43.4	33.0	1,100	1	1,500	1	.00	18.8	37	37	37	37	1,400	4,000	6,000	430
BC35	50	50	32.9	33.9	33.2	1,100	1	1,500	1	.00	17.5	36	36	36		1,400	4,000	6,000	
BC36	40	60	39.4	27.1	33.5	1,100	1	1,450	1	.00	16.7	37	37	37	36	2,000	4,000	9,000	350
BC37	29	71	46.6	19.7	33.7	1,100	1	1,470	1	.00	15.8	37	37	36	38	1,400	2,000	5,000	370
BC375	25	75	49.5	16.7	33.8	1,100	1	1,500	1	.00	15.9	60	60	60		1,300	5,000	5,000	
BC38	16	84	55.0	11.0	34.0	1,245	1	1,430	1	.00	14.6	640	630	620		300	300	200	
BC39 [b]	10	90	59.1	6.8	34.1	1,245	1	1,410	1	.00	13.6	1,640	1,630	1,620		170	190	110	
BC395 [b]	5	95	62.4	3.4	34.2	1,100	1	1,410	1	.01	14.0	2,680	2,670	2,640		140	120	55	
BT		100	65.7		34.3	1,245	1	1,385	2	.05	10.6	1,400	1,400	1,400		100	130	70	

* Not matured.

[b] K and Q values obtained after 6 months.

[c] Three heats at 1,500° C for 1 hr.

The relation between the maturing temperature and the composition of the specimens is shown in figure 2. No attempt was made to determine in all cases the range of temperatures within which mature specimens could be produced, but it was noted that, in general, this range was about 10° C. When the compositions were in the region of $CaO:2TiO_2$[2], containing a few percent of BaO, the maturing range was less than 10° C. This region may be near a ternary eutectic. In another area two mixtures, designated BC2 and BC3, and three other mixtures (BC326, BC327, and B2C28) did not yield mature specimens, despite many attempts with systematic variations in the duration and temperature of heat treatments. The lowest absorption obtained for these specimens was between 0.5 and 1.6 percent.

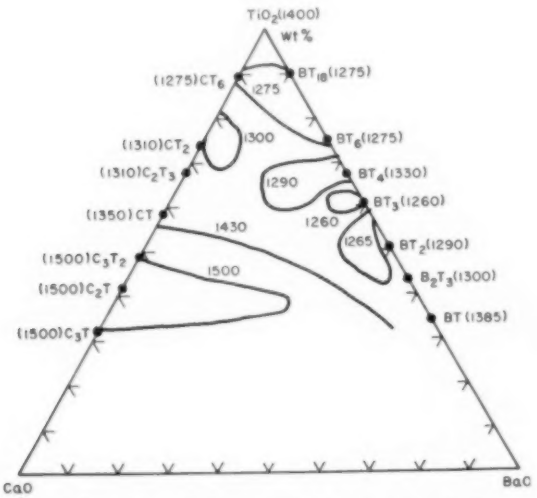

FIGURE 2. *Approximate maturing temperature (° C) after calcining treatment.*

B = BaO; C = CaO; T = TiO_2.

Small amounts of impurities have a pronounced effect on the maturing temperature of some preparations, particularly those representing a definite compound. If calcium titanate is prepared with titania containing 1.3 percent of impurities, the range in maturing temperature extends from 1,350° to 1,400° C. However, when less than a tenth of 1 percent of impurities is present, a maturing temperature of about 1,500° C is required.

[2] A colon indicates that the composition may or may not be a compound. A known compound is represented by a single dot separating the oxide formulae, or by a single formula, as $CaTiO_3$.

At 25° C the variations in K and Q, with composition, measured at 1 mc/s, are shown in figures 3 and 4, respectively. The ternary parts of these diagrams exhibit isodielectric-constant lines plotted from the data on K and Q given in table 1. Underneath and to the right side of the ternary diagram, the values of K (or Q) are plotted for the binary systems of CaO-TiO_2 and BaO-TiO_2. Systematically varying the compositions of the specimens affected the values of K and Q, as given in table 1.

In the CaO-TiO_2 system, the substitution of CaO for TiO_2, up to about 41 percent of CaO, raised the K value from near 100 for TiO_2 to about

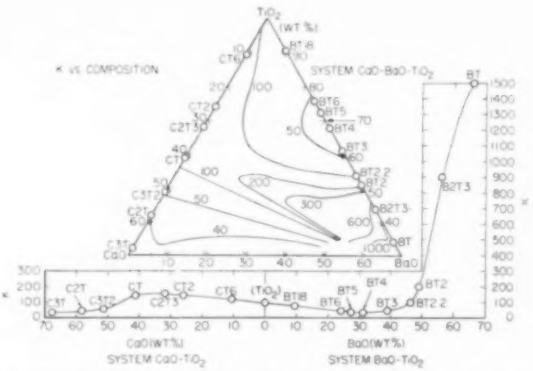

FIGURE 3. *Dielectric constant, at 25° C and 1 mc/s, with varying composition within the ternary system,* $3CaO:TiO_2$-$BaTiO_3$-TiO_2, *and the binary systems,* CaO-TiO_2 and BaO-TiO_2.

B = BaO; C = CaO; T = TiO_2.

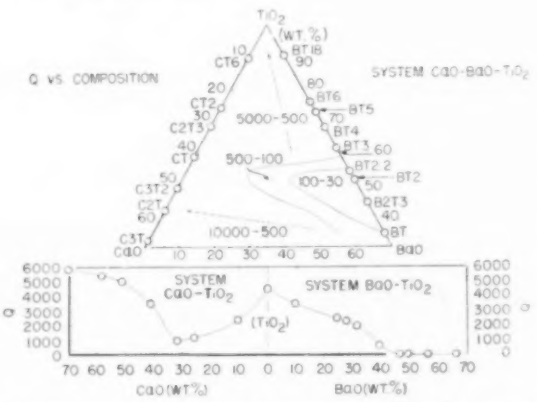

FIGURE 4. *Q values, at 25° C and 1 mc/s, with varying composition within the ternary system,* $3CaO:TiO_2$-$BaTiO_3$-TiO_2, *and the binary systems,* CaO-TiO_2 and BaO-TiO_2.

B = BaO; C = CaO; T = TiO_2.

140 for $CaTiO_3$ (fig. 3). Higher values, up to 168, have been reported by others [4]. The different values obtained were probably due to variations in the crystal development as influenced by impurities and heat-treatment. Q values (fig. 4) were progressively lowered when CaO replaced TiO_2 and became a minimum when the CaO content reached about 31 percent. Further additions of CaO increased the Q values.

Within the ternary system for dielectrics having percentages of TiO_2 greater than about 60, the replacement of BaO by CaO increased the values of K but did not greatly decrease those of Q, in contrast to the effect of replacing BaO by MgO [2]. However, for dielectrics having compositions on the join $CaTiO_3$-$BaTiO_3$, increasing the content of $CaTiO_3$ resulted in a continuous decrease in K, from about 1,400 for $BaTiO_3$ to near 140 for $CaTiO_3$, and in an increase in Q, from 130 for $BaTiO_3$ to 3,500 for $CaTiO_3$, measured at 25° C and 1 mc/s. For specimens having compositions along the join $3CaO:2TiO_2$-$BaO:2TiO_2$, the initial substitution of CaO for BaO resulted in a decrease in K from 200 to 180 and in Q from 70 to 50. Further increase in CaO content increased K to a maximum of 265 at 33 percent of $3CaO:2TiO_2$, followed by a decrease in K to 55 for 100 percent of $3CaO:2TiO_2$. Q values were below 100 for specimens containing less than about 50 percent of $3CaO:2TiO_2$ and above 200 at higher CaO content. Along the join $2CaO:TiO_2$-$2BaO:3TiO_2$, K for the dielectrics was continuously reduced, as CaO replaced BaO, from 900 for $2BaO:3TiO_2$ to 40 for $2CaO:TiO_2$. The Q value, although less than 100 when the percentage of $2CaO:TiO_2$ was 17 percent or less, was several hundred at higher CaO content. On the join $3CaO:TiO_2$-$BaTiO_3$, the replacement of $BaTiO_3$ by 5 percent of $3CaO:TiO_2$ increased K from 1,400 to 2,670, but additional replacement to 10 percent of $3CaO:TiO_2$ reduced K to 1,630. Further increase in the content of $3CaO:TiO_2$ to 25 percent resulted in a rapid decrease in K to a value of 60. From 29 percent to 100 percent, K remained near 40. The Q value was not over 300 from 0 to 16 percent of $3CaO:TiO_2$, but for higher percentages Q ranged from 2,000 to 5,000.

Certain specimens, indicated in figure 1, were found to decrease in K and increase in Q with time after the final heat treatment. Similar behavior was noted and described for some of the titanate dielectrics previously studied [2]. Data showing the extent of these changes after storage for 6 months under room conditions are given in table 2. Although the maximum decrease in K for any specimen was less than 25 percent, the maximum increase in Q was 225 percent. These changes appear only in the dielectrics containing less than about 50 percent of titania and more than about 25 percent of baria. In this region, the presence of the crystalline forms of $BaTiO_3$, with some solid solution, might be expected, and changes in this crystalline structure may be associated with the instability of the specimens. The data in table 1 were obtained after the K and Q values had been stabilized by aging these specimens for 6 months.

TABLE 2.—*Changes in K and Q of some specimens after 6 months of storage*

[Measured at 1 mc/s and 25° C]

Specimen designation	Dielectric constant, K			Quality factor, Q		
	After 1 day	After 6 months	Change	After 1 day	After 6 months	Change
			%			%
CB3	228	217	−4.8	305	680	128
CB35	249	238	−4.4	215	700	225
CB4	285	264	−7.4	200	480	140
CB5	347	315	−9.2	151	390	160
CB6	426	380	−10.8	105	310	195
CB64	464	401	−13.6	94	270	187
CB7	516	440	−14.7	90	264	193
CB8	657	542	−17.5	102	325	219
CB9	696	599	−13.9	66	159	141
CB95	860	838	−2.6	94	117	24
B2C26	213	209	−1.9	780	1,030	32
B2C28	495	477	−3.6	47	55	17
B2C29	542	514	−5.2	31	32.5	5
B2C295	560	571	−3.2	26	27	4
BC38	611	538	−12.0	290	294	1
BC39	1,630	1,397	−14.3	169	216	22
BC395	2,200	1,692	−23.1	65	117	80

All of the dielectrics containing less than 50 percent of titania and greater than about 30 percent of calcia (fig. 1) decreased in K and Q values after exposure to room conditions for over a year. These changes are probably due to the presence of free lime, which slowly hydrates as a result of exposure to moisture in the air. Specimens in the region of $3CaO:TiO_2$ disintegrate after storage for several weeks. The data given in table 1 for these dielectrics were obtained within a day or two after they were matured.

Changes in the dielectric constant due to variations in temperature are given in table 3. At 1

mc/s these data were obtained by measurements at temperatures given in the table. Equilibrium values of K were not attained for the specimens listed in table 2 for the reason that the temperature at each interval was held constant for only 15 min before measurements were made. For stable specimens, the average values of temperature coefficient of K per degree centigrade are considered to be within ± 10 ppm, or 5 percent, whichever is greater. All but seven of these stable values are negative and lie within the range of 0 to $-2{,}250$ ppm per degree centigrade. Where no values are given, computations of the coefficient were not made because the coefficient either changed sign or showed large irregularities within this range of temperature. To illustrate the variation of K resulting from changes in temperature and composition, diagrams were constructed for temperatures of $-60°$, 0°, and 60° C (fig. 5). These diagrams exhibit isodielectric-constant lines plotted from the data in table 3. In contrast to specimens with compositions in the join $SrTiO_3$-$BaTiO_3$ [1], the dielectrics with compositions in the join $CaTiO_3$-$BaTiO_3$ do not have peak values of K within the temperature range of $-60°$ to 85° C.

TABLE 3. *Dielectric constant, at 1 mc/s, from −60° to 85° C, and average temperature coefficient of dielectric constant per ° C*

Specimen designation	Values of K at—															Average temperature coefficient of K per ° C
	−60° C	−50° C	−40° C	−30° C	−20° C	−10° C	0° C	10° C	20° C	30° C	40° C	50° C	60° C	70° C	80° C	85° C	
																	ppm
CT6	131	129	127	125	123	121.5	120	119	117.5	116.5	115	114	113	112	111	110.5	−1,200
18BC6	87.8	86.8	85.9	85.1	84.4	83.7	83.0	82.4	81.7	81.0	80.4	79.9	79.4	78.8	78.3	78.0	−820
BT18	80.5	79.7	78.9	78.3	77.6	77.0	76.5	76.0	75.4	74.8	74.3	73.8	73.4	73.0	72.7	72.5	−730
CT2	163.5	160	157	154	151	148.5	146	144	141.5	139.5	138	136	134.5	133	131.5	130.5	−1,590
6BC2	120	118	116	114	112	110.5	109	108	106.5	105.5	104.5	103.5	102.5	102	101.5	101	−1,220
6BC5	91.7	90.4	89.2	88.1	87.1	86.2	85.6	85.0	84.4	83.8	83.2	82.5	81.8	81.1	80.4	80.1	−940
6BC8	61.5	60.9	60.4	59.9	59.6	59.2	58.9	58.7	58.6	58.5	58.4	58.1	57.8	57.5	57.1	57.0	−530
6BC9	50.3	50.1	49.9	49.7	49.5	49.4	49.2	49.1	48.9	48.7	48.6	48.5	48.4	48.3	48.2	48.1	−310
BT6	46.5	46.3	46.2	46.0	45.8	45.6	45.4	45.3	45.1	45.0	44.9	44.8	44.7	44.6	44.5	44.5	−300
5BC8	58.6	58.2	57.7	57.3	56.9	56.6	56.3	56.0	55.8	55.5	55.2	55.0	54.7	54.5	54.3	54.2	−530
5BC9	50.4	50.1	49.9	49.7	49.5	49.4	49.2	49.1	49.0	48.9	48.7	48.5	48.4	48.3	48.2	48.15	−320
5BC95	46.0	45.8	45.7	45.5	45.4	45.3	45.2	45.1	45.0	44.9	44.8	44.7	44.65	44.6	44.5	44.45	−230
BT5	36.7	36.7	36.7	36.7	36.7	36.7	36.7	36.7	36.7	36.7	36.7	36.7	36.7	36.7	36.7	36.7	0
C2T3	169	165.5	162	158.5	156	152.5	150	147.5	145.5	143.5	141.5	139.5	138	136	134.5	133.5	−1,650
BC22	114	112	110	108	106	104.5	102.8	101.5	100.2	99.4	98.1	97.0	96.0	95.0	94.0	93.4	−1,370
BC24	98.4	96.3	94.5	93.1	91.7	90.6	89.5	88.5	87.5	86.5	85.6	84.8	84.1	83.4	82.7	82.3	−1,260
BC26	73.0	71.5	70.5	69.6	68.9	68.3	67.8	67.3	66.9	66.5	66.1	65.6	65.1	64.7	64.2	64.0	−920
BC27	61.9	61.4	60.9	60.3	59.9	59.5	59.1	58.6	58.3	58.1	57.9	57.7	57.5	57.4	57.2	57.1	−570
BC28	52.4	52.0	51.6	51.2	51.0	50.7	50.4	50.2	50.0	49.9	49.7	49.5	49.4	49.3	49.2	49.1	−460
BC29	41.9	41.8	41.7	41.6	41.6	41.5	41.5	41.5	41.5	41.5	41.5	41.5	41.5	41.5	41.5	41.5	−70
BT4	33.0	33.1	33.2	33.3	33.4	33.5	33.6	33.7	33.7	33.8	33.9	33.9	34.0	34.0	34.0	34.0	210
CT	169	165	161.5	158	155	152	149	146.5	144	142	139	137	135	133.5	132	131	−1,800
BC5	106.4	104.8	103.0	101.5	99.8	98.5	97.2	96.2	95.2	94.2	93.2	92.2	91.3	90.3	89.3	88.9	−1,240
BC6	80.2	79.2	78.0	77.00	76.0	75.2	74.4	73.8	73.3	72.6	72.0	71.4	70.8	70.2	69.7	69.4	−980
BC7	73.9	73.0	72.2	71.4	70.6	70.0	69.4	68.9	68.4	67.9	67.4	66.9	66.4	65.9	65.5	65.3	−790
BC8	59.9	59.4	58.8	58.4	58.0	57.5	57.2	56.8	56.5	56.2	55.9	55.7	55.4	55.2	54.9	54.8	−620
BC9	53.4	53.1	52.8	52.6	52.3	52.1	51.8	51.6	51.4	51.2	51.0	50.8	50.6	50.4	50.2	50.1	−440
BT3	44.6	44.5	44.5	44.4	44.3	44.3	44.2	44.1	44.1	44.0	43.9	43.9	43.8	43.8	43.7	43.7	−160
CT	169	165	161.5	158	155	152	149	146.5	144	142	139	137	135	133.5	132	131	−1,800
CB1	186	181	176	171.5	168	164.5	161.5	159	156	154	151.5	149.5	147	145	143	141.5	−1,940
CB2	237	229	223	216	211	206	201	197	193	189	185	181	178	176	174	173	−2,250
CB3 *	254	248	244	238	234	230	227	225	224	225	226	228	231	236	242	250	.....
CB35 *	290	282	275	269	264	260	256	253	251	250	250	251	253	257	264	271	.....
CB4 *	295	290	285	282	279	276	274	273	275	279	284	291	302	315	331	346	.....
CB5 *	349	347	345	343	341	341	339	341	342	348	353	365	378	398	423	444	.....
CB6 *	409	407	407	406	404	405	406	410	413	427	440	460	483	517	570	604	.....
CB64 *	410	408	407	407	408	409	412	413	420	435	455	480	515	570	635	690	.....
CB7 *	415	420	420	425	430	435	440	445	450	480	510	550	600	660	770	835	4,600
CB8 *	455	470	485	490	515	520	530	540	550	600	660	740	860	1,020	1,250	1,600	7,700

See footnote at end of table.

TABLE 3. *Dielectric constant, at 1 mc/s, from −60° to 85° C, and average temperature coefficient of dielectric constant per °C*—Continued

Specimen designation	Values of K at—															Average temperature coefficient of K per °C
	−60° C	−50° C	−40° C	−30° C	−20° C	−10° C	0° C	10° C	20° C	30° C	40° C	50° C	60° C	70° C	80° C	85° C	
																	ppm
CB9 *	670	655	640	640	635	640	640	640	640	660	680	720	765	825	905	960	
CB95 *	610	720	920	1,110	1,005	950	910	875	860	855	860	875	910	950	1,020	1,060	
BT	805	815	860	910	980	1,060	1,160	1,310	1,570	1,450	1,360	1,320	1,300	1,330	1,400	1,440	
C3T2	51.3	51.2	51.0	51.0	50.8	50.7	50.6	50.5	50.4	50.2	50.1	50.0	49.9	49.7	49.6	49.5	−260
BC321	67.7	67.3	66.9	66.5	66.1	65.7	65.3	65.0	64.6	64.2	63.9	63.6	63.3	63.0	62.7	62.5	−550
BC323	90.5	89.5	88.5	87.4	86.4	85.7	84.8	84.1	83.3	82.6	81.8	81.2	80.6	79.9	79.3	79.0	−950
BC324	174	169	165	161	157.5	154	152	150	149	146.5	144.5	142	140	138	136.5	135.5	−1,780
BC325	254	250	246	243	240	237	235	233	232	233	234	236	240	245	253	258	
BC327	260	260	261	261	262	263	264	265	266.5	268	270	272.5	275	277.5	280.5	282.5	590
BC328	200	201	202	203.5	205	206	208	210	212	214.5	217	220	223	227	232	235	1,150
BC329	151	153	155	157	160	162	165	167	171	174	177	181	185	191	197	204	2,200
BT2	163	168	173	177	182	187	192	196	200	202	204	207	210	214	219	221	2,100
C2T	40.23	40.2	40.15	40.1	40.0	39.95	39.9	39.85	39.8	39.7	39.65	39.6	39.5	39.45	39.4	39.37	−155
B2C21	46.3	46.2	46.15	46.1	45.95	45.9	45.8	45.7	45.6	45.45	45.4	45.3	45.25	45.15	45.1	45.05	−190
B2C22	45.7	45.6	45.5	45.4	45.35	45.3	45.2	45.1	45.05	44.95	44.85	44.8	44.7	44.6	44.5	44.45	−180
B2C23	47.4	47.55	47.7	47.8	47.95	48.1	48.2	48.3	48.4	48.25	48.1	48.0	47.9	47.8	47.7	47.68	
B2C24	59.2	58.8	58.3	57.9	57.5	57.15	56.8	56.6	56.3	56.0	55.75	55.5	55.25	55.05	54.8	54.6	−550
B2C25	79.7	78.8	77.9	77.0	76.2	75.5	74.8	74.2	73.6	72.9	72.4	71.9	71.4	70.9	70.4	70.2	−870
B2C26 *	236	233	230	227	224	221	217	214	210	207	204	200	196	192	187	185	−1,670
B2C28 *	464	470	480	487	495	503	512	518	525	535	547	560	573	590	608	617	2,020
B2C29 *	449	457	465	475	485	495	504	512	525	542	555	575	592	620	642	660	2,820
B2C295 *	474	485	497	510	523	535	550	560	580	593	610	633	655	685	715	742	3,270
B2T3	600	630	660	690	720	745	780	825	870	890	900	910	920	935	965	980	
C3T	34.35	34.3	34.25	34.2	34.15	34.1	34.1	34.05	34.0	33.95	33.9	33.9	33.85	33.8	33.75	33.72	−100
BC31	40.35	40.3	40.2	40.15	40.1	40.05	40.0	39.95	39.9	39.85	39.8	39.7	39.65	39.6	39.55	39.5	−145
BC32	39.02	38.95	38.9	38.85	38.8	38.75	38.7	38.65	38.62	38.6	38.5	38.45	38.4	38.35	38.3	38.28	−130
BC33	37.45	37.4	37.37	37.33	37.3	37.23	37.2	37.15	37.1	37.05	37.0	36.95	36.9	36.85	36.8	36.78	−130
BC35	35.92	35.85	35.83	35.8	35.8	35.75	35.75	35.7	35.7	35.65	35.6	35.55	35.5	35.45	35.4	35.38	−100
BC36	38.0	37.95	37.85	37.8	37.75	37.75	37.7	37.7	37.7	37.65	37.6	37.55	37.5	37.45	37.4	37.35	−50
BC37	38.55	38.3	38.0	37.8	37.5	37.3	37.15	37.05	36.9	36.75	36.6	36.4	36.3	36.15	36.05	35.95	−480
BC375	70.0	69.3	68.4	67.7	66.9	66.2	65.4	64.7	63.9	63.2	62.5	61.8	61.1	60.3	59.6	59.2	−1,130
BC38	500	520	540	555	575	590	600	600	600	600	580	555	525	495	460	440	
BC39 *	1,100	1,130	1,190	1,260	1,330	1,420	1,520	1,640	1,730	1,750	1,710	1,610	1,500	1,400	1,300	1,230	
BC395 *	1,400	1,460	1,520	1,570	1,640	1,710	1,800	1,860	1,880	2,000	2,460	2,920	3,020	2,860	2,580	2,500	
BT	805	815	860	910	980	1,060	1,160	1,310	1,570	1,450	1,360	1,320	1,300	1,330	1,400	1,440	

* Values of K depend upon length of time at each temperature.

Greater variation was obtained for the Q values than for the K values. At all frequencies used, dielectrics of high calcia or high titania content had Q values greater than 300; those of high baria content had Q values less than 300. For nearly all of the specimens tested at 3,000 mc/s, the Q values were lower than those measured at lower frequencies. In general, no great improvement in K or Q was obtained by the use of highest purity titania (99.9%) in the preparation of the dielectrics.

Linear thermal expansion was fairly high for all the specimens measured, as shown in table 4. Since local heating to elevated temperatures cracks all these dielectrics, except in thin sections they should be preheated when solder connections are made directly to the metal electrodes on them.

TABLE 4. *Linear thermal expansion*

Specimen designation	Temperature range from 25° C to—						
	100° C	200° C	300° C	400° C	500° C	600° C	700° C
	Percent	*Percent*	*Percent*	*Percent*	*Percent*	*Percent*	*Percent*
C2T	0.07	0.18	0.30	0.42	0.555	0.68	0.82
CT	.07	.185	.31	.43	.56	.69	.82
C2T3	.07	.175	.29	.405	.51	.63	.75
CT2	.065	.17	.28	.39	.50	.62	.735
CT6	.06	.15	.25	.35	.45	.555	.655
CB5	.055	.16	.285	.41	.545	.68	.81
BC26	.06	.155	.265	.365	.475	.585	.705
6BC5	.055	.15	.255	.355	.46	.57	.685
BC6	.065	.175	.285	.40	.52	.64	.765
B2C25	.07	.19	.325	.45	.59	.725	.87
BC35	.07	.18	.34	.47	.605	.71	.85

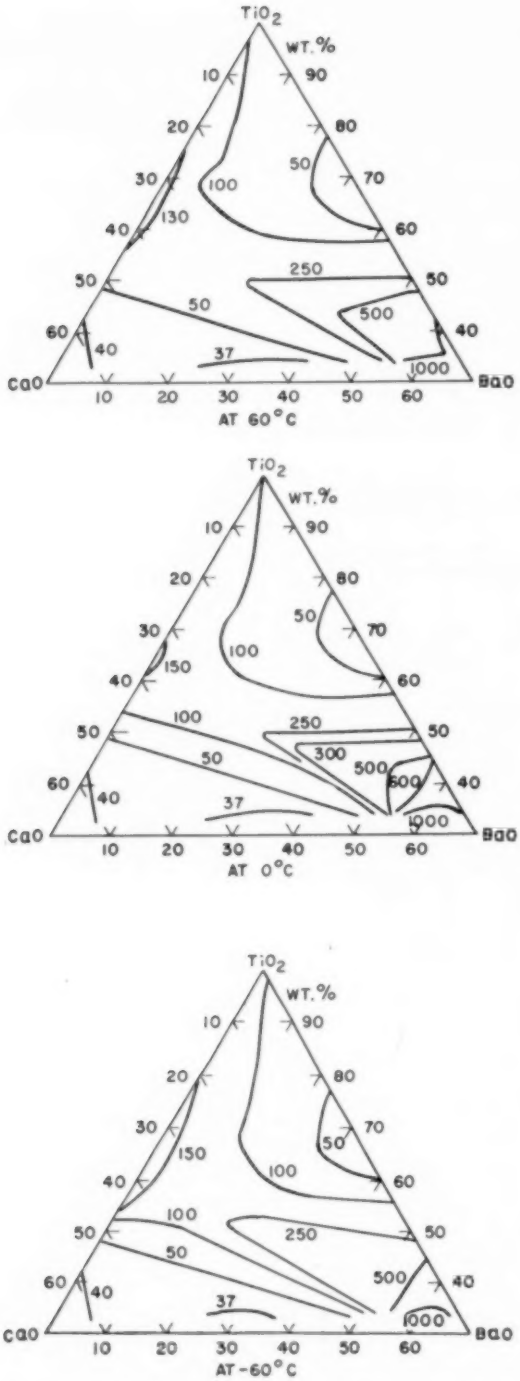

FIGURE 5. *Variation in dielectric constant K with composition at 1 mc/s and at 60°, 0°, and −60° C.*

IV. Summary

Dielectrics having compositions in the system $3CaO:TiO_2$–$BaTiO_3$–TiO_2 can be prepared from mixtures of titanium dioxide with calcium and barium carbonates. Mature dielectrics (less than 0.1% absorption) were obtained by dry-pressing the calcined mixtures and heating the disks thus formed to various temperatures within the range 1,260° to 1,500° C. Matured specimens containing less than 50 percent of titania and greater than about 30 percent of calcia deteriorate in electrical properties after exposure to room conditions for several months.

The dielectric constant, K, varies from 34 for $BaO:4TiO_2$ and $3CaO:TiO_2$ to several hundred for dielectrics having compositions in the region of barium titanate. Most of the temperature coefficients of K are negative. The Q values range from 20 to 10,000 and are lowest for dielectrics of high baria content. K and Q values of some of the dielectrics are affected by their past thermal history, the K decreasing and the Q increasing for several weeks after these specimens are matured.

Relatively high values of the linear thermal expansion (0.65 to 0.81% at 25° to 700° C) were obtained for dielectrics having compositions in all regions of the system.

V. References

[1] E. N. Bunting, G. R. Shelton, and A. S. Creamer, J. Research NBS **38,** 337 (1947) RP1776; J. Am. Ceram. Soc. **30,** 4 (1947).

[2] G. R. Shelton, A. S. Creamer, and E. N. Bunting, J. Research NBS **41,** 17 (1948) RP1899.

[3] U. S. Pat. 2,394,030 and 2,402,515–8, by E. Wainer.

[4] A. von Hippel, et al., Ind. Eng. Chem. **38,** 1097 (1946).

WASHINGTON, April 3, 1949.

U. S. Department of Commerce
National Bureau of Standards

Research Paper RP2026
Volume 43, September 1949

Part of the Journal of Research of the National Bureau of Standards

Heats, Equilibrium Constants, and Free Energies of Formation of the Dimethylcyclopentanes [1]

By Morton B. Epstein,[2] Gordon M. Barrow,[3] Kenneth S. Pitzer,[4] and Frederick D. Rossini [5]

For the five dimethylcyclopentanes, values are presented for the following thermodynamic properties to 1,500° K: heat content function, free energy function, entropy, heat content, heat capacity, heat of formation from the elements, free energy of formation from the elements, and logarithm of the equilibrium constant of formation from the elements. Equilibrium constants and concentrations are given in tabular and graphical form for some reactions of isomerization.

I. Introduction

As part of the work of the American Petroleum Institute Research Project 44 at the National Bureau of Standards and the University of California, values have been compiled for the thermodynamic properties in the gaseous state to 1,500 °K of the heat content function, free energy function, entropy, heat content, heat capacity, heat of formation, free energy of formation, and logarithm of the equilibrium constant of formation for the five dimethylcyclopentanes. Calculations have also been made of the free energies and equilibrium constants of some reactions of isomerization.

II. Constants

The values of the constants used in the present calculations are the same as in the previous report [1].[6]

III. Heat Content Function, Free Energy Function, Entropy, Heat Content, and Heat Capacity

For the dimethylcyclopentanes, the available thermal, spectroscopic, and other molecular data are either insufficient or too uncertain to permit a satisfactory statistical treatment at the present time. However, the thermodynamic functions may be calculated by adding the necessary increment to the corresponding function of methylcyclopentane, for which the appropriate values have already been calculated [2].

For the calculation by the method of increments, the following equation was used:

$$G(\text{dimethlcyclopentane}) = G(\text{methylcyclopentane}) + G(\text{methyl}) + 2G(\text{restricted rotation of methyl group with appropriate barrier}) - 2G(\text{restricted rotation of methyl group with barrier as in methylcyclopentane}). \quad (1)$$

In eq 1, G represents the contribution to the heat content function, the free energy function, or the heat capacity, the entropy and heat content being simply derived from these functions. In calculating the contribution of the restricted rotation of the methyl group in methylcyclopentane, the barrier was taken to be 3,600 cal/mole [2].

The barriers restricting the internal rotation of the methyl groups in the dimethylcyclopentanes have been chosen to fit the known entropies of 1,1-dimethylcyclopentane, *cis*-1,2-dimethylcyclopentane, and *trans*-1,3-dimethylcyclopentane [3]. These barriers are 5,320, 4,680, and 4,360 cal/mole, respectively. For *trans*-1,2-dimethylcyclopentane and *cis*-1,3-dimethylcyclopentane, the barriers were taken to be equal to that in *trans*-1,3-dimethylcyclopentane. The barrier restricting ring puckering for all of the dimethylcyclopentane isomers is taken unchanged from that in methylcyclopentane [2].

[1] This investigation was performed as a part of the work of the American Petroleum Institute Research Project 44 at the National Bureau of Standards and the University of California.

[2] Research Associate on the American Petroleum Institute Research Project 44 at the National Bureau of Standards.

[3] Junior Research Fellow on the American Petroleum Institute Research Project 44 at the University of California, Berkeley, California.

[4] Associate Director of the American Petroleum Institute Research Project 44 at the University of California, Berkeley, California, on leave.

[5] Director of the American Petroleum Institute Research Project 44 at the National Bureau of Standards.

[6] Figures in brackets indicate the literature references at the end of this paper.

847618—49——5

TABLE 1. *Values of the thermodynamic functions, for the ideal gas state, to 1,500 ° K, for the five dimethylcyclopentanes*

Compound (gas)	Temperature in ° K														
	0	298.16	300	400	500	600	700	800	900	1000	1100	1200	1300	1400	1500
	HEAT CONTENT FUNCTION, $(H^\circ - H_0^\circ)/T$, IN CAL/DEG MOLE														
1,1-Dimethylcyclopentane	0	18.66	18.77	23.51	28.59	33.63	38.32	42.64	46.69	50.38	53.77	56.92	59.78	62.42	64.87
cis-1,2-Dimethylcyclopentane	0	18.86	18.95	23.63	28.71	33.71	38.38	42.70	46.69	50.36	53.73	56.86	59.72	62.36	64.79
trans-1,2-Dimethylcyclopentane	0	18.94	19.05	23.71	28.78	33.77	38.42	42.68	46.69	50.34	53.69	56.82	59.68	62.30	64.73
cis-1,3-Dimethylcyclopentane	0	18.94	19.05	23.71	28.78	33.77	38.42	42.68	46.69	50.34	53.69	56.82	59.68	62.30	64.73
trans-1,3-Dimethylcyclopentane	0	18.94	19.05	23.71	28.78	33.77	38.42	42.68	46.69	50.34	53.69	56.82	59.68	62.30	64.73
	FREE ENERGY FUNCTION, $(F^\circ - H_0^\circ)/T$, IN CAL/DEG MOLE														
1,1-Dimethylcyclopentane	0	−67.21	−67.36	−73.36	−79.14	−84.72	−90.28	−95.75	−101.02	−106.13	−111.05	−115.87	−120.51	−125.04	−129.51
cis-1,2-Dimethylcyclopentane	0	−68.65	−68.81	−74.91	−80.71	−86.34	−91.91	−97.36	−102.65	−107.76	−112.70	−117.50	−122.12	−126.63	−131.10
trans-1,2-Dimethylcyclopentane	0	−68.73	−68.87	−75.01	−80.81	−86.45	−92.03	−97.54	−102.79	−107.90	−112.84	−117.64	−122.26	−126.77	−131.24
cis-1,3-Dimethylcyclopentane	0	−68.73	−68.87	−75.01	−80.81	−86.45	−92.03	−97.54	−102.79	−107.90	−112.84	−117.64	−122.26	−126.77	−131.24
trans-1,3-Dimethylcyclopentane	0	−68.73	−68.87	−75.01	−80.81	−86.45	−92.03	−97.54	−102.79	−107.90	−112.84	−117.64	−122.26	−126.77	−131.24
	ENTROPY, S°, IN CAL/DEG MOLE														
1,1-Dimethylcyclopentane	0	85.87	86.13	96.87	107.73	118.35	128.60	138.39	147.71	156.51	164.82	172.79	180.29	187.46	194.38
cis-1,2-Dimethylcyclopentane	0	87.51	87.76	98.54	109.42	120.06	130.29	140.06	149.34	158.12	166.43	174.36	181.84	188.99	195.89
trans-1,2-Dimethylcyclopentane	0	87.67	87.92	98.72	109.60	120.22	130.45	140.22	149.48	158.24	166.53	174.46	181.94	189.07	195.97
cis-1,3-Dimethylcyclopentane	0	87.67	87.92	98.72	109.60	120.22	130.45	140.22	149.48	158.24	166.53	174.46	181.94	189.07	195.97
trans-1,3-Dimethylcyclopentane	0	87.67	87.92	98.72	109.60	120.22	130.45	140.22	149.48	158.24	166.53	174.46	181.94	189.07	195.97
	HEAT CONTENT, $(H^\circ - H_0^\circ)$, IN CAL/MOLE														
1,1-Dimethylcyclopentane	0	5564	5631	9404	14300	20180	26820	34110	42020	50380	59150	68300	77710	87390	97300
cis-1,2-Dimethylcyclopentane	0	5623	5685	9452	14360	20230	26870	34160	42020	50360	59100	68230	77640	87300	97180
trans-1,2-Dimethylcyclopentane	0	5647	5715	9484	14400	20260	26890	34140	42020	50340	59060	68180	77580	87220	97100
cis-1,3-Dimethylcyclopentane	0	5647	5715	9484	14400	20260	26890	34140	42020	50340	59060	68180	77580	87220	97100
trans-1,3-Dimethylcyclopentane	0	5647	5715	9484	14400	20260	26890	34140	42020	50340	59060	68180	77580	87220	97100

	0	298.16	300	400	500	600	700	800	900	1000	1100	1200	1300	1400	1500
HEAT CAPACITY, C_p°, IN CAL/DEG MOLE															
1,1-Dimethylcyclopentane	0	31.86	32.16	43.55	54.01	62.78	70.08	76.18	81.38	85.83	89.62	92.89	95.75	98.19	100.31
cis-1,2-Dimethylcyclopentane	0	32.06	32.34	43.67	54.03	62.72	69.92	75.98	81.14	85.57	89.38	92.65	95.51	97.97	100.11
trans-1,2-Dimethylcyclopentane	0	32.14	32.44	43.71	54.03	62.66	69.88	75.84	80.98	85.43	89.24	92.51	95.39	97.85	100.01
cis-1,3-Dimethylcyclopentane	0	32.14	32.44	43.71	54.03	62.66	69.88	75.84	80.98	85.43	89.24	92.51	95.39	97.85	100.01
trans-1,3-Dimethylcyclopentane	0	32.14	32.44	43.71	54.03	62.66	69.88	75.84	80.98	85.43	89.24	92.51	95.39	97.85	100.01
HEAT OF FORMATION, ΔHf°, IN KCAL/MOLE															
1,1-Dimethylcyclopentane	−22.69	−33.05	−33.10	−35.92	−38.14	−39.79	−41.04	−41.91	−42.39	−42.59	−42.55	−42.29	−41.94	−41.49	−40.94
cis-1,2-Dimethylcyclopentane	−20.66	−30.96	−31.01	−33.84	−36.05	−37.72	−38.96	−39.83	−40.36	−40.58	−40.57	−40.33	−39.99	−39.54	−39.03
trans-1,2-Dimethylcyclopentane	−22.39	−32.67	−32.72	−35.54	−37.75	−39.41	−40.67	−41.58	−42.09	−42.33	−42.35	−42.11	−41.78	−41.36	−40.85
cis-1,3-Dimethylcyclopentane	−21.65	−31.93	−31.98	−34.80	−37.01	−38.67	−39.93	−40.84	−41.35	−41.59	−41.61	−41.37	−41.04	−40.62	−40.11
trans-1,3-Dimethylcyclopentane	−22.19	−32.47	−32.52	−35.34	−37.55	−39.21	−40.47	−41.38	−41.89	−42.13	−42.15	−41.91	−41.58	−41.16	−40.65
FREE ENERGY OF FORMATION, ΔFf°, IN KCAL/MOLE															
1,1-Dimethylcyclopentane	−22.69	+9.33	9.58	24.26	39.58	55.34	71.29	87.33	103.51	119.75	136.02	152.24	168.48	184.62	200.64
cis-1,2-Dimethylcyclopentane	−20.66	+10.93	11.18	25.67	40.83	56.39	72.17	88.07	104.08	120.15	136.23	152.31	168.42	184.43	200.29
trans-1,2-Dimethylcyclopentane	−22.39	+9.17	9.42	23.90	39.04	54.60	70.36	86.19	102.22	118.27	134.34	150.41	166.50	182.50	198.35
cis-1,3-Dimethylcyclopentane	−21.65	+9.91	10.16	24.64	39.78	55.34	71.10	86.93	102.96	119.01	135.08	151.15	167.24	183.24	199.09
trans-1,3-Dimethylcyclopentane	−22.19	+9.37	9.62	24.10	39.24	54.80	70.56	86.39	102.42	118.47	134.54	150.61	166.70	182.70	198.55
LOGARITHM OF EQUILIBRIUM CONSTANT OF FORMATION, $\log_{10}Kf$															
1,1-Dimethylcyclopentane	Infinite	−6.8372	−6.9791	−13.2550	−17.3902	−20.1566	−22.2561	−23.8567	−25.1361	−26.1704	−27.0236	−27.7258	−28.3238	−28.8208	−29.2335
cis-1,2-Dimethylcyclopentane	Infinite	−8.0107	−8.1413	−14.0255	−17.8445	−20.5399	−22.5337	−24.0595	−25.2729	−26.2579	−27.0664	−27.7393	−28.3132	−28.7903	−29.1818
trans-1,2-Dimethylcyclopentane	Infinite	−6.7224	−6.8651	−13.0564	−17.0648	−19.8865	−21.9662	−23.5465	−24.8213	−25.8483	−26.6914	−27.3930	−27.9912	−28.4890	−28.8986
cis-1,3-Dimethylcyclopentane	Infinite	−7.2648	−7.4042	−13.4607	−17.3882	−20.1561	−22.1972	−23.7487	−25.0009	−26.0101	−26.8384	−27.5277	−28.1156	−28.6046	−29.0064
trans-1,3-Dimethylcyclopentane	Infinite	−6.8690	−7.0108	−13.1657	−17.1522	−19.9594	−22.0286	−23.6011	−24.8698	−25.8921	−26.7311	−27.4294	−28.0248	−28.5203	−28.9278

The term G(methyl) represents the contribution of a methyl group with a barrier to internal rotation of 3,600 cal/mole and is calculated from the following relation:

G(methyl) = G(methylcyclopentane) − G(cyclopentane) − G(restricted rotation of ring puckering in methylcyclopentane),

where the term G(cyclopentane) includes all contributions to that function for cyclopentane exclusive of symmetry. From the method of calculation of the function for methylcyclopentane [2], the term G(methyl) is the same as the contribution of a methyl group to the functions for methylcyclohexane with a barrier of 3,600 cal/mole. This contribution is equal to the difference between the functions for methylcyclohexane and cyclohexane, exclusive of contributions due to symmetry and to equatorial-polar tautomerism [4].

For 1,1-dimethylcyclopentane, *trans*-1,2-dimethylcyclopentane, and *trans*-1,3-dimethylcyclopentane, an additional symmetry term, R ln 2, was subtracted from the entropy and the negative of the free energy function. For *trans*-1,2-dimethylcyclopentane and *trans*-1,3-dimethylcyclopentane, a mixing term R ln 2 was added to allow for the mixing of equal amounts of the dextro and levo optical isomers. The values tabulated for these two compounds, therefore, are for the mixture of the optical isomers. It will be noted that the mixing term, where applicable, exactly cancels the symmetry term. The resulting values for the heat content function, the free energy function, the entropy, the heat content, and the heat capacity are included in table 1. Where the second decimal place is given, the uncertainty is several tenths of a unit.

IV. Heat, Free Energy, and Equilibrium Constants of Formation

Values for the standard heat of formation at 25° C of the five dimethylcyclopentanes in the gaseous state, from carbon (solid, graphite) and hydrogen (gaseous), are taken from reference [5].

The method of calculating values of the standard heat of formation, the standard free energy of formation, and the logarithm of the equilibrium constant of formation for the different temperatures in the range 0° to 1,500° K is the same as that described in section IV–1 of reference [6].

The resulting values for the formation of the given hydrocarbon in the gaseous state, from the elements carbon (solid, graphite) and hydrogen (gaseous), each in its thermodynamic standard reference state, are included in table 1, which gives values of the following properties to 1,500° K: heat of formation, free energy of formation, and logarithm of the equilibrium constant of formation.

V. Free Energies and Equilibria of Some Reactions of Isomerization

In figure 1 are plotted, as a function of temperature, for the five dimethylcyclopentanes and ethylcyclopentane, the amounts, in mole fraction, of each of the isomers present at equilibrium with the other isomers in the gaseous state. The corresponding numerical values are given in table 2.

TABLE 2. *Values of the equilibrium concentrations for the isomerization of the C_7 alkylcyclopentanes in the ideal gaseous state to 1,500° K*

Temperature	Composition, in mole fraction, of equilibrium mixture of isomers					
	Ethylcyclopentane	1,1-Dimethylcyclopentane	*cis*-1,2-Dimethylcyclopentane	*trans*-1,2-Dimethylcyclopentane	*cis*-1,3-Dimethylcyclopentane	*trans*-1,3-Dimethylcyclopentane
°K						
298.16	0.031	0.264	0.018	0.343	0.099	0.245
300	.032	.264	.018	.342	.099	.245
400	.075	.201	.034	.318	.125	.247
500	.122	.168	.048	.289	.137	.236
600	.164	.143	.059	.267	.142	.225
700	.196	.127	.068	.249	.145	.215
800	.221	.116	.075	.235	.147	.206
900	.243	.108	.080	.223	.147	.199
1000	.262	.102	.084	.213	.147	.192
1100	.278	.098	.087	.204	.147	.186
1200	.292	.094	.089	.197	.146	.182
1300	.303	.090	.091	.193	.145	.178
1400	.310	.088	.094	.188	.145	.175
1500	.313	.087	.097	.185	.144	.174

In figure 2 are plotted, as a function of temperature, values of the logarithm of the equilibrium constant for the isomerization to methylcyclohexane of ethylcyclopentane and each of the five dimethylcyclopentanes.

FIGURE 1. *Equilibrium concentrations of the six C_7H_{14} alkyl cyclopentanes.*

The vertical width of a band measures the mole fraction as a function of temperature of a given isomer when at equilibrium with all of the isomeric alkylcyclopentanes in the gas phase.

FIGURE 2. *Isomerization of ethylcyclopentane and each of the five dimethylcyclopentanes to methylcyclohexane.*

The curves give the logarithm of the equilibrium constant as a function of temperature for the following reactions in the gaseous state: C_7H_{14} (gas, ethylcyclopentane or a dimethylcyclopentane) $\rightleftharpoons C_7H_{14}$ (gas, methylcyclohexane).

VI. References

[1] M. B. Epstein, K. S. Pitzer, and F. D. Rossini, J. Research NBS **42,** 379 (1949) RP1976.

[2] J. E. Kilpatrick, H. G. Werner, C. W. Beckett, K. S. Pitzer, and F. D. Rossini, J. Research NBS **39,** 523 (1947) RP1845.

[3] H. M. Huffman and others, U. S. Bureau of Mines, Bartlesville, Oklahoma. Unpublished.

[4] C. W. Beckett, K. S. Pitzer, and R. Spitzer, J. Am. Chem. Soc. **69,** 2488 (1947).

[5] W. H. Johnson, E. J. Prosen, and F. D. Rossini, J. Research NBS **42,** 251 (1949) RP1966.

[6] D. D. Wagman, J. E. Kilpatrick, W. J. Taylor, K. S. Pitzer, and F. D. Rossini, J. Research NBS **34,** 143 (1945) RP1634.

WASHINGTON, May 13, 1949.

U. S. Department of Commerce
National Bureau of Standards

Research Paper RP2027
Volume 43, September 1949

Part of the Journal of Research of the National Bureau of Standards

Cathode Heater Compensation as Applied to Degenerative Voltage-Stabilized Direct-Current Power Supplies

By Robert C. Ellenwood and Howard E. Sorrows

A new method of compensating a degenerative-type voltage stabilizer that simplifies the design of precision stabilized direct-current power supplies is discussed. If the operating voltages of the direct-current amplifier in the comparator circuit of the stabilizer are properly chosen, compensation for line voltage changes is obtained from the corresponding changes in the "heater-to-plate transconductance." An equation for the over-all stabilization factor of the compensated stabilizer is presented in terms of the stabilization factor of a simple degenerative stabilizer. Output voltage changes of less than 0.005 percent for ± 10-percent change in line voltage were obtained from experimental tests of sample power supplies with 350 volts output.

I. Introduction

To improve the accuracy of ultrahigh frequency measurements, it was found expedient to develop several precision stabilized d-c power supplies [1].[1] Although each power supply was designed for use with a specific instrument, it was required that each:

1. Produce the required d-c output of several hundred volts.
2. Be designed for a current drain of several hundred milliamperes with an approximately constant load resistance.
3. Have stability such that the output voltage be practically independent of line voltage changes expected in the laboratory.
4. Have as simple a circuit as possible to facilitate repairs and adjustments.

Neher and Pickering, in a 1939 report [2], observed that under certain conditions the experimental performance of a stabilized power supply was better than their theoretical prediction. They found that the lower the screen grid voltage of one of the component tubes, the better the voltage stabilization. This phenomenon could be attributed to the greater cathode temperature control of the amplifier-tube plate current at lower screen voltages. Since the cathode temperature depends on the heater voltage, the variations in heater voltage can be employed to improve the voltage stabilization for variations in line voltage.

In view of the disagreement in literature in the usage of the terms "regulation" and "stabilization", it is desirable to define these terms as used in this paper. Stabilization refers to the reduction of output voltage or current fluctuations. Regulation refers to the percentage change of output voltage of a power supply as the power-supply output current is changed.

II. General Theory and Design Considerations

The majority of commercially available general-purpose stabilized power supplies that furnish several hundred milliamperes at several hundred volts are of the degenerative amplifier type. The basic circuit of this type of stabilizer is shown in figure 1. The degenerative d–c amplifier (T_2 in fig. 1) is in a comparator circuit [3] that compares the output voltage of the stabilizer with some reference voltage. The over-all stability of the

[1] Figures in brackets indicate the literature references at the end of this paper.

power supply is no better than the stability of the reference voltage. Dry cells or standard cells can be used as precision reference-voltage standards. VR tubes are too unstable for reference voltages when precision stabilization is desired [4].

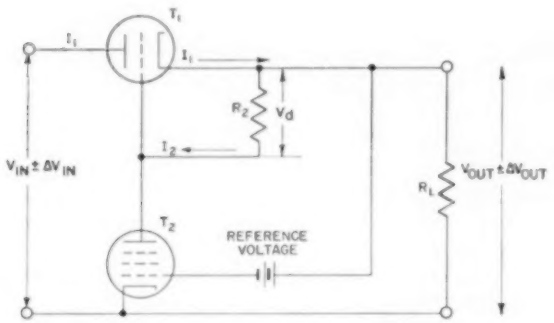

FIGURE 1. *Simplified degenerative-voltage-stabilizer schematic.*

The equation of stabilization for figure 1 is usually given as follows:

$$F=1+\frac{r_{p1}}{R_L}+\frac{R_2\mu_1(\mu_2+1)}{r_{p2}+R_2}, \qquad (1)$$

where

F=stabilization factor ($\Delta V_{in}/\Delta V_{out}$).
ΔV_{in}=change in d-c voltage input to stabilizer.
r_{p1}=plate resistance of the control tube (T_1).
R_L=external load resistance.
R_2=plate load resistance of d-c amplifier (T_2).
μ_1=amplification factor of the current control tube (T_1).
μ_2=amplification factor of the d-c amplifier (T_2).
r_{p2}=plate resistance of the d-c amplifier (T_2).

It is seen from the above equation that the theoretical stabilization factor (F) for a given load (R_L) is limited by the amplification factors and the plate resistances of the given tubes. It is noted that the stabilization factor (eq 1) does not directly consider the effect of line voltage changes on the heater voltage. The heater voltage is proportional to the line voltage in most power supplies.

Precision measurements often require the use of a d-c power supply with output voltage practically independent of line voltage changes. A stabilization factor (F_L), which includes the effect of variations in the line voltage on the heater voltage, is given in eq 2, in terms of the stabilization factor (F) of eq 1.

$$F_L=\frac{F}{N_p\left(1-\frac{R_2\mu_1 r_{p2}S_{h2}N_h}{r_{p2}+R_2}\right)}, \qquad (2)$$

where

$$F_L=\frac{\text{Change in line voltage } (\Delta V_L)}{\text{Resultant change of output voltage } (\Delta V_{out})},$$

N_p≈Turns ratio of plate transformer.
N_h≈Turns ratio of heater transformer.
$S_{h2}=\Delta i_{p2}/\Delta e_{h2}$=heater-to-plate transconductance.

The term "transconductance" is used for want of a better term to describe the effect on the plate current of heater voltage acting through its control upon the initial velocity of the electrons emitted by the cathode. Although the expression is dimensionally correct, no attempt is made to defend it as rigorously correct. It is evident from eq 2 that, if the denominator equals zero, F_L approaches infinity, which indicates perfect stabilization with respect to line voltage changes. If the other factors in the denominator are of the proper order of magnitude, nearly perfect stabilization can be obtained by adjusting the heater to plate transconductance (S_{h2}) of the d-c amplifier tube (T_2). Therefore, the design of a heater-compensated power supply requires a family of characteristic curves for the d-c amplifier tube (T_2 of fig. 1) that presents the plate current as a function of heater voltage and screengrid voltage.

III. Description of Operation

Measurements were made on the stabilized power supply shown in figure 2 for the purpose of analyzing its heater compensation. It was found that the output voltage is sensitive to small changes in the heater voltage of the d-c amplifier tube (T_2) but independent of the heater voltage of the control tube (T_1).

Since the compensation is effected through the d-c amplifier tube, T_2, a study was made of the operation of the amplifier circuit. When a change occurs in the heater voltage, the change in the plate current of the amplifier tube results in a proportional change in the voltage V_d across R_2, which appears on the grid of the control tube T_1.

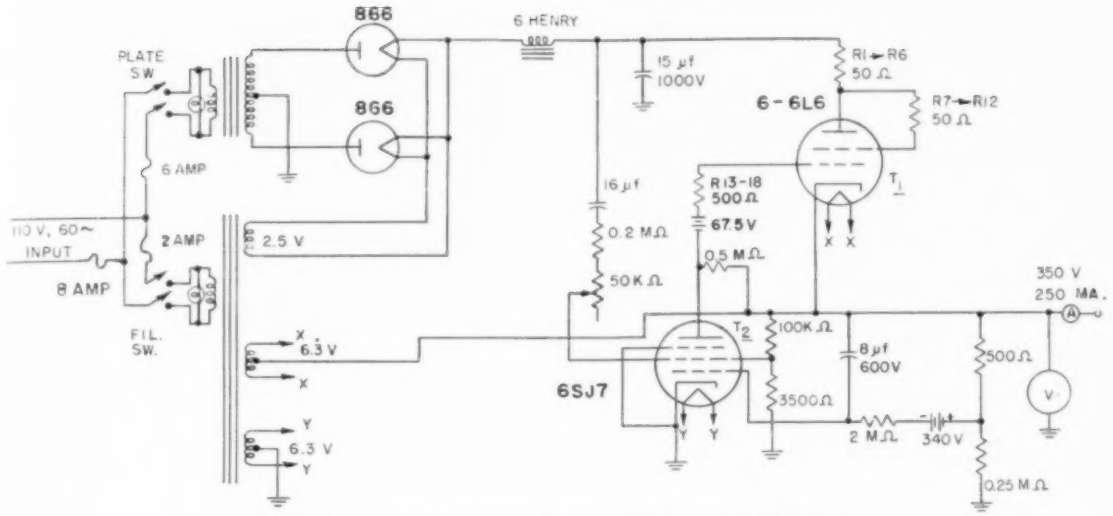

FIGURE 2. *Heater-compensated power supply, 350-v d-c, 250 ma.*

In this way additional compensation for a line voltage change can be obtained from the heater voltage change. The change in voltage V_d per 20-v change (100 to 120 v) in line voltage was measured for various values of screen voltage. It was found that the lower the screen voltage, the greater the incremental change in the voltage drop per unit change in heater voltage (See fig. 3).

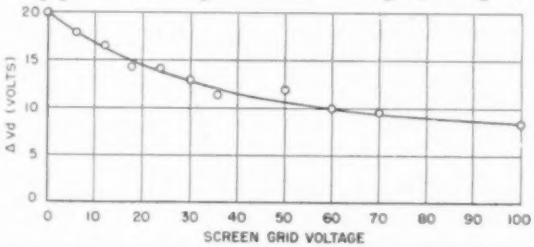

FIGURE 3. *Change in voltage drop across resistor (R_2) for 20-v change in a-c line voltage versus screen-grid voltage.*

As the heater-to-plate transconductance, S_{h2} in eq 2, is defined as the change in plate current per unit change in heater voltage with all other tube voltages held constant, it is seen that the incremental change in the voltage drop per unit change in heater voltage, the ordinate of figure 3, is proportional to S_{h2}. Therefore the transconductance, S_{h2}, varies with the screen-grid voltage as in figure 3. The screen-grid voltage, at which S_{h2} has the proper value for maximum stabilization, can be selected from experimental data such as is shown in figure 4.

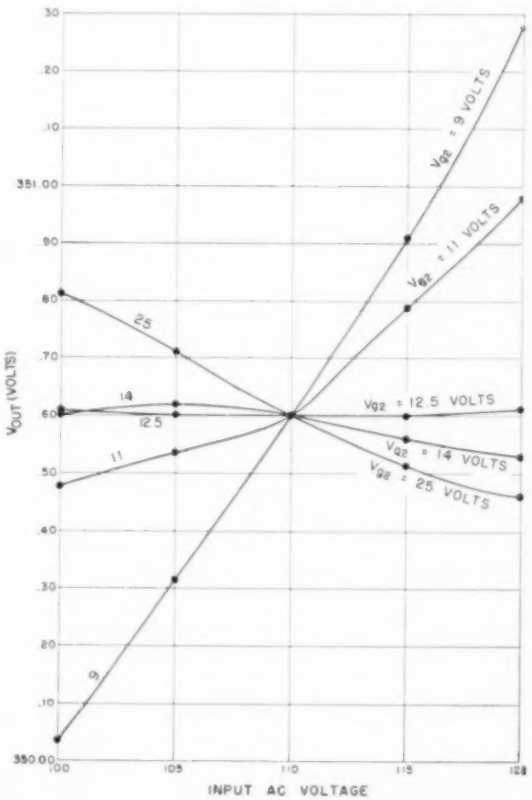

FIGURE 4. *Stabilized d-c output voltage for various screen grid voltages.*

847618—49——6

The improvement with heater compensation of the stabilization of a power supply is shown in figure 5, a, b, and c. The performance of the power supply without heater compensation is shown in figure 5, a. It is seen that with a constant heater voltage an increase in line voltage of 10 v resulted in an increase in output voltage of about 0.1 v. The effect of changes in heater voltage is presented in figure 5, b. With the input voltage to the stabilizer, V_{in}, held constant and the screen grid voltage set at the value for maximum stabilization, an increase of 10 v in the primary voltage of the heater transformer resulted in a decrease in the output voltage of about 0.1 v. Thus it is seen that the heater voltage can be employed to provide the additional compensation that the degenerative-type voltage stabilizer usually lacks for perfect stabilization with respect to line voltage changes. Figure 5, c shows that, with the primaries of the high voltage and heater transformers connected to a common line voltage and the screen grid voltage set at its proper value, the heater-compensated power supply has a maximum deviation of output voltage of 0.01 v for a line voltage change of ±10 percent. This is a variation of less than 0.0005 percent in output voltage per volt change in the line. The performance appeared to be unaffected by changing from one amplifier tube (T_2) to others of the same kind, and over the period of time the power supply was used there appears to be no effect from aging.

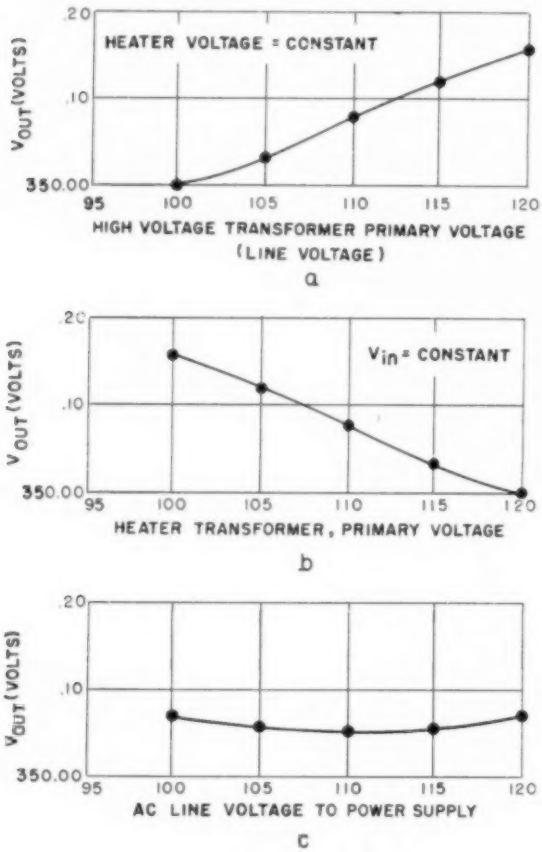

FIGURE 5.

a, Stabilized d-c output voltage versus primary voltage of high-voltage transformer; b, stabilized d-c output voltage versus primary voltage of heater transformer; c, stabilized d-c output voltage versus a-c line voltage.

The following measurements were obtained from the sample power supply (fig. 2):

Parameter	Measured value
Output voltage	350 v d-c
Input voltage to stabilizer	550 v d-c
Amplifier screen-grid voltage	12.5 v d-c
Amplifier control-grid voltage	−0.95 v d-c
Output ripple	1.9 mv (rms)
Internal resistance	2 ohms
Over-all stabilization factor.[a]	500
Percent voltage change [b]	0.003 percent for ±10-percent line voltage change

[a] Stabilization factor is $\left(\frac{\Delta \text{line voltage}}{\Delta \text{output voltage}}\right)$.

[b] Percent voltage change is $\left(\frac{\Delta \text{output voltage}}{\text{output voltage}}\right)$.

Figure 6 shows the performance of this power supply for a wide range of input voltage.

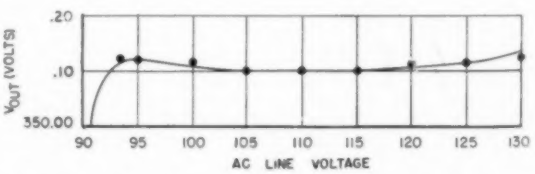

FIGURE 6. *Direct-current output voltage versus line voltage for 12.5 screen-grid volts.*

IV. Compensation for Time Lag

A compensating voltage determined by the heater voltage of an indirectly heated cathode-type tube has a time lag dependent on the time necessary for the cathode temperature to come to equilibrium [5, 6]. To reduce the effect of this time lag, an RC circuit is applied between the input terminal (V_{in}, fig. 1) and the screen grid of the d-c amplifier. When a sudden change of line voltage occurs, the RC circuit applies the proper value of voltage to the screen grid of the d-c amplifier to compensate for the thermal time lag of the cathode temperature. The time constant of the RC network was chosen to be equal to that of the temperature change of the cathode.

V. Summary

Heater compensation has been applied to a degenerative voltage stabilizer to obtain a variation of less than 0.0005 percent in output voltage per volt change in line voltage. The high stability was obtained without sacrificing simplicity of design. The amount of compensation from the heater voltage action is a function of the screen-grid voltage of the amplifier tube. Experimental methods are given for determining the correct screen-grid voltage for maximum stability.

VI. References

[1] H. E. Sorrows, R. C. Ellenwood, and W. E. Ryan, National Bureau of Standards, CRPL Report 9–1 (November 8, 1946).

[2] H. V. Neher and W. H. Pickering, Rev. Sci. Instruments **10,** 35 (1939).

[3] F. V. Hunt and R. W. Hickman, Rev. Sci. Instruments **10,** 6 (1939).

[4] G. N. Kirkpatrick, Proc. Inst. Radio Engrs. **35,** 485 (1947).

[5] R. C. Evans, Rev. Sci. Instruments **5,** 371 (1934).

[6] J. S. Ashworth and J. C. Mouzon, Rev. Sci. Instruments **8,** 127 (1937).

WASHINGTON. June 3, 1949.

U. S. Department of Commerce
National Bureau of Standards

Research Paper RP2028
Volume 43, September 1949

Part of the Journal of Research of the National Bureau of Standards

Mechanical Properties of Laminated Plastics at −70°, 77°, and 200° F[1]

By John J. Lamb, Isabelle Albrecht, and Benjamin M. Axilrod

Laminates of an unsaturated polyester reinforced with glass fabric and of phenolic resin reinforced with asbestos fabric, high-strength paper, cotton fabric, and rayon fabric were tested in impact, bending, tension, and compression at −70°, 77°, and 200° F. Special apparatus was constructed for conducting the tests at the extreme temperature conditions. The impact strength of the glass-fabric laminate increases at −70° and decreases at 200° F relative to 77° F; the impact strengths of cotton- and rayon-fabric laminates decrease at −70° and increase at 200° F; the paper and asbestos-fabric laminates have small changes in impact strength with temperature. The flexural, tensile, and compressive strengths and moduli of elasticity increase at −70° and decrease at 200° F relative to the 77° F values.

Tests made at room temperature after heating the materials at 200° F for 24 hr indicate that prolonged heating with consequent loss of moisture content and further cure of the resin may offset the effect of high temperature alone. In flexural tests made at 150° F and 90-percent relative humidity, two laminates showed considerable loss in strength.

I. Introduction

A knowledge of the effect of temperature on the strength properties of plastics is of considerable importance in application of the materials for aircraft purposes. Results obtained by various investigators [1, 2, 3] [2] on plastic materials indicate that considerable variation in mechanical properties with temperature may be expected.

Oberg, Schwartz, and Shinn [2] reported variations of 10 to 30 percent in the tensile and flexural properties of Grades C, L, and XX phenolic laminates for the range −38° to 78° F.

Norelli and Gard [3] reported data for tensile, compressive, and shear strengths and tensile moduli of elasticity for various phenolic laminates for temperatures ranging from −67° F to as high as 392° F in some instances. They concluded that the percentage change in strength for cellulose laminates is greater than for those made with mineral reinforcement.

Meyer and Erickson [4] determined the mechanical properties of high-strength-paper phenolic laminates for temperatures from −69° to 200° F. For this temperature range they found large variations in tensile, compressive, and flexural strengths and somewhat smaller variations in modulus of elasticity. The strength and modulus of elasticity values diminished with increasing temperature.

In investigations by the Naval Air Experimental Station [5] considerable data have been obtained at 77° and 160° F on the mechanical properties of a variety of plastic laminates. The ultimate strength and modulus of elasticity values were generally lower at the higher temperature, but the percentage changes varied greatly for the different materials.

Witt, Wolfe, and Rust [6] obtained tensile and compressive data at 160° F and flexural and impact data at −70° and 160° F on a large number of samples of Grades C and L laminates from various manufacturers. They reported decreases in flexural, tensile, and compressive strengths and moduli of elasticity at 160° F rang-

[1] The data presented in this paper are a summary of results reported in NACA Technical Notes 1054 and 1550.

[2] Figures in brackets indicate the literature references at the end of this paper.

TABLE 1. *Description of materials*

NBS Designation	Type of laminate [a]	Density	Thickness, average	Manufacturer	Resin		Reinforcement					Molding conditions			
					Type	Content by weight	Type	Thread count		Number of plies	Ply arrangement	Pressure	Temp. [b]	Time of heating [b]	Time of cooling [b]
								Warp	Filling						
		g/cm³	*in.*			*Percent*						*lb/in²*	°F	*min*	*min*
L1	Low-pressure cotton-fabric phenolic.	1.36	0.15	Bakelite Corp.	Bakelite—BV-16887.	52	Enameled duck 8 oz/yd²	84	28	9	Cross	250	325	30	
L2		1.32	.60							35					
V1	Low-pressure Grade C phenolic.	1.27	.15	Synthane Corp.	do	51	Army duck 10.4 oz/yd²	50	40	7	do	180	320	50	
V2		1.29	.55							[c] 26					
W1	High-pressure Grade C phenolic.	1.36	.14	do	Bakelite—BV-1112.	47	do	50	40	7	do	1,800	320	50	
W2		1.36	.45							25					
I2	Grade C phenolic	1.34	.53	do	do	48	Cotton fabric	50	40	27	Parallel	1,800	340±20	50	20
Z1 [d]	Rayon-cotton-fabric phenolic.	1.37	.16	Formica Insulation Co.	Ironsides Co.—Phenolic 91-L.	37 to 40	Fortisan WE-3975 3/1 twill, 12.5 oz/yd²	Rayon 75	Cotton 12	7 23	Cross	1,100	300	20	20
Z2		1.37	.48												
S1	High-strength-paper phenolic.	1.42	.12	Consolidated Water Power and Paper Co.	Bakelite—16526	30	High-strength Mitscherlich paper 32.5 lb/ream of 480 sheets, 24×36 in.			27/0.060-in. thickness.	do	250	310±10	12	
S2		1.42	.50											30	
K1	Grade AA asbestos-fabric phenolic.	1.50	.15	Synthane Corp.	Bakelite—2427	47	Asbestos fabric 18 oz/yd²	18	16	5	Parallel	1,800	340±20	50	20
K2		1.48	.57							20					
AB1	Glass-fabric unsaturated-polyester.	1.82	.13	Army Air Forces Technical Service Command.	Plaskon—900	43	Fiberglas ECC-11-112	38	38	45	do	40	180	120	
													220	120	
AB2	do	1.86	.49	do	do	43	do	38	38	166	do	40	160	120	
													180	120	
													200	120	
													220	120	
U2	do	1.78	.60	Plaskon Div., Libbey-Owens-Ford Glass Co.	do	50	do	38	38	160	do	50	122	720	
													230	240	

[a] Grade AA and Grade C refer to NEHA designations.

[b] If two or more temperature-time conditions are listed for one laminate, they were applied in succession to cure the laminates.

[c] Warp directions at right angles in the two face plies.

[d] The ⅛-in.-thick sample and the ½-in.-thick sample of the Z material used in the impact, flexural, and tensile tests were received at the same time. The ½-in.-thick sample used in the compressive tests was received 10 months later.

ing from 20 to 25 percent relative to the corresponding values at 77° F. The impact strength of these cotton-fabric phenolic laminates decreased about 40 percent at −70° F and increased about 25 percent at 160° F.

Izod-impact test data reported by Fuller [7] for Grades L and XX phenolic laminates and for a glass-cotton-fabric phenolic laminate indicate an increase in Izod-impact strength with temperature for the cellulose laminates and an opposite trend for the glass-cotton-fabric laminate for the range −67° to 158° F. Shinn [8] also found that the Izod-impact strength of paper and cotton-fabric phenolic laminates increased with temperature over the temperature range −67° to 158° F; a similar trend was observed for paper and cotton-fabric unsaturated-polyester laminates between −67° and 77° F.

The present investigation was undertaken to obtain the impact, flexural, tensile, and compressive properties of representative laminates in the temperature range −70° to 200° F. Since testing at these temperatures presents many problems not met in testing at room temperature, a major part of the project was concerned with the development of apparatus and techniques.

This investigation, conducted at the National Bureau of Standards, was sponsored by and conducted with financial assistance from the National Advisory Committee for Aeronautics.

II. Materials

The materials tested were a group of laminates, which at the beginning of the project (1943) were considered for possible application in structural members of aircraft. The samples were supplied in nominal ⅛-in. and ½-in. thicknesses in the form of sheets 3 ft square or larger. A detailed description of the samples is contained in table 1.

Five of these laminates were tested at the University of Illinois [9] and the Pennsylvania State College [10] in research investigations of the mechanical properties of the materials. Creep at room temperature and flexural fatigue at various temperatures were determined at the former laboratory; static and dynamic creep were investigated at the latter institution. Limited measurements of the tensile and compressive properties of the laminates were made at 77° F in both of these projects. Some of these materials were included in other investigations at this Bureau [11, 12], which were undertaken to determine (a) the tensile stress-strain characteristics of laminates and (b) the effect of simulated service conditions on laminates. Findley, Adams, and Worley [13] made creep tests on the low-pressure Grade C laminate and the rayon-cotton-fabric laminate at three temperatures and 50-percent relative humidity. In all instances except (a) the tests were made on different sheets of the samples of the laminates.

III. Apparatus and Test Procedures

1. Sampling Procedures and Statistical Considerations

Each sample consisted of only one sheet. Impact, flexural, and compression specimens were cut from the same sheet of ½-in.-thick laminate. Initially the sheets were cut into quarters. Impact and flexural specimens were cut from the four quarters of the sheet. A similar procedure was followed in cutting tensile and impact specimens from the ⅛-in.-thick samples. The compression specimens were cut from the same quarter of the sheet, from an area of less than 1 square foot.

Since only one sheet of each sample was tested, the standard error as given in this report measures only variations due to the precision of the test method and variation within a sheet, but does not include sheet-to-sheet variability.

In section II of this report it has been mentioned that five of these same materials were tested concurrently at two other laboratories [9, 10]. Both of these laboratories had one ½-in.-thick sheet of each of the five types of laminates. When the results of compressive strength tests made at 77° F at the three laboratories were compared, it was found that, except for the second sheet of ½-in.-thick rayon-fabric phenolic laminate received at the National Bureau of Standards, the three sheets of each type of laminate had the same compressive strength within 15 percent. Therefore, the sheets tested at this Bureau are considered typical of the manufacturer's product.

For Izod impact tests the average ratio of standard error to impact strength for the 153 values given in table 2 is 2.3 percent. This ratio increases with temperature, being 2.0, 2.1, 2.3, and 2.7 for tests at −70°, 0°, 77°, and 200° F, respectively. In general, this ratio was smaller for

impact tests made edgewise than for tests made flatwise. For the other tests the relative values of the standard errors are summarized as follows:

Average ratio of standard error to individual mean value

Type of test	Number of mean values	Strength	Modulus of elasticity
		Percent	*Percent*
Flexure	108	1.5	1.7
Tension	40	2.0	2.8
Compression	24	1.5	1.3

2. Preparation of Specimens

The testing procedures outlined in Federal Specification L–P–406a [14] were followed as closely as possible. The specimens, however, were not polished with fine emery paper after machining. The flexure specimens of glass-fabric laminate U2 were cut with a diamond abrasive saw. All the specimens of glass-fabric laminate sample AB were machined with carbide-tipped tools. Specimens of all other samples were machined with high-speed steel tools, which gave a finish considered satisfactory. The tensile specimens (fig. 1) were milled with a machine having a cam-operated milling fixture for duplicating the desired contour (fig. 2). The ends of the compressive specimens were ground, while the latter were held in a fixture designed to give parallel, square ends.

Specimens tested at 77° F and 50-percent relative humidity were conditioned at least 96 hr prior to test. Specimens tested at other temperatures were first conditioned the same as the 77° F specimens and then were kept at the testing temperature for 24 ±2 hr prior to test.

3. Impact Tests

The impact tests were made according to Method 1071 in Federal Specification L–P–406a [14], using a Baldwin-Southwark pendulum-type Izod impact machine, which had ranges of 2, 8, and 16-ft-lb. The specimens were centered and the notch located properly with alinement jigs.

The tests were made at temperatures of −70°, 0°, 77°, and 200° F. The relative humidity was controlled at 50 percent in testing at 77° F and was not controlled at the other temperatures.

The samples in the ½-in. thickness were tested flatwise and edgewise for both the lengthwise and crosswise orientations. Since the Izod impact machine had a limited capacity (16 ft-lb), the specimens of the glass-fabric laminate sample tested flatwise were made only 0.25 to 0.30 in. wide. Edgewise tests were made on specimens of the ½-in.-thick sheets of some of the samples for both lengthwise and crosswise orientations.

4. Flexural Tests

The flexural tests were made according to Method 1031 of Federal Specification L–P–406a [14], using a 2,400-lb-capacity Baldwin-Southwark hydraulic universal testing machine that had ranges of 240, 1,200, and 2,400 lb. This machine was located in a room in which the atmosphere was controlled at 77° F and 50-percent relative humidity. Tests to obtain flexural strength and load-deflection graphs were made at −70°, 77°, and 200° F.

A variable-span flexure test jig with a deflection indicator [15] was used in all tests (figs. 3 and 4). The deflection of the specimen at the center of the span relative to the supports was indicated by an equal-arm lever actuating a gage. The gage, a Southwark-Peters Plastics Extensometer, was coupled to the recorder on the testing machine to obtain load-deflection records. Two models of the Plastics Extensometer were used with this apparatus: the Type PS–6, a high-magnification gage with a range of 0.23 in., and the Type PS–7, a low-magnification gage with a range of 1 in.

The span of the flexure test jig is adjustable from 1.6 to 9 in., and the screw is graduated to 0.002 in. The combination of recording gage and lever is accurate to about 5 percent in the measurement of deflections over 0.01 in. with the PS–6 gage and to about 3 percent for deflections over 0.1 in. with the PS–7 gage. The percentage error diminishes as the deflection increases. Calibrations were made only at 77° F. Additional errors due to thermal expansion would have a maximum value of 0.2 percent.

The flexural properties were determined only for the 0.5-in.-thick samples. Each sample was tested four ways, flatwise and edgewise for specimens cut both lengthwise and crosswise. At least five specimens were tested for each sample for all orientations. The only deviation from Method 1031 of Federal Specification L–P–406a was the

TABLE 2. *Izod impact strengths of laminates at various temperatures* [a]

Material designation	Orientation of specimen	Direction of load	Impact strength for tests made at [b]—			
			−70° F	0° F	77° F	200° F
½-IN.-THICK MATERIAL						
			ft-lb/in. of notch	*ft-lb/in. of notch*	*ft-lb/in. of notch*	*ft-lb/in. of notch*
L2, Low-pressure cotton-fabric phenolic	Lengthwise	Flatwise	3.30 ±0.04	4.17 ±0.06	5.98 ±0.08	6.09 ±0.05
	Crosswise	do	3.32 ± .05	4.12 ± .06	5.96 ± .06	5.82 ± .07
	Lengthwise	Edgewise	1.87 ± .02	2.32 ± .02	3.22 ± .03	3.28 ± .02
	Crosswise	do	1.85 ± .03	2.39 ± .02	3.09 ± .01	3.22 ± .05
V2, Low-pressure Grade C phenolic	Lengthwise	Flatwise	3.93 ± .07	5.40 ± .19	6.57 ± .14	6.64 ± .14
	Crosswise	do	3.79 ± .14	5.04 ± .11	6.26 ± .13	6.39 ± .20
	Lengthwise	Edgewise		2.51 ± .05	3.30 ± .08	3.35 ± .11
	Crosswise	do		2.59 ± .06	3.31 ± .06	3.57 ± .06
W2, High-pressure Grade C phenolic	Lengthwise	Flatwise	4.15 ± .07	5.12 ± .25	5.69 ± .29	5.80 ± .28
	Crosswise	do	3.87 ± .08	4.34 ± .15	5.27 ± .37	6.46 ± .60
	Lengthwise	Edgewise	2.12 ± .05	2.40 ± .11	2.75 ± .14	3.02 ± .14
	Crosswise	do	2.42 ± .02	2.46 ± .11	3.22 ± .17	3.87 ± .26
I2, Grade C phenolic	Lengthwise	Flatwise	2.81 ± .07	3.89 ± .10	5.06 ± .14	6.69 ± .07
	Crosswise	do	2.45 ± .06	3.13 ± .05	4.03 ± .05	5.25 ± .13
	Lengthwise	Edgewise	1.74 ± .02	2.26 ± .02	2.69 ± .03	3.85 ± .04
	Crosswise	do	1.46 ± .01	1.91 ± .02	2.34 ± .03	3.19 ± .04
Z2, Rayon-cotton-fabric phenolic	Lengthwise	Flatwise	17.0 ± .6	18.4 ± .6	17.6 ± .6	15.8 ± .4
	Crosswise	do	18.6 ± .9	19.1 ± .6	17.4 ± .7	16.4 ± .6
	Lengthwise	Edgewise	9.02 ± .32	7.96 ± .10	6.62 ± .09	5.94 ± .35
	Crosswise	do	7.70 ± .15	6.94 ± .21	5.91 ± .15	5.00 ± .28
S2, High-strength-paper phenolic	Lengthwise	Flatwise	4.07 ± .08	4.21 ± .09	4.18 ± .10	4.36 ± .24
	Crosswise	do	4.21 ± .11	4.18 ± .11	4.17 ± .14	4.53 ± .17
	Lengthwise	Edgewise	0.694± .005	0.726± .008	0.841± .012	0.688± .009
	Crosswise	do	.709± .007	.741± .010	.867± .008	.686± .005
K2, Asbestos-fabric phenolic	Lengthwise	Flatwise	4.13 ± .09	4.26 ± .04	4.58 ± .07	4.22 ± .08
	Crosswise	do	1.63 ± .06	1.99 ± .05	2.01 ± .14	1.75 ± .07
	Lengthwise	Edgewise	3.19 ± .08	3.40 ± .06	3.84 ± .03	3.46 ± .03
	Crosswise	do	1.33 ± .05	1.46 ± .02	1.60 ± .05	1.50 ± .04
AB2, Glass-fabric unsaturated-polyester	Lengthwise	Flatwise	46.1 ± .7	39.8 ± .9	31.5 ± .6	26.6 ± .5
	Crosswise	do			29.4 ± .8	
	Lengthwise	Edgewise			9.88 ± .05	
	Crosswise	do			9.03 ± .03	
⅛-IN.-THICK MATERIAL [c]						
V1, Low-pressure Grade C phenolic	Lengthwise	Edgewise	1.94 ±0.02	2.46 ±0.02	3.23 ±0.06	3.15 ±0.05
	Crosswise	do	1.86 ± .03	2.39 ± .02	2.94 ± .04	3.11 ± .05
W1, High-pressure Grade C phenolic	Lengthwise	do	1.84 ± .04	2.21 ± .05	2.72 ± .05	3.13 ± .09
	Crosswise	do	1.67 ± .03	2.16 ± .05	2.71 ± .03	2.96 ± .04
Z1, Rayon-cotton-fabric phenolic	Lengthwise	do	12.9 ± .3	13.0 ± .6	11.8 ± .2	12.2 ± .3
	Crosswise	do	8.74 ± .17	7.82 ± .14	7.13 ± .09	6.91 ± .16
S1, High-strength-paper phenolic	Lengthwise	do	0.612± .006	0.608± .005	0.640± .008	0.664± .007
	Crosswise	do	.622± .004	.638± .007	.629± .015	.623± .004
AB1, Glass-fabric unsaturated-polyester	Lengthwise	do	14.4 ± .2	12.0 ± .4	10.0 ± .3	9.58 ± .16
	Crosswise	do			10.9 ± .2	

[a] The tests were made in accordance with method 1071, Federal Specification L–P–406a.

[b] Mean value for 9 to 12 specimens for all materials except glass fabric laminate AB2, for which 20 to 25 specimens were tested. The accompanying plus or minus value is the standard error.

[c] The specimens were tested individually in the ⅛-in. thickness; composite specimens were not used.

use of a span-depth ratio of 8:1 instead of 16:1 in order to conserve materials. However, for comparative purposes flexure tests were made also at 77° F with a span-depth ratio of 16:1.

5. Tensile Tests

Tensile tests were made according to Method 1011 in Federal Specification L–P–406a [14], using the 1,200-lb range of a 2,400-lb capacity Baldwin-Southwark universal hydraulic testing machine and the 2,400- and 12,000-lb ranges of a 60,000-lb capacity Baldwin-Southwark universal hydraulic testing machine.

The Model PS–6 Southwark-Peters Plastics Extensometer, referred to previously was used. This instrument is a nonaveraging type with a 2-in. gage length, a strain magnification of 400, and a strain range of 10 percent. This gage sepa-

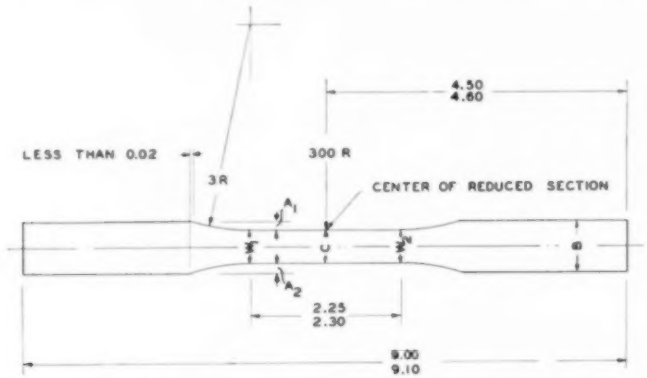

FIGURE 1. *Tensile specimen for plastic materials less than 0.25 in. thick.*

Notes on dimensions—All dimensions are in inches. Specimens shall besymmetrical about line-connecting centers of tab ends. W_1 W_2=0.505$\frac{1}{2}$±0.002; W_1-W_2=less than 0.001; $C=W_1-0.004$; A_1-A_2=less than 0.004; B=0.750±0.002. Blanks, before machining reduced section, shall be parallel to within 0.002.

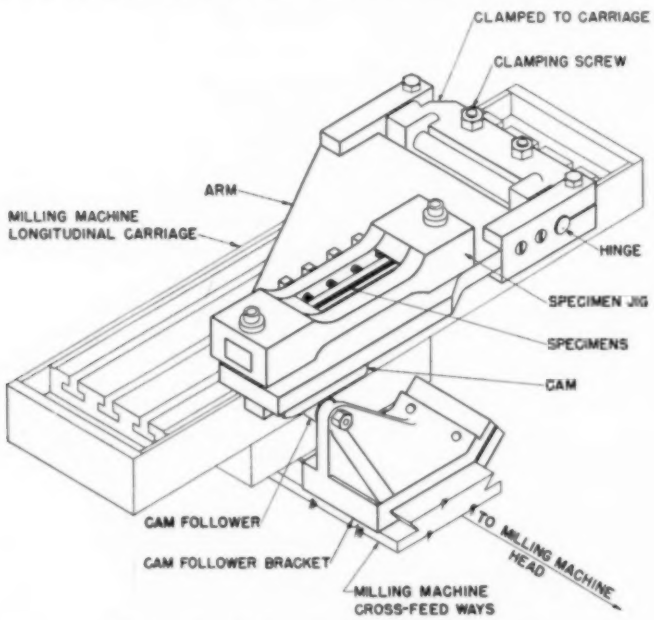

FIGURE 2. *Jig for milling tensile test specimen.*

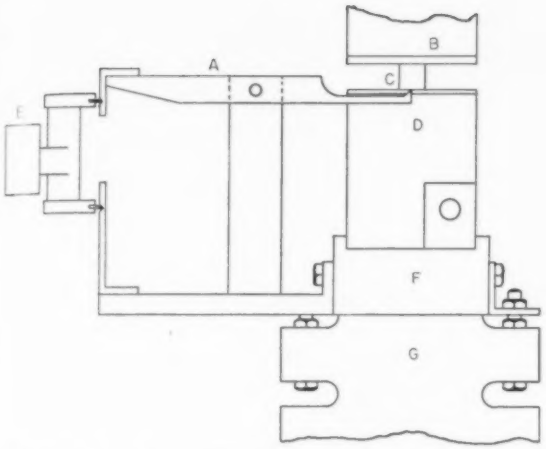

FIGURE 3. *Cross-sectional view of flexural test jig and deflection indicator.*

A, Equal-arm lever; *B*, loading head; *C*, specimen; *D*, specimen support; *E*, autographic tensile strain gage; *F*, base of flexural test jig; *G*, paper phenolic laminate support for flexural test jig. This support used at high and low temperatures.

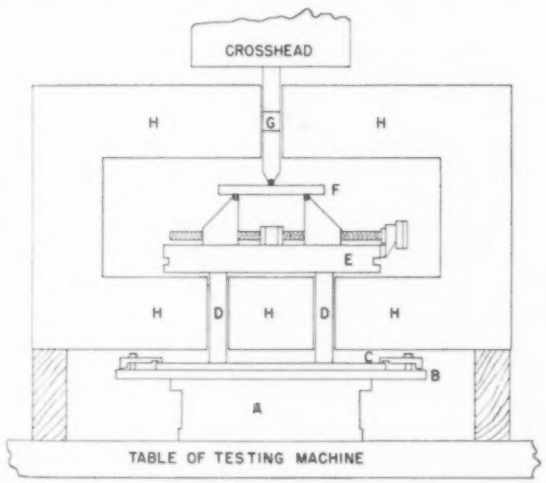

FIGURE 4. *Cross-sectional view of flexural test jig and insulated test cabinet.*

A, Magnetic chuck; *B*, flat steel plate screwed to magnetic chuck; *C*, flat steel plate; *D*, paper phenolic pieces, attached by screws to both *C* and *E*; *E*, base of flexural test jig; *F*, specimen; *G*, paper phenolic piece in loading head; *H*, insulation of test cabinet.

rates into two parts and hence was left on the specimen until failure. In all tests the relative rate of head motion was kept constant at 0.05 in./min until the specimen failed.

Tests to obtain tensile strength and load-elongation graphs were made at −70°, 77°, and 200° F. Tensile tests were made on nominal ⅛-in. thick samples. Both the lengthwise and crosswise directions of most of the samples were tested at the three temperatures. The 45°-diagonal direction was tested only at room temperature. The tensile specimens for a given sample were all taken from the same sheet and those for testing at the three temperatures sampled appropriately from the four quarters of the sheet.

6. Compressive Tests

The compressive tests were made according to Method No. 1021 in Federal Specification L-P-406a [14] on the 2,400-, 12,000-, and 60,000-lb ranges of a 60,000-lb capacity Baldwin-Southwark universal hydraulic testing machine.

The compression tool is shown in figure 5, together with the insulated loading and supporting pieces used in the high- and low-temperature testing. The compression tool incorporates several features of one designed by Aitchison and Miller [16].

(1) A spherical seat at the bottom of the plunger compensates for specimens that have ends that are nonparallel.

(2) The load is transmitted from the testing machine to the plunger by means of a steel push rod and a spherical bearing at the lower end of the push rod. The upper end of the push rod is a spherical surface concentric with the bearing, so that the line of application of the load remains, as nearly as possible, coaxial with the plunger during a lateral displacement of the heads of the testing machine relative to each other.

(3) The seat for the cylindrical lower bearing block was bored concentric with the plunger bushings. A jig, adjustable for specimens of slightly different thickness, was used to center the specimen on the lower bearing block to approximately 0.01 in. This made rapid centering of the specimen possible in the high-temperature and low-temperature tests.

An averaging type Southwark-Peters compressometer, model PC–4, with a gage length of 1 in., a strain magnification of 1,000, and a strain range of 4 percent was used in obtaining stress-strain data. In testing, the relative rate of head motion was 0.01 in./min until about 50 percent of the maximum load was attained. Then the strain gage was removed and the rate of loading increased to 0.03 in./min.

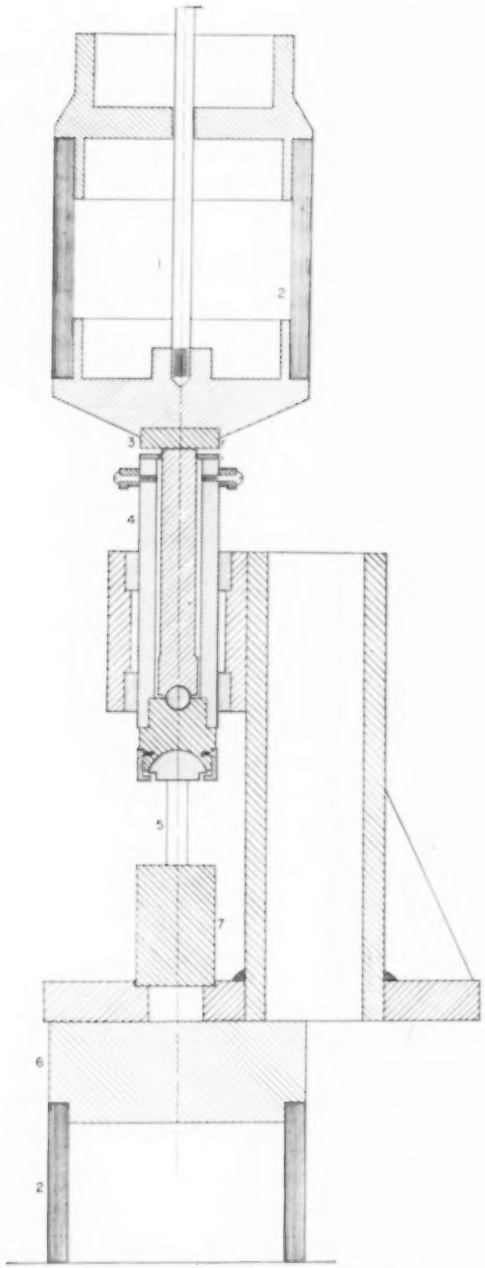

FIGURE 5. *Subpress for compression testing.*

(1), Rod, ½-in. diameter, 16 in. long, to hold loading head in lower crosshead of universal testing machine; (2), laminated paper phenolic tubing, 6½-in. outside diameter and ½-in. thickness; (3), hardened steel insert, 2-in. diameter and ½ in. thick, in loading head; (4), compression plunger; (5), specimen; (6), steel, 6½-in. outside diameter and 2½ in. thick; (7), case-hardened steel cylinder, 2-in. diameter and 3 in. high.

The compression specimen was 2 in. long and 0.50 in. wide; the thickness (0.45 to 0.60 in.) was that of the material (table 1). Compression tests were made for both the lengthwise and crosswise directions of the samples at 77° F, but only the lengthwise directions were tested at −70° and 200° F. For some of the samples, specimens oriented at 45° were tested at 77° F. The compression specimens for a given sample were all taken from the same section of the same sheet but were not otherwise sampled, since all the specimens were taken from a piece of the sheet less than 1 ft² in area.

An additional set of specimens was tested at 77° F to obtain the strain at failure. A Southwark-Peters deflectometer, model PD–1, was used to measure the motion of the plunger in the compression tool relative to the base of the tool. The deflectometer has low magnifications of 5, 10, and 20 with a range of 2 in. and high magnifications of 50, 100, and 200 with a range of 0.2 in.

7. High- and Low-Temperature Testing

In all tests at −77° and 200° F, the specimens were kept in a conditioning cabinet at the test temperature for about 20 hr and were then placed in the testing cabinet 1 to 4 hr prior to testing, resulting in a total conditioning period of 24 hr.

The impact tests at 0° and 77° F were made in rooms controlled at these temperatures. For the −70° and 200° F tests, the impact machine was housed in an insulated cabinet. The air in the cabinet was circulated by a fan except during the impact tests. Dry ice was used to cool the air; heating was done with electric heaters. In testing conducted in the insulated cabinet the operator kept his hands, which were protected with woolen gloves, inside the cabinet for periods of about 15 min at a time. This was sufficient for testing about 5 to 10 specimens.

For the low- and high-temperature flexural tests, the specimen, the flexural jig, and the deflection indicator were enclosed in a temperature-controlled cabinet equipped with a blower. The arrangement of the flexural apparatus for the low- and high-temperature tests is shown in figure 4.

For the low- and high-temperature tensile tests, the specimen, the grips, and the strain gage were enclosed in an insulated temperature-con-

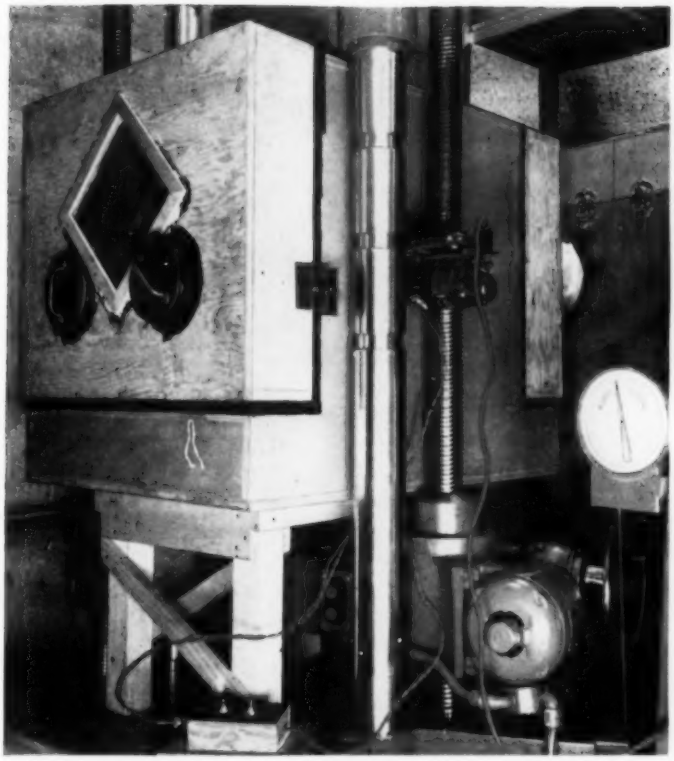

FIGURE 6. *Front view of tensile test enclosure in place in testing machine.*

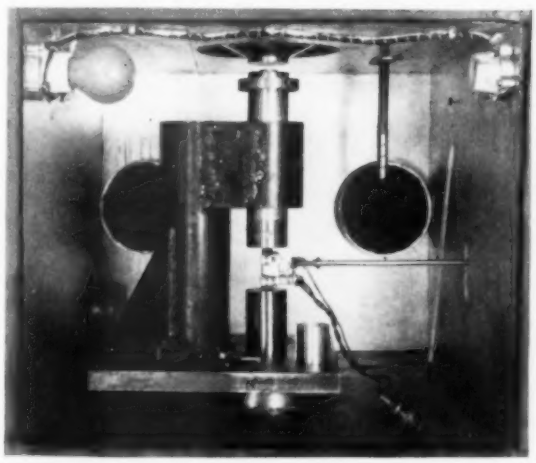

FIGURE 7. *Interior view of compression test enclosure with specimen in place in compression tool and compressometer attached to specimen.*

trolled cabinet (fig. 6). A triple-paned 12- by 12-in. window in the front, armholes, and interior lights enabled convenient handling of the specimens and equipment. Dry ice was used to cool the air; heating was done with electric heaters.

The arrangement for compression testing at low and high temperatures was similar to that for tensile testing. The specimen, compressometer, and compression tool were enclosed in an insulated temperature-controlled cabinet that was heated and cooled in the same way as the tensile test cabinet. Figure 7 shows the compression tool in the cabinet with the specimen and strain gage in position for testing. The method of supporting and loading the compression tool is indicated in figure 5. The steel supporting and loading blocks are insulated from the platen and cross-head, respectively, by tubular phenolic laminate pieces. The two holes shown in the

rear of the box in figure 7 were used to circulate either hot or cold air from the conditioning unit shown in figure 6.

Little difficulty was encountered in the high-temperature testing with this equipment. At low temperature several problems were encountered, such as lubricants freezing, frost on the electrical contacts of the gage, and rusting of the gage and loading parts. The testing was carried out with no lubricant on the bearings of the pendulum impact machine, or on the flexural jig, or on the compression tool bushings. The bearings of the pendulum were oiled with heptane prior to warming up to room temperature. Frost on the electrical contacts of the strain gage was washed off with ethanol. Rusting of the strain gage, flexural jig, tensile grips, and compression tool plunger was avoided by immersing them in alcohol until they attained room temperature. They were then disassembled and dried thoroughly.

IV. Results of Tests and Discussions

1. Impact Strength

The data for Izod impact strength of the various samples at temperatures of —70°, 0°, 77°, and 200° F are presented in table 2 and figures 8 to 10. The variation in impact strength with temperature is shown in figures 8 and 9 for lengthwise specimens of the 0.5-in.-thick samples tested flatwise.

The Izod impact strengths at 77° F for samples of the laminates tested flatwise are approximately as follows:

Type of laminate	Izod impact strength
	ft-lb/in. of notch
Grade C phenolic, high-pressure and low-pressure (L, V, W, I).	4 to 7
Rayon-cotton-fabric phenolic (Z)	17
High-strength-paper phenolic (S)	4
Asbestos-fabric phenolic (K)	2 to 4½
Glass-fabric unsaturated-polyester (AB)	30

All the cotton-fabric samples exhibited a steady decrease in impact strength as the temperature was reduced from 77° to —70° F (fig. 9). For samples I2, L2, and V2, the impact strength at —70° F was between 55 and 65 percent of the

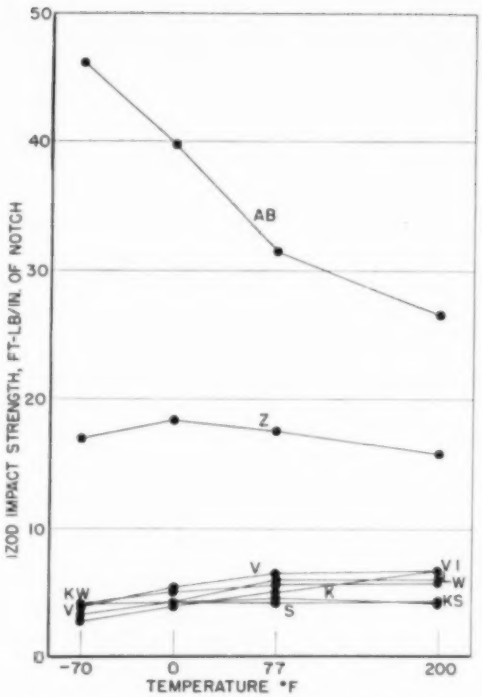

FIGURE 8. *Variation of Izod impact strength with temperature for ½-in.-thick laminates.*

Lengthwise specimens tested flatwise. *I*, Grade C phenolic; *K*, asbestos-fabric phenolic; *L*, low-pressure cotton-fabric phenolic; *S*, high-strength-paper phenolic; *V*, low-pressure Grade C phenolic; *W*, high-pressure Grade C phenolic; *Z*, rayon-cotton-fabric phenolic; AB, glass-fabric unsaturated-polyester.

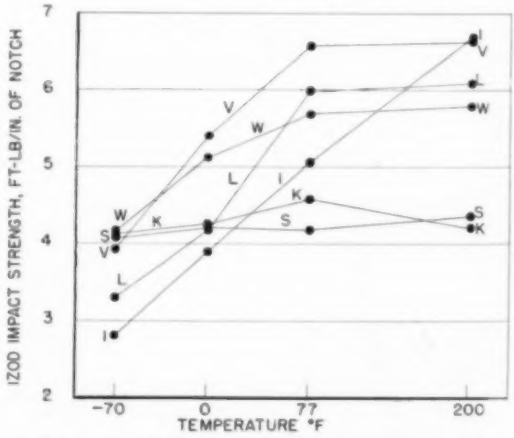

FIGURE 9. *Variation of Izod impact strength with temperature for ½-in.-thick laminates.*

Lengthwise specimens tested flatwise. *I*, Grade C phenolic; *K*, asbestos-fabric phenolic; *L*, low-pressure cotton-fabric phenolic; *S*, high-strength-paper phenolic; *V*, low-pressure Grade C phenolic; *W*, high-pressure Grade C phenolic.

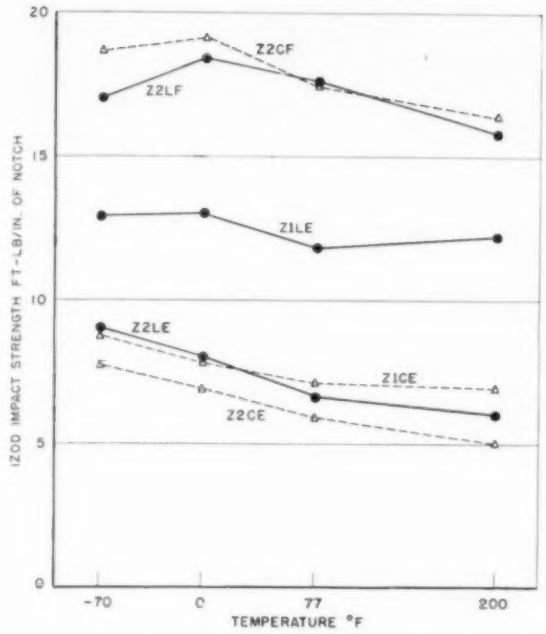

FIGURE 10. *Variation of Izod impact strength with temperature for rayon-cotton-fabric phenolic laminate.*

Z1, Sheet ¼ in. thick; *Z2*, sheet ½ in. thick; *LF*, lengthwise specimens tested flatwise; *LE*, lengthwise specimens tested edgewise; *CF*, crosswise specimens tested flatwise; *CE*, crosswise specimens tested edgewise.

77° F value for all orientations of specimen and directions of load employed. The corresponding range for W2, a high-pressure grade C laminate sample, was 73 to 77 percent. Little change in impact strength at 200° F compared to 77° F was observed for the cotton-fabric laminates with the exception of the I2 sample. The latter showed a steady increase in impact strength with temperature up to 200° F. These results are in good agreement with values reported for Grade C laminates by Shinn [8], who found that in flatwise tests impact strengths at −67° and 158° F were 66 and 113 percent, respectively, of the value at 77° F.

The paper, S2, and asbestos, K2, laminate samples showed less than 25-percent variation in impact strength over the range of temperature and orientations of specimen and loading investigated (table 2). The variation in impact strength was less than 10 percent for the 0.5-in.-thick paper laminate sample tested flatwise.

The temperature-impact strength trend for the high-strength-paper laminate sample agrees quite well with Shinn's data [8] for flatwise tests where a very slight increase in strength with temperature was found for the range −67° to 158° F. Meyer and Erickson [4] reported that the impact strengths for "Papreg" at the extremes of temperature were slightly less than the normal temperature values, a trend found in this laboratory only for the 0.5-in. sheet tested edgewise. In their impact tests at 158° and 200° F, Meyer and Erickson stated that the specimen was "tested at room temperature within 15 to 30 sec after removal from the conditioning medium"; this test condition is believed to introduce some uncertainty into the results.

The rayon, Z, and glass-fabric, AB, laminate samples had much higher impact strengths than the other samples and also show different impact strength versus temperature trends (fig. 8). When tested edgewise, the rayon laminate sample in both the ⅛- and ½-in. thicknesses showed a slight but steady decrease in impact strength as the temperature was varied from −70° to 200° F (fig. 10). The glass-fabric laminate sample, AB2, showed a constant trend toward higher impact strength at low temperatures. This agrees with data on glass-fabric laminates given by both Field [1] and Fuller [7]. The values for the impact strength of the glass-fabric laminate sample in this paper agree very well with the 77° F data for the same combination of cloth and resin tested by C. D. Jones [17].

The increase in the impact strength of the glass-fabric laminate sample at low temperature is anomalous; it may be related to the interlaminar shear failure that occurs in impact testing of the glass fabric. Thus, if the shear strength increases at low temperature in proportion to the increase in tensile and compressive strengths at low temperature, the impact strength as measured by the Izod method should likewise increase.

The approximate values for the percentage

changes in Izod impact strength at −70° and 200° F based on 77° F values are as follows:

Type of laminate	Change in Izod impact strength	
	−70° F	200° F
Grade C phenolic, low-pressure (L, V)	*Percent* −40	*Percent* 0 to +5
Grade C phenolic, high-pressure (W, I)	−25 to −40	+10 to +35
Rayon-fabric phenolic (Z)	0 to +35	0 to −10
High-strength-paper phenolic (S)	0 to −20	+5 to −20
Asbestos-fabric phenolic (K)	−15	−10
Glass-fabric unsaturated-polyester (AB)	+45	−5 to −15

In the tests at 200° F the specimens may have lost some moisture as compared to those tested at the lower temperatures and may have undergone further cure as a result of the heating. To obtain information relative to these effects, Izod impact specimens were tested at 77° F after being heated at 200° F for 24 hr and cooled to room temperature for 1 to 2 hr over calcium chloride in a desiccator. The results of these tests are shown in table 3. The low-pressure cotton-fabric phenolic samples, L2 and V2, were about 10 percent weaker and the glass-fabric laminate, sample AB2, about 10 percent stronger after the 200° F heating. A decrease of 10 percent in impact strength was noted for the rayon laminate, Z2. No definite effect of the heating on the strength of the other samples was noted.

TABLE 3. *Effect of heating at 200° F for 24 hr on Izod impact strengths of ½-in.-thick laminates* [a]

Material designation	Orientation of specimen	Direction of load	Impact strength [b]	
			No heating [c]	Heated at 200° F [d]
			ft-lb/in. of notch	*ft-lb/in. of notch*
L2, Low-pressure cotton-fabric phenolic	Lengthwise	Edgewise	3.22 ±0.03	2.88 ±0.04
	Crosswise	do	3.09 ± .01	2.85 ± .02
V2, Low-pressure Grade C phenolic	Lengthwise	Flatwise	6.57 ± .14	5.95 ± .21
	Crosswise	do	6.26 ± .13	5.55 ± .10
W2, High-pressure Grade C phenolic	Crosswise	Flatwise	5.27 ± .37	4.93 ± .12
I2, Grade C phenolic	Lengthwise	Flatwise	5.06 ± .14	5.13 ± .13
	Crosswise	do	4.03 ± .05	4.21 ± .07
Z2, Rayon-cotton-fabric phenolic	Lengthwise	Flatwise	17.6 ± .6	16.0 ± .4
	Crosswise	do	17.4 ± .7	15.8 ±1.0
S2, High-strength-paper phenolic	Lengthwise	Flatwise	4.18 ± .10	4.02 ±0.18
	Crosswise	do	4.17 ± .14	4.29 ± .20
K2, Asbestos-fabric phenolic	Lengthwise	Edgewise	3.84 ± .03	3.86 ± .06
	Crosswise	do	1.60 ± .05	1.48 ± .03
AB2, Glass-fabric unsaturated-polyester	Lengthwise	Flatwise	31.5 ± 6	35.5 ± .8

[a] The tests were made in accordance with method 1071, Federal Specification L–P–406a.

[b] Mean value for 9 to 12 specimens for all materials except glass-fabric laminate AB2, for which 20 to 25 specimens were tested. The accompanying plus or minus value is the standard error.

[c] Specimens conditioned and tested at 77° F and 50 % relative humidity. Data from table 2.

[d] Specimens tested at 77° F after being allowed to cool to room temperature for 1 to 2 hr in a desiccator containing calcium chloride.

2. Flexural Properties

The flexural properties of some of the laminates tested flatwise at 77° F were approximately as follows:

Type of laminate	Flexural strength	Initial flexural modulus of elasticity
	10^3 lb/in.²	*10^6 lb/in.²*
Grade C phenolic, low-pressure (L, V)	16	0.80
Grade C phenolic, high-pressure (W, I)	18 to 22	1.0 to 1.1
Rayon-cotton-fabric phenolic (Z)	34	1.6
High-strength-paper phenolic (S)	33	2.4
Asbestos-fabric phenolic (K)	[a] 16 (L) 9 (C)	[a] 1.2 (L) 1.0 (C)
Glass-fabric unsaturated-polyester (U, AB)	55 (L) 45 (C)	2.5 to 2.9

[a] L=lengthwise; C=crosswise.

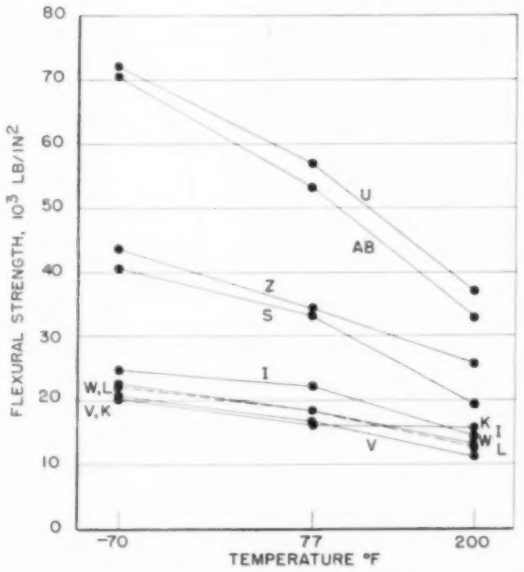

FIGURE 11. *Variation of flexural strength with temperature for ½-in.-thick laminates.*

Lengthwise specimens tested flatwise. Span-depth ratio 8:1. I, Grade C phenolic; *K*, asbestos-fabric phenolic; *L*, low-pressure cotton-fabric phenolic; *S*, high-strength-paper phenolic; *U*, glass-fabric unsaturated-polyester; *V*, low-pressure Grade C phenolic; *W*, high-pressure Grade C phenolic; *Z*, rayon-cotton-fabric phenolic; *AB*, glass-fabric unsaturated-polyester.

(a) Temperature Dependence

The variation of the flexural properties of the samples with temperature is shown graphically in figure 11 to 21.

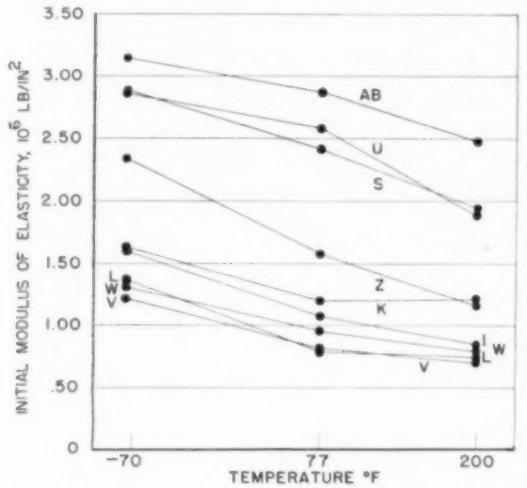

FIGURE 12. *Variation of initial flexural modulus of elasticity with temperature for ½-in.-thick laminates.*

Lengthwise specimens tested flatwise. Span-depth ratio 8:1. *I*, Grade C phenolic; *K*, asbestos-fabric phenolic; *L*, low-pressure cotton-fabric phenolic; *S*, high-strength-paper phenolic; *U*, glass-fabric unsaturated-polyester; *V*, low-pressure Grade C phenolic; *W*, high-pressure Grade C phenolic; *Z*, rayon-cotton-fabric phenolic; *AB*, glass-fabric unsaturated-polyester.

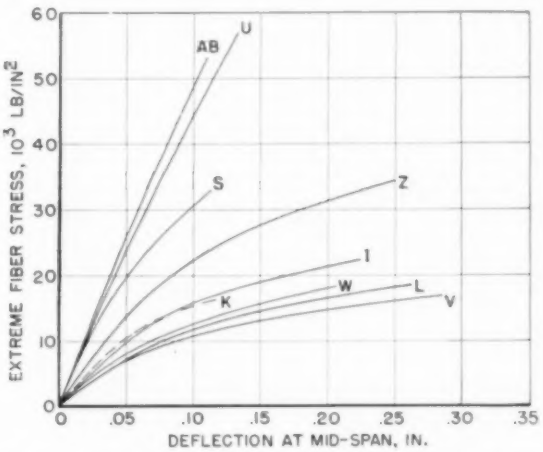

FIGURE 13. *Flexural stress-deflection curves for ½-in.-thick laminates at 77° F.*

Lengthwise specimens tested flatwise. Span-depth ratio 8:1. *I*, Grade C phenolic; *K*, asbestos-fabric phenolic; *L*, low-pressure cotton-fabric phenolic; *S*, high-strength-paper phenolic; *U*, glass-fabric unsaturated-polyester; *V*, low-pressure Grade C phenolic; *W*, high-pressure Grade C phenolic; *Z*, rayon-cotton-fabric phenolic; *AB*, glass-fabric unsaturated-polyester.

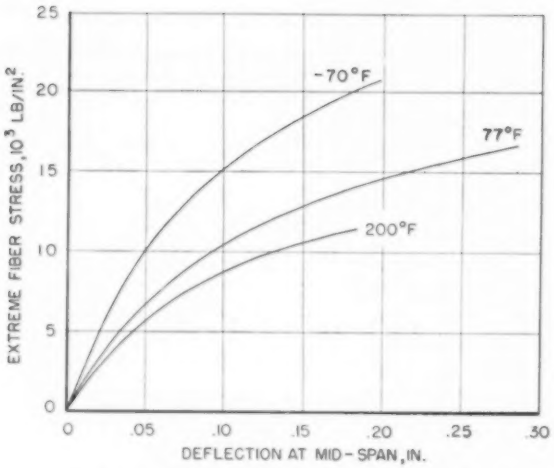

FIGURE 14. *Flexural stress-deflection curves for low-pressure Grade C cotton-fabric phenolic laminate, V2.*

Lengthwise specimens tested flatwise. Span-depth ratio 8:1. Initial modulus of elasticity: −70° F, 1,220,000 lb/in.^{2}; 77° F, 820,000 lb/in.^{2}; 200° F, 710,000 lb/in.^{2}

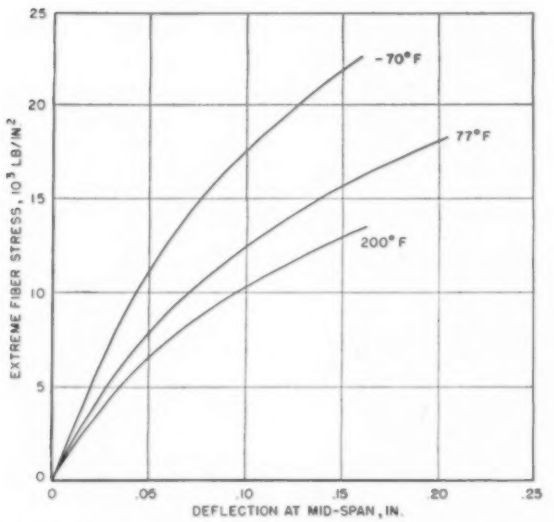

FIGURE 15. *Flexural stress-deflection curves for high-pressure Grade C cotton-fabric phenolic laminate, W2.*

Lengthwise specimens tested flatwise. Span-depth ration 8:1. Initial modulus of elasticity: −70° F, 1,310,000 lb/in.^{2}; 77° F, 960,000 lb/in.^{2}; 200° F, 800,000 lb/in.^{2}

The four samples of cotton-fabric phenolic laminates, I2, L2, V2, and W2, exhibited quite similar properties. The flexural strength of these cotton-fabric laminates increased about 10 to 30 percent at −70° F and decreased very nearly 30

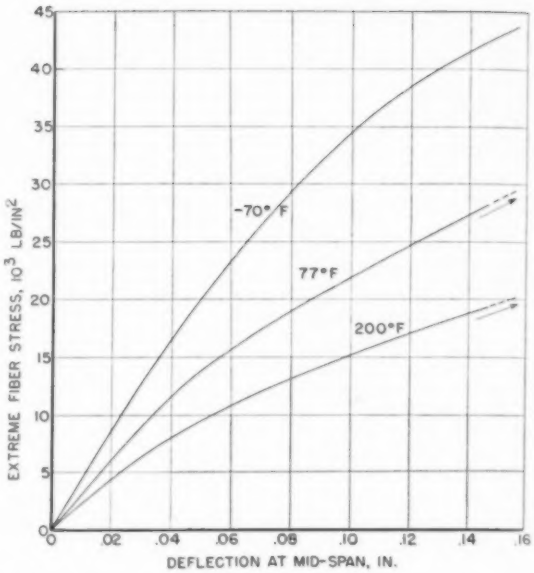

FIGURE 16. *Flexural stress-deflection curves for rayon-cotton-fabric phenolic laminate, Z2.*

Lengthwise specimens tested flatwise at three temperatures. Span-depth ration 8:1.

Temperature	Initial flexural modulus of elasticity	Flexural strength	Total deflection
°F	lb/in.^{2}	lb/in.^{2}	in.
−70	2, 340, 000	43, 700	0. 16
77	1, 580, 000	34, 400	. 25
200	1, 160, 000	25, 800	. 23

percent at 200° F, compared to the 77° F values (fig. 11). Corresponding changes for the initial modulus of elasticity (fig. 12) were increases of 40 to 80 percent at −70° F and moderate decreases up to about 25 percent at 200° F. The variations of secant modulus values with temperature were greater than for the initial modulus of elasticity.

These results are in fair agreement with data for grade C phenolic laminate given by Oberg, Schwartz, and Shinn [2]. They observed increases in flexural strength and flexural modulus of elasticity of about 17 percent at −38° F compared to values at 78° F and 40-percent relative humidity. Witt, Wolfe, and Rust [6] reported a 20-percent increase in flexural strength and 35-percent increase in modulus of elasticity at −70° F for eleven Grade C materials based on values at 77° F and 50-percent relative humidity.

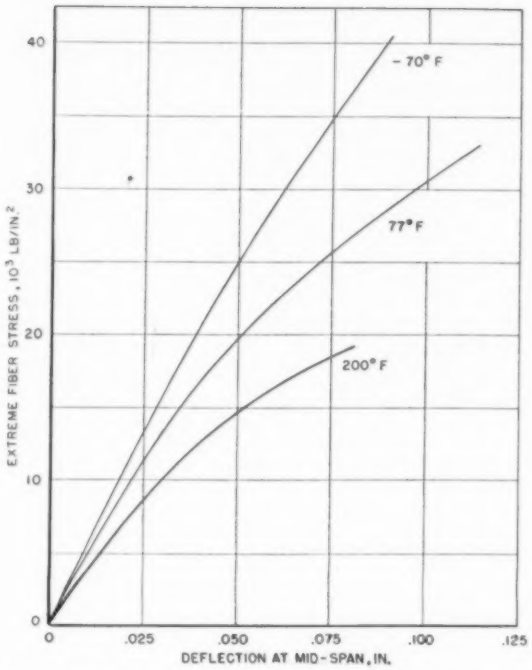

FIGURE 17. *Flexural stress-deflection curves for high-strength-paper phenolic laminate, S2.*

Lengthwise specimens tested flatwise. Span-depth ration 8:1. Initial modulus of elasticity: −70° F, 2,880,000 lb/in.^{2}; 77° F, 2,420,000 lb/in.^{2}; 200° F, 1,950,000 lb/in.^{2}

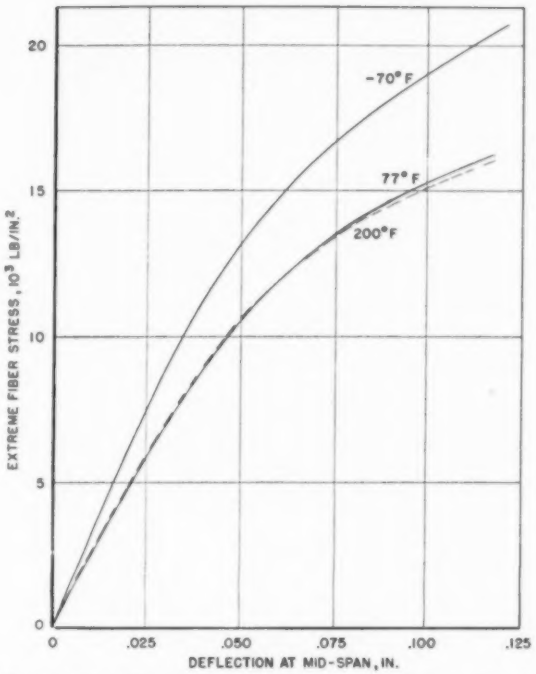

FIGURE 18. *Flexural stress-deflection curves for Grade AA asbestos-fabric phenolic laminate, K2.*

Lengthwise specimens tested flatwise. Span-depth ratio 8:1. Initial modulus of elasticity: −70° F, 1,640,000 lb/in.^{2}; 77° F, 1,200,000 lb/in.^{2}; 200° F, 1,220,000 lb/in.^{2}

The flexural strength and initial flexural modulus of elasticity of the paper phenolic laminate, S2, varied with temperature in a manner similar to the values for the cotton-fabric laminates, except that the initial modulus of elasticity increased only 20 percent between 77° and −70° F. Meyer and Erickson [4] reported that the flexural strength and flexural modulus of elasticity for high-strength-paper phenolic laminate decreased at elevated temperatures and increased at subnormal temperatures. The magnitudes of the changes that they recorded agree fairly well with the data given in this report. In tests at the Naval Air Experimental Station [5] on a phenolic material laminated with a spruce sulfite paper, probably of the high-strength type, it was noted that the flexural strength and flexural modulus of elasticity at 160° F were about a third less than at 77° F.

The variation of the flexural properties of the Grade AA asbestos-fabric-laminate, K2, with temperature was less than that of the cotton-fabric

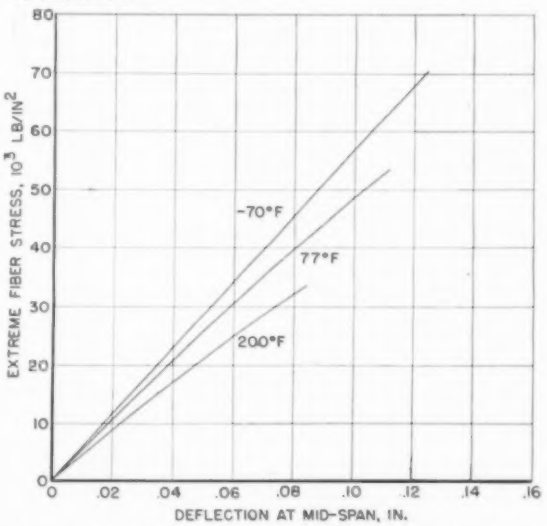

FIGURE 19. *Flexural stress-deflection curves for glass-fabric laminate, AB2.*

Lengthwise specimens tested flatwise. Span-depth ratio 8:1. Initial flexural modulus of elasticity: −70° F, 3,150,000 lb/in.^{2}; 77° F, 2,880,000 lb./in.^{2}; 200° F, 2,480,000 lb./in.^{2}

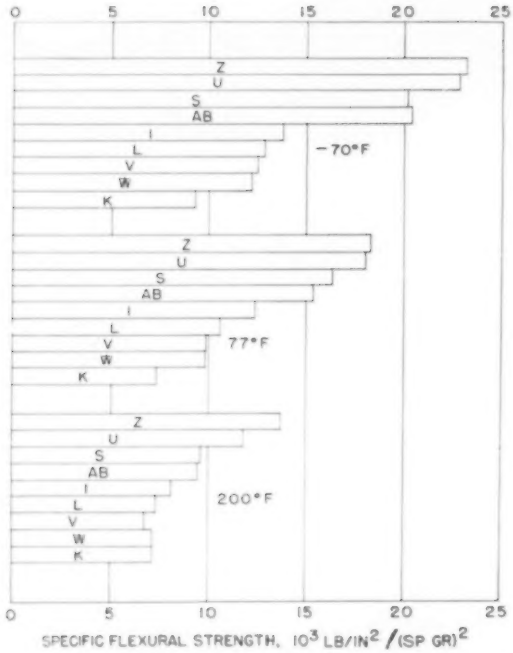

FIGURE 20. *Comparison of specific flexural strength of ½-in.-thick laminates at three temperatures.*

Lengthwise specimens tested flatwise. Span-depth ratio 8:1. *I*, Grade C phenolic; *K*, asbestos-fabric phenolic; L, low-pressure cotton-fabric phenolic; *S*, high-strength-paper phenolic; *U*, glass-fabric unsaturated-polyester; *V*, low-pressure Grade C phenolic; *W*, high-pressure Grade C phenolic; Z, rayon-cotton-fabric phenolic; *AP*, glass-fabric unsaturated-polyester.

laminates and the trend is different. Most of the change in flexural properties of the asbestos-fabric laminate occurred between 77° and −70° F; the flexural strength and initial modulus of elasticity increased roughly 20 and 35 percent of the 77° F values, respectively, at −70° F. The average change in flexural properties at 200° F was not over 5 percent. The stress-deflection curves for this material (fig. 18) indicate the similarity between the properties at 77° and 200° F.

The two glass-fabric laminates, U2 and AB2, showed the same trend in change of flexural strength and modulus of elasticity with temperature (figs. 11, 12, 19). The flexural strength increased about one-third at −70° F and decreased about one-third at 200° F. The flexural strengths of the two materials did not differ significantly. The AB2 sample was superior to the U2 sample in flexural modulus of elasticity, having greater values at all temperatures and for all directions of testing. The percentage decrease in modulus of elasticity at 200° F was less for the AB2 than for the U2 sample.

For both glass-fabric laminates the stress-deflection diagrams were less curved than for any other samples tested. In the lengthwise and crosswise directions the secant modulus of elasticity for the range 0 to 25,000 lb/in.^{2} showed a decrease of less than 10 percent from the initial modulus of elasticity at all the temperatures.

The approximate values for the percentage changes in flexural strength and flexural modulus of elasticity at −70° and 200° F, based on 77° F values, for the lengthwise and crosswise directions of the laminates investigated may be summarized as follows:

Type of laminate	Change in flexural strength		Change in initial flexural modulus of elasticity	
	−70° F	200° F	−70° F	200° F
	Percent	*Percent*	*Percent*	*Percent*
Grade C phenolic (L, V, W, I)	10 to 30	−30	40 to 80	−8 to −25
Rayon-cotton-fabric phenolic (Z)	30	−25	40	−30
High-strength-paper phenolic (S)	25	−40	20	−18
Asbestos-fabric phenolic (K)	20	−5	35	0
Glass-fabric unsaturated-polyester (U, AB)	30	−30 to −35	10 to 15	−15 to −25

(b) Effects of Other Environmental Conditions

Flexural tests were also made at 77° F on specimens heated at 200° F for 24 hr to determine whether changes in the strength properties occurred in the 200° F tests. Such changes may be brought about by (a) additional cure of the resin, (b) loss of moisture, (c) deterioration of the filler if organic, or (d) a combination of these factors. The results of these tests and of tests on unheated specimens are shown in table 4. The flexural strength values showed an average decrease of about 8 to 13 percent for the cotton-fabric and

TABLE 4. *Effect of heating at 200° F for 24 hr on flexural properties of ¼-in.-thick laminates* [a]

Material designation	Orientation of specimen	Direction of load	Flexural strength		Flexural modulus of elasticity			
					Initial		Secant	
			No heating [b]	Heated at 200° F [c]	No heating [b]	Heated at 200° F [c]	No heating [b]	Heated at 200° F [c]
			10^3 lb/in.^{2}	10^3 lb/in.^{2}	10^6 lb/in.^{2}	10^6 lb/in.^{2}	10^6 lb/in.^{2}	10^6 lb/in.^{2}
							0 to 10,000 LB/IN.^{2}	
L2, Low-pressure cotton-fabric phenolic	Crosswise	Flatwise	18.1±0.2	15.4±0.1	0.80±0.01	0.86±0.01	0.67±0.01	0.72±0.01
	do	Edgewise	17.5± .4	15.7± .1	.76± .02	.88± .01	.64± .01	.72± .01
V2, Low-pressure Grade C phenolic	Lengthwise	Flatwise	16.7± .3	14.7± .2	.82± .01	.79± .01	.58± .01	.56± .01
	Crosswise	do	16.3± .2	14.6± .2	.81± .02	.77± .01	.59± .02	.59± .01
	Lengthwise	Edgewise	16.3± .1	14.7± .1	.79± .01	.74± .01	.58± .01	.56± .01
	Crosswise	do	16.5± .2	14.5± .5	.79± .01	.74± .02	.60± .01	.59± .01
W2, High-pressure Grade C phenolic	Lengthwise	Flatwise	18.3± .4	16.9± .4	.96± .02	.89± .02	.76± .02	.76± .03
	Crosswise	do	18.4± .2	17.2± .2	.99± .02	.91± .03	.79± .02	.79± .03
	Lengthwise	Edgewise	17.9± .1	16.5± .2	1.00± .03	.91± .01	.78± .02	.78± .02
	Crosswise	do	18.0± .1	16.3± .2	1.03± .02	.94± .02	.81± .02	.81± .02
I2, Grade C phenolic	Crosswise	Flatwise	20.7± .3	18.8± .2	1.07± .07	1.07± .02	1.02± .04	.99± .02
	Lengthwise	Edgewise	21.2± .2	19.7± .3	1.14± .03	1.11± .03	1.09± .02	1.04± .01
							0 to 15,000 LB/IN.^{2}	
Z2, Rayon-cotton-fabric phenolic	Lengthwise	Flatwise	34.4± .5	31.0± .4	1.58± .02	1.71± .01	1.42±0.03	1.56±0.004
	Crosswise	do	32.7± .5	30.8± .7	1.40± .01	1.39± .02	1.25± .02	1.24± .02
S2, High-strength-paper phenolic	Lengthwise	Flatwise	33.2± .4	27.2± .6	2.42± .02	2.43± .02	2.28± .01	2.23± .01
	Crosswise	Edgewise	33.6± .4	30.4± .1	2.71± .06	2.88± .05	2.60± .06	2.64± .02
							0 to 7,500 LB/IN.^{2}	
K2, Asbestos-fabric phenolic	Crosswise	Flatwise	8.9± .2	9.6± .1	0.99± .01	1.11± .01	0.92±0.01	1.04±0.02
	do	Edgewise	9.4± .1	9.9± .2	.97± .02	1.07± .01	.90± .02	0.99± .02
							0 to 20,000 LB/IN.^{2}	
U2, Glass-fabric unsaturated-polyester	Crosswise	Flatwise	45.1± .7	53.0± .3	2.45± .01	2.55± .01	2.35±0.02	2.48±0.01
	do	Edgewise	48.6± .5	51.3± .5	2.43± .02	2.52± .03	2.37± .03	2.46± .03
AB2, Glass-fabric unsaturated-polyester	Lengthwise	Flatwise	53.2± .1	57.8± .7	2.88± .01	2.91± .04	2.80± .02	2.80± .02

[a] Tests were made in accordance with method 1031, Federal Specification L–P–406a, using an 8:1 span-depth ratio. Each value in the table represents the mean for five specimens. The accompanying plus or minus value is the standard error.

[b] Specimens conditioned and tested at 77° F and 50% relative humidity.

[c] Specimens tested at 77° F after being allowed to cool to room temperature for 1 to 2 hr in a desiccator containing calcium chloride.

paper laminates. The changes in the flexural moduli of elasticity were small and not consistent except for the low-pressure sample, L2, which exhibited increases of 10 percent after heating. The glass-fabric laminate, U2, exhibited average increases of 11 and 4 percent, respectively, in flexural strength and moduli of elasticity on heating. The asbestos-fabric laminate, K2, also exhibited higher flexural properties after heating, the increases in flexural strength and moduli of elasticity being about 7 and 12 percent, respectively.

It seems reasonable that the strength and modulus of elasticity values of these organic plastics should diminish with increase in temperature if no change in composition or structure takes place. If heating a laminate at 200° F for 24 hr causes an increase in the strength properties due to a change in composition or structure, then in the flexural tests at 200° F (table 4) the effects of prolonged heating and of an elevated test temperature may oppose one another. This may explain the very small differences between the flexural properties at 77° and 200° F (fig. 18) for the asbestos-fabric laminate, which had increased flex-

ural properties at 77° F after heating (table 4). The effect of prolonged heating on the flexural strength of laminates was investigated by Hausmann, Parkinson, and Mains [18]. They found that the flexural strength of Grades C, X, and XXX phenolic laminates at 190° F increased with the length of time the specimens were at the test temperature (see table 1, [18]). For the Grade XXX laminate, the flexural strength values at 194° F after a month of heating were nearly equal to the 77° F values on unheated specimens.

Flexural strength tests were made on six samples at 150° F and 90-percent relative humidity after 24 hr of conditioning at the test temperature, combining the effects of elevated temperature and high relative humidity. The results of these tests are given in table 5, together with corresponding data for the 77° and 200° F tests.

The deleterious effect of these extreme conditions was most pronounced for the paper laminate,

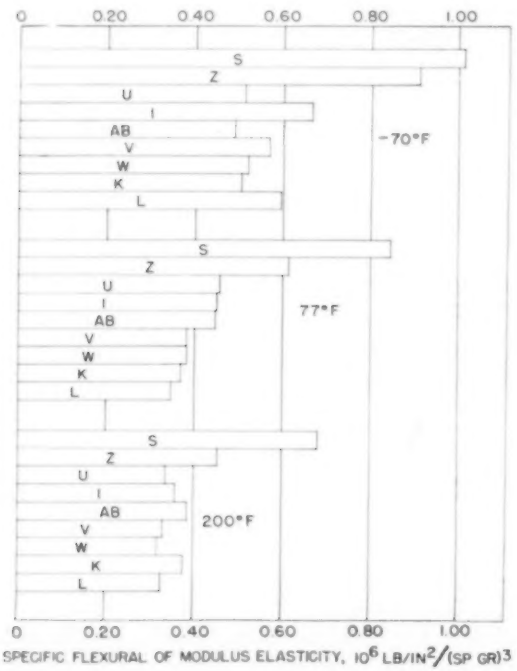

FIGURE 21. *Comparison of specific flexural modulus of elasticity of ½-in.-thick laminates at three temperatures.*

Lengthwise specimens tested flatwise. Span-depth ratio 8:1. *J*, Grade C phenolic; *K*, asbestos-fabric phenolic; *L*, low-pressure cotton-fabric phenolic; *S*, high-strength-paper phenolic; *U*, glass-fabric unsaturated-polyester; *V*, low-pressure Grade C phenolic; *W*, high-pressure Grade C phenolic; *Z*, rayon-cotton-fabric phenolic; *AB*, glass-fabric unsaturated-polyester.

TABLE 5. *Flexural strength of ½-in.-thick laminates at various temperatures and relative humidities* [a]

Material designation	Flexural strength at—		
	77° F, 50-percent relative humidity [b]	150° F, 90-percent relative humidity [c]	200° F, < 6-percent relative humidity [d]
	10^3 lb/in.^{2}	10^3 lb/in.^{2}	10^3 lb/in.^{2}
V2, Low-pressure Grade C phenolic	16.7 ±0.3	7.0 ±0.1	11.4 ±0.2
W2, High-pressure Grade C phenolic	18.3 ± .4	15.4 ± .3	13.3 ± .2
I2, Grade C phenolic	22.2 ± .3	19.8 ± .2	14.5 ± .1
Z2, Rayon-cotton-fabric phenolic	34.4 ± .5	26.0 ± .3	25.8 ± .5
S2, High-strength-paper phenolic	33.2 ± .4	13.2 ± .6	19.4 ± .2
AB2, Glass-fabric unsaturated-polyester	53.2 ± .1	34.7 ± .4	33.8 ± .8

[a] Lengthwise specimens tested flatwise. Tests were made in accordance with method 1031, Federal Specification L-P-406a, using an 8:1 span-depth ratio. Each value in the table represents the mean for 5 specimens. The accompanying plus or minus value is the standard error.

[b] Specimens conditioned and tested at 77° F and 50% relative humidity.

[c] Specimens tested at 150° F and 90% relative humidity after 24 hr at the test conditions.

[d] Specimens tested at 200° F and less than 6% relative humidity after 24 hr at the test conditions.

sample S2, and the low-pressure Grade C laminate, V2. The other four samples were not so greatly affected by these conditions as they were by 24 hr at 200° F and a low relative humidity. The effect of moisture content on the strength properties of high-strength-paper laminate was studied by Erickson and Mackin [19]. They tested specimens from a series of panels conditioned 100 days at 80° F at various relative humidities. They found decreases in ultimate strength in tension, compression, and flexure of 25 percent or more and decreases of about 35 percent in modulus of elasticity as the relative humidity was varied from 30 to 97 percent, corresponding to moisture contents ranging from 0.2 to 9.5 percent.

The above results and the results obtained in this laboratory indicate the necessity for studying the effect of relative humidity as well as temperature on the strength properties of laminates, especially those with cellulosic fillers.

(c) Strength-Density Considerations

When the density is considered in evaluating the flexural properties of these samples, the cellulose laminates, with lower densities than the mineral laminates, compare more favorably with the latter materials and are superior in some

TABLE 6. *Effect of span-depth ratio on flexural properties of ½-in.-thick laminates* [a]

Material designation	Orientation of specimen	Direction of load	Flexural strength at span-depth ratio:		Flexural modulus of elasticity			
					Initial modulus of elasticity at span-depth ratio:		Secant modulus of elasticity at span-depth ratio:	
			8:1	16:1	8:1	16:1	8:1	16:1
			10^3 lb/in.^{2}	10^3 lb/in.^{2}	10^6 lb/in.^{2}	10^6 lb/in.^{2}	10^6 lb/in.^{2}	10^6 lb/in.^{2}
							0 TO 10,000 LB/IN.^{2}	
L2, Low-pressure cotton-fabric phenolic	Lengthwise	Flatwise	18.4±0.2		0.80±0.01		0.67±0.01	
	Crosswise	do	18.1± .2		.80± .01		.67± .01	
	Lengthwise	Edgewise	17.5± .2		.78± .01		.65± .01	
	Crosswise	do	17.5± .4	16.5±0.2	.76± .02	0.87±0.01	.64± .01	0.64±0.01
V2, Low-pressure Grade C phenolic	Lengthwise	Flatwise	16.7± .3	15.3± .1	.82± .01	.84± .01	.58± .01	.56± .01
	Crosswise	do	16.3± .2	15.0± .2	.81± .02	.82± .01	.59± .02	.54± .02
	Lengthwise	Edgewise	16.3± .1	15.2± .2	.79± .01	.84± .02	.58± .01	.58± .01
	Crosswise	do	16.5± .2	14.8± .1	.79± .01	.80± .01	.60± .01	.54± .01
W2, High-pressure Grade C phenolic	Lengthwise	Flatwise	18.3± .4	17.1± .2	.96± .02	1.03± .03	.76± .02	.78± .04
	Crosswise	do	18.4± .2	17.4± .1	.99± .02	1.02± .05	.79± .02	.76± .06
	Lengthwise	Edgewise	17.9± .1	17.1± .1	1.00± .03	1.01± .02	.78± .02	.76± .04
	Crosswise	do	18.0± .1	16.6± .1	1.03± .02	1.00± .04	.81± .02	.74± .06
I2, Grade C phenolic	Lengthwise	Flatwise	22.2± .3	20.9± .1	1.08± .02	1.24± .02	1.07± .02	1.10± .02
	Crosswise	do	20.7± .3	19.7± .3	1.07± .07	1.22± .03	1.02± .04	1.08± .02
	Lengthwise	Edgewise	21.2± .2	19.8± .2	1.14± .03	1.30± .08	1.09± .02	1.09± .02
	Crosswise	do	21.4± .4	19.5± .1	1.11± .08	1.31± .04	1.04± .07	1.07± .03
							0 TO 15,000 LB/IN.^{2}	
Z2, Rayon-cotton-fabric phenolic	Lengthwise	Flatwise	34.4± .5	35.0± .4	1.58± .02	1.76± .03	1.42±0.03	1.58±0.03
	Crosswise	do	32.7± .5	30.4± .3	1.40± .01	1.42± .02	1.25± .02	1.20± .04
	Lengthwise	Edgewise	33.4± .5	31.9± .3	1.57± .03	1.66± .02	1.43± .03	1.47± .01
	Crosswise	do	31.7± .2	29.1± .4	1.50± .01	1.48± .04	1.37± .01	1.21± .04
							0 TO 20,000 LB/IN.^{2}	
S2, High-strength-paper phenolic	Lengthwise	Flatwise	33.2± .4	32.4± .2	2.42± .02	2.54± .02	2.10±0.01	2.15±0.03
	Crosswise	do	34.2± .6	32.4± .5	2.30± .02	2.52± .03	2.05± .01	2.12± .02
	Lengthwise	Edgewise	33.5± .5	32.6± .4	2.65± .03	2.57± .04	2.31± .01	2.17± .02
	Crosswise	do	33.6± .4	31.8± .5	2.71± .06	2.54± .03	2.35± .05	2.12± .04
							0 TO 5,000 LB/IN.^{2}	
K2, Asbestos-fabric phenolic	Lengthwise	Flatwise	16.3± .6		1.20± .02		1.20±0.02	
	Crosswise	do	8.9± .2		.90± .01		.99± .01	
	Lengthwise	Edgewise	16.4± .2		1.15± .02		1.15± .02	
	Crosswise	do	9.4± .1	9.0± .1	.97± .02	1.06± .02	.97± .02	1.02±0.02
							0 TO 20,000 LB/IN.^{2}	
U2, Glass-fabric unsaturated-polyester	Lengthwise	Flatwise	56.9± .1	55.7± .7	2.50± .02	2.82± .05	2.57±0.02	2.70±0.05
	Crosswise	do	45.1± .7	44.5± .4	2.45± .01	2.56± .02	2.35± .02	2.39± .02
	Lengthwise	Edgewise	54.8± .9	54.2± .5	2.70± .03	2.80± .02	2.67± .03	2.71± .02
	Crosswise	do	48.6± .5	45.1± .4	2.43± .03	2.57± .02	2.37± .03	2.40± .02
							0 TO 15,000 LB/IN.^{2}	
AB2, Glass-fabric unsaturated-polyester	Lengthwise	Flatwise	53.2± .1	52.1± .5	2.88± .01	3.14± .02	2.80±0.02	2.97±0.03
	Crosswise	do	46.0± .7		2.84± .03		2.61± .01	
	Lengthwise	Edgewise	60.8± .5	57.9± .8	2.89± .02	3.18± .04	2.87± .01	2.95± .03
	Crosswise	do	53.5± .7		2.82± .02		2.66± .01	

[a] Specimens were conditioned and tested at 77° F and 50% relative humidity in accordance with Method 1031, Federal Specifications L–P–406a. Each value in the table represents the mean for 5 to 10 specimens. The accompanying plus or minus value is the standard error.

instances. This may be seen by comparing figures 20 and 21 with figures 11 and 12. Figures 20 and 21 also show that there is no difference in specific strength properties between the low-pressure and high-pressure laminates, V2 and W2, made with the same Grade C fabric. When comparisons are based on density, the flexural strength and stiffness of the asbestos-fabric laminate, K2, are greater than those of the cotton-fabric laminates at 200° F.

(d) Effect of Span-Depth Ratio

The results of tests made at 77° F using span-depth ratios of 16:1 and 8:1 are given in table 6. The flexural strength obtained with a 16:1 span-depth ratio was slightly less for all samples, the decreases ranging from about 2 percent for the glass-fabric laminate, U2, to about 7 percent for the cotton-fabric phenolic laminates. The initial flexural modulus of elasticity values were usually a little greater for the tests with the larger span-depth ratio. The I2 material, a high-pressure phenolic Grade C laminate, showed significant changes in both flexural strength and initial modulus of elasticity with the change in span-depth ratio.

3. Tensile Properties

The results of the tensile tests of the plastic laminates at temperatures of −70°, 77°, and 200° F are shown in figures 22 to 30.

The tensile properties of representative laminates at 77° F are approximately as follows:

Type of laminate	Tensile strength	Tensile secant modulus of elasticity for lowest stress range in table 8
	10^3 lb/in.²	10^6 lb/in.²
Grade C phenolic, low-pressure (V)	9	0.8
Grade C phenolic, high-pressure (W)	10.5	1.0
Rayon-cotton-fabric phenolic (Z)	* 32 (L) 26 (C)	* 1.9 (L) 1.2 (C)
High-strength-paper phenolic (S)	30	2.6
Asbestos-fabric phenolic (K)	8 (L) 5 (C)	1.5 (L) 1.2 (C)
Glass-fabric unsaturated-polyester (AB)	43 (L) 33 (C)	3.0 (L) 2.6 (C)

* L=lengthwise; C=crosswise.

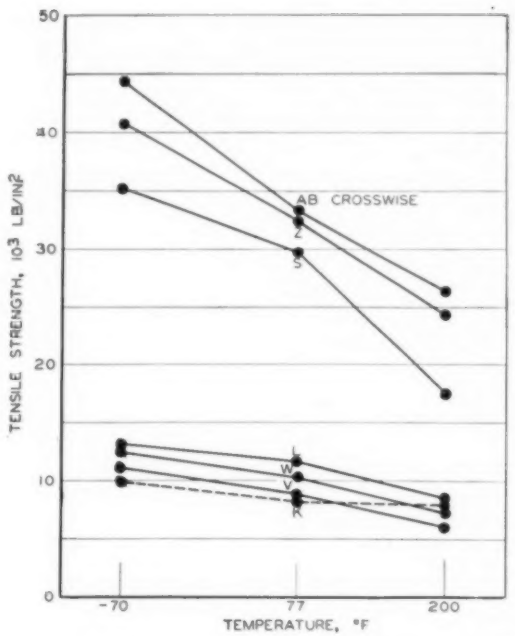

FIGURE 22. *Variation of tensile strength with temperature for ⅛-in.-thick laminates.*

Lengthwise specimens unless otherwise noted. Types of laminates shown are: *K*, asbestos-fabric phenolic; *L*, low-pressure cotton-fabric phenolic; *S*, high-strength-paper phenolic; *V*, low-pressure Grade C phenolic; *W*, high-pressure Grade C phenolic; *Z*, rayon-cotton-fabric phenolic; *AB*, glass-fabric unsaturated-polyester.

The tensile strengths and moduli of elasticity of all the samples increased at −70° F and decreased at 200° F relative to the 77° F values (figs. 22 and 23).

The three cotton-fabric phenolic laminates, L1, V1, and W1, exhibited similar changes in tensile strength properties with change in temperature. The tensile strengths of these samples increased 15 to 25 percent at −70° F and decreased 25 to 30 percent at 200° F compared to the 77° F values. Corresponding changes for the secant modulus of elasticity at 2,500 lb/in.² were increases of about 40 to 50 percent at −70° F and decreases of about 20 to 30 percent at 200° F. Witt, Wolfe, and Rust [6], in tensile tests at 77° F and 160° F on a number of samples of Grade C phenolic laminates, found average decreases in strength and modulus of elasticity of about 18 and 22 percent, respectively.

The rayon-fabric phenolic laminate, Z1, showed the greatest percentage increase (55 crosswise and 70 lengthwise) in tensile modulus of elasticity at

−70° F. Other changes in the tensile properties of this laminate were similar to those for the three cotton-fabric phenolic laminates.

Of the samples tested, the high-strength-paper phenolic laminate, S1, showed the largest percentage decrease (40%) in tensile strength at 200° F. The percentage changes in modulus of elasticity at both −70° and 200° F were less for the paper (10 to 20%) than for the other four laminates with cellulosic reinforcement.

Meyer and Erickson [4] reported that the tensile strength and modulus of elasticity for high-strength-paper laminates decreased about 35 and 15 percent, respectively, at 200° F relative to 75° F; these values agree with the data in table 8. The changes found by them at subnormal temperatures were much less than those given in this report and included slightly negative values.[3]

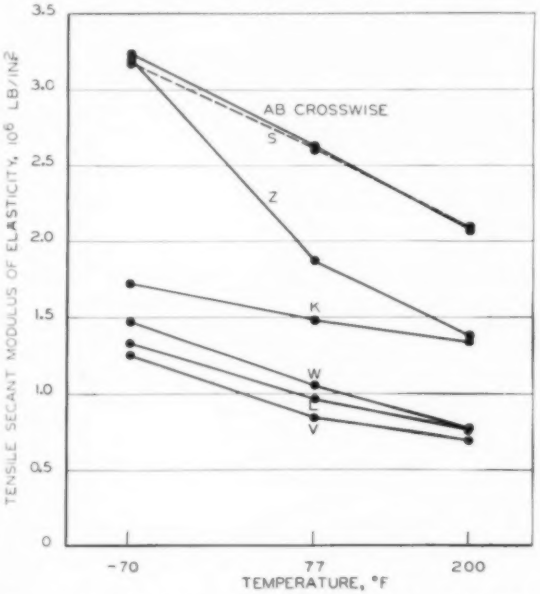

FIGURE 23. *Variation of tensile secant modulus of elasticity with temperature for ⅛-in.-thick laminates.*

Lengthwise specimens unless otherwise noted. Stress ranges: 0 to 5,000 lb/in.² for *AB*, *S*, *Z*; 0 to 2,500 lb/in.² for *K*, *W*, *L*, *V*. Types of laminates shown are: *K*, asbestos-fabric phenolic; *L*, low-pressure cotton-fabric phenolic; *S*, high-strength-paper phenolic; *V*, low-pressure Grade C phenolic; *W*, high-pressure Grade C phenolic; *Z*, rayon-cotton-fabric phenolic; *AB*, glass-fabric unsaturated-polyester.

[3] A possible reason for the small changes in both the tensile and compressive moduli of elasticity at −69° F reported by Meyer and Erickson is that their tests at the low temperature were made at a different laboratory and with different means of measuring the strain from those made at 75° F and higher temperatures. Hence the uncertainty in the changes they report for low temperatures may be somewhat greater than the uncertainty in corresponding changes obtained in this laboratory where all tests were made with the same equipment.

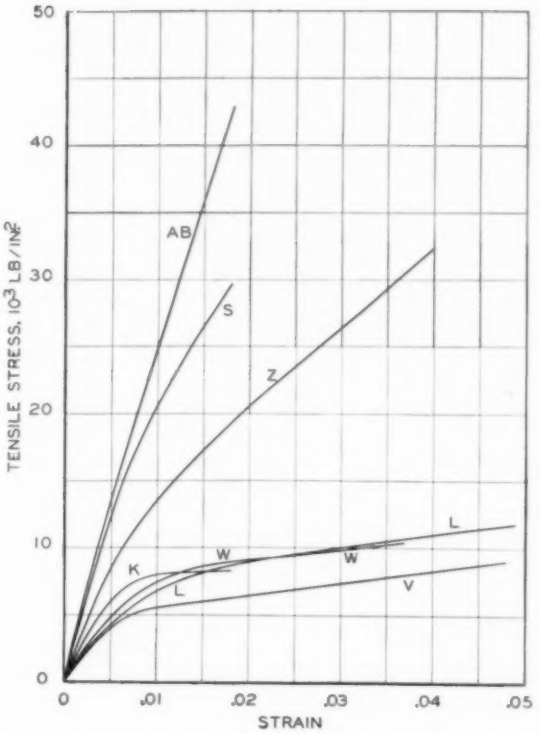

FIGURE 24. *Tensile stress-strain curves of ⅛-in.-thick laminates at 77° F.*

Lengthwise specimens. Types of laminates shown are: *AB*, glass-fabric unsaturated-polyester; *S*, high-strength-paper phenolic; *Z*, rayon-cotton-fabric phenolic; *K*, asbestos-fabric phenolic; *L*, low-pressure cotton fabric phenolic; *W*, high-pressure Grade C phenolic; *V*, low-pressure Grade C phenolic.

The material investigated by Meyer and Erickson was quite similar to that tested in this laboratory as regards resin, molding conditions, and paper base.

The asbestos-fabric laminate, K1, (fig. 33), with decreases in tensile properties of less than 10 percent at 200° F, exhibited the least change of all the samples. Witt and others [6] tested several Grade AA asbestos-fabric phenolic laminates in tension. They found that average decreases in strength and modulus of elasticity at 160° F relative to 77° F were 6 and 15 percent, respectively.

Next to the asbestos-fabric laminate, the glass-fabric laminate, AB1, (fig. 30) showed the smallest percentage loss (20%) in strength at 200° F. This change was approximately half that of the high-strength-paper laminate, S1. The glass-fabric laminate also had the highest percentage

847618—49——7

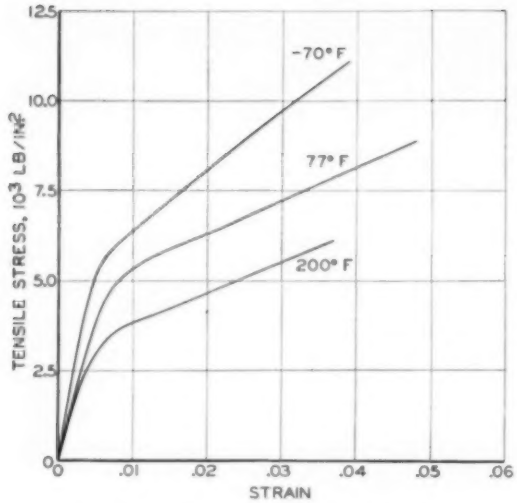

FIGURE 25. *Tensile stress-strain curves for low-pressure Grade C phenolic laminate, V1.*

Lengthwise specimens. Secant modulus of elasticity (0 to 2,500 lb/in.²): −70° F, 1,250,000 lb/in.²; 77° F, 840,000 lb/in.²; 200° F, 680,000 lb/in.²

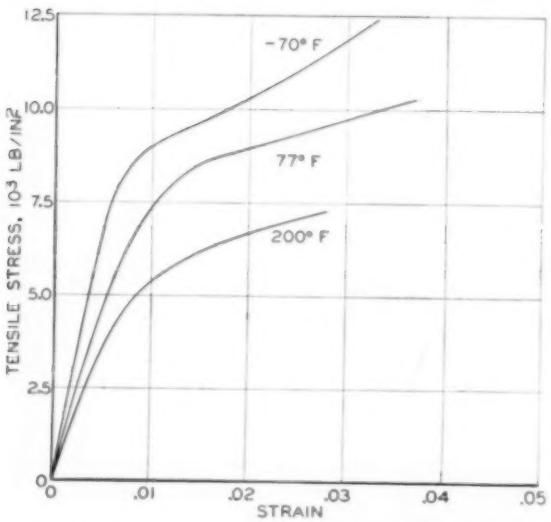

FIGURE 26. *Tensile stress-strain curves for high-pressure Grade C phenolic laminate, W1.*

Lengthwise specimens. Secant modulus of elasticity (0 to 2,500 lb/in.²): −70° F, 1,470,000 lb/in.²; 77° F, 1,050,000 lb/in.²; 200° F, 770,000 lb/in.²

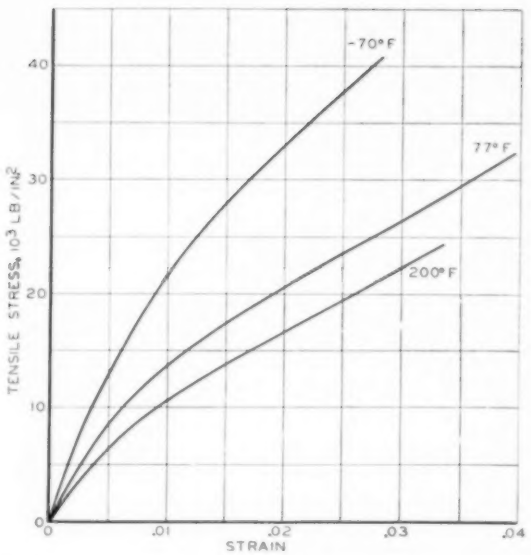

FIGURE 27. *Tensile stress-strain curves for rayon-cotton-fabric phenolic laminate, Z1.*

Lengthwise specimens. Secant modulus of elasticity (0 to 5,000 lb/in.²): −70° F, 3,200,000 lb/in.²; 77° F, 1,870,000 lb/in.²; 200° F, 1,380,000 lb/in.²

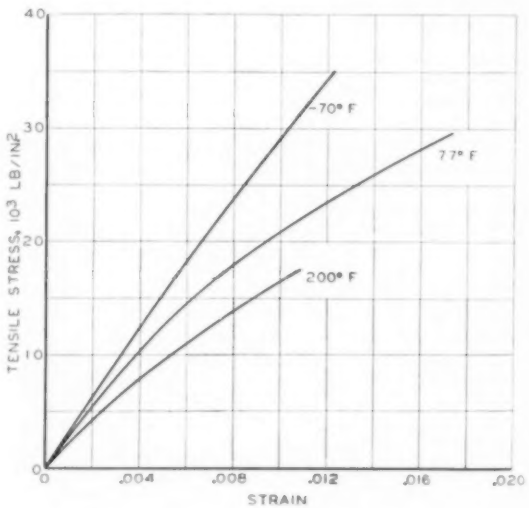

FIGURE 28. *Tensile stress-strain curves of high-strength-paper phenolic laminate, S1.*

Lengthwise specimens. Secant modulus of elasticity (0 to 5,000 lb/in.²): −70° F, 3,180,000 lb/in.²; 77° F, 2,610,000 lb/in.²; 200° F, 2,090,000 lb/in.²

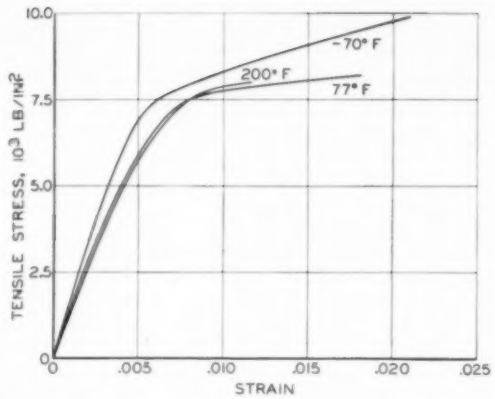

FIGURE 29. *Tensile stress-strain curves for Grade AA asbestos-fabric phenolic laminate, K1.*

Lengthwise specimens. Secant modulus of elasticity (0 to 2,500 lb/in.²): −70° F, 1,720,000 lb/in.²; 77° F, 1,480,000 lb/in.²; 200° F, 1,340,000 lb/in.²

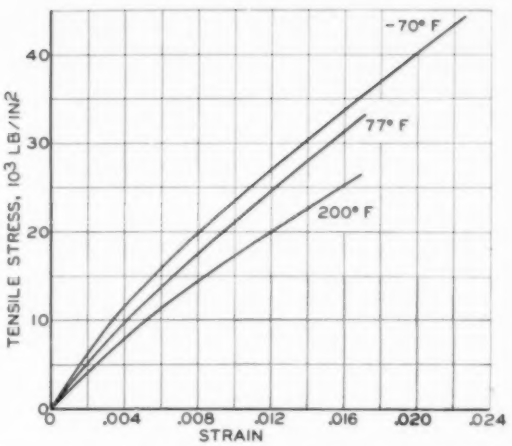

FIGURE 30. *Tensile stress-strain curves for glass-fabric unsaturated-polyester laminate, AB1.*

Crosswise specimens. Secant modulus of elasticity (0 to 5,000 lb/in.²): −70° F, 3,240,000 lb./in.²; 77° F, 2,630,000 lb/in.²; 200° F, 2,080,000 lb/in.²

increase (33%) in tensile strength at −70° F. The percentage change in the tensile modulus of elasticity of the glass-fabric laminate was about the same as for the high-strength-paper laminate at both the high and low temperatures.

The approximate values for the percentage changes in tensile strength and tensile secant modulus of elasticity at −70° and 200° F, relative to the value at 77° F for the laminates investigated, may be summarized as follows:

Type of laminate	Change in tensile strength		Change in tensile secant modulus of elasticity	
	−70° F	200° F	−70° F	200° F
	Percent	*Percent*	*Percent*	*Percent*
Grade C phenolic, low-pressure (V)	25	−30	47	−18
Grade C phenolic, high-pressure (W)	20	−30	45	−30
Rayon-cotton-fabric phenolic (Z)	25	−25	60	−30
High-strength-paper phenolic (S)	15	−40	23	−15
Asbestos-fabric phenolic (K)	15	−3	23	−10
Glass-fabric unsaturated-polyester (crosswise only) (AB)	33	−20	23	−20

The types of failure obtained in tension were similar to those shown by Findley and Worley (see fig. 49, [9]) and by Marin (see fig. 41, [10]) for the same laminates. The cotton-fabric phenolic laminates had a clean break, with the exception of the low-pressure molded laminate, V1, which also split on a central ply. The high-strength-paper laminate, S1, had a brittle and slightly jagged break. In the glass-fabric laminate AB1, the failure was very irregular and of the tongue and groove type, extending throughout the reduced section. The manner of failure in the rayon-fabric laminate, Z1, was between that of the glass-fabric and the cotton-fabric laminates.

4. Compressive Properties

The results of the compressive tests of the plastic laminates at temperatures of −70°, 77°, and 200° F are shown in figures 31 to 35.

The compressive properties of the laminates at 77° F are approximately as follows:

Type of laminate	Compressive strength	Compressive modulus of elasticity
	10^3 lb/in.^{2}	10^6 lb/in.^{2}
Grade C phenolic, low-pressure (V)	19	0.9
Grade C phenolic, high-pressure (W, I)	20 to 25	1.1 to 1.3
Rayon-cotton-fabric phenolic (Z)	24	[a] 2.0 (L) 1.9 (C)
High-strength-paper phenolic (S)	19	2.7
Asbestos-fabric phenolic (K)	21	1.5 (L) 1.2 (C)
Glass-fabric unsaturated-polyester (AB)	[a] 42 (L) 36 (C)	3.3 (L) 3.1 (C)

[a] L=lengthwise; C=crosswise.

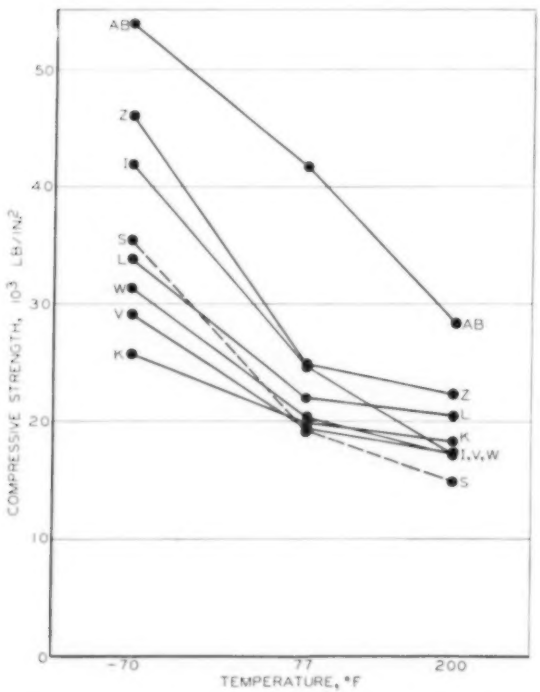

FIGURE 31. *Variation of compressive strength with temperature for ½-in.-thick laminates.*

Lengthwise specimens. Types of laminates shown are: *I*, Grade C phenolic; *K*, asbestos-fabric phenolic; *L*, low-pressure cotton-fabric phenolic; *S*, high-strength-paper phenolic; *V*, low-pressure Grade C phenolic; *W*, high-pressure Grade C phenolic; *Z*, rayon-cotton-fabric phenolic; *AB*, glass-fabric unsaturated-polyester.

The compressive strengths and moduli of elasticity of all the laminates increased at −70° F and decreased at 200° F, relative to the 77° F values (figs. 31 and 32).

The compressive strengths of the four cotton-fabric phenolic laminates increased 50 to 70 percent at −70° F and decreased 10 to 30 percent at 200° F. The compressive secant modulus of elasticity increased 30 to 60 percent at −70° F, with the greatest change in the low-pressure samples, and decreased 20 to 30 percent at 200° F. The two low-pressure cotton-fabric phenolic laminates, L2 and V2, made with the same resin, showed nearly identical variation in compressive properties with temperature. Witt, Wolfe, and Rust [6], who tested a large group of samples of Grade C phenolic laminate in compression at 77° and 160° F, found average decreases in compressive strength and modulus of elasticity of about 22 and 27 percent, respectively. Norelli and Gard [3], who tested a Grade C sample at various temperatures, indicated an increase in compressive strength of about 50 percent at −67° F and a decrease of 35 percent at 167° F, relative to 77° F.

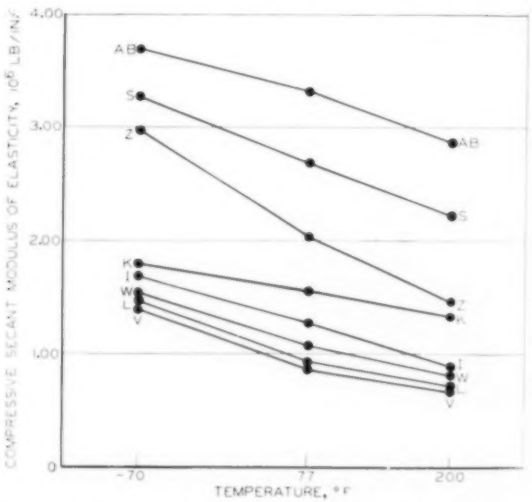

FIGURE 32. *Variation of compressive secant modulus of elasticity (0 to 2,500 lb/in.^{2}) with temperature for ½-in.-thick laminates.*

Lengthwise specimens. Types of laminates shown are: *I*, Grade C phenolic; *K*, asbestos-fabric phenolic; *L*, low-pressure cotton-fabric phenolic; *S*, high-strength-paper phenolic; *V*, low-pressure Grade C phenolic; *W*, high-pressure Grade C phenolic; *Z*, rayon-cotton-fabric phenolic; *AB*, glass-fabric unsaturated-polyester.

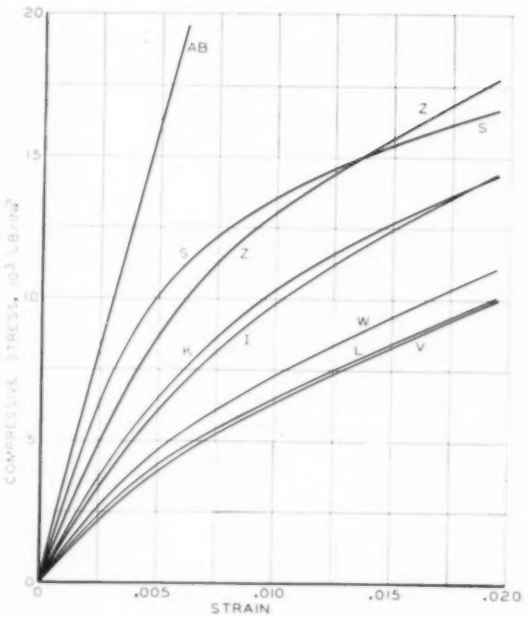

FIGURE 33. *Compressive stress-strain curves of laminates at 77° F.*

Lengthwise specimens. Types of laminates shown are: *I*, Grade C phenolic; *K*, asbestos-fabric phenolic; *L*, low-pressure cotton-fabric phenolic; *S*, high-strength-paper phenolic; *V*, low-pressure Grade C phenolic; *W*, high-pressure grade C phenolic; *Z*, rayon-cotton-fabric phenolic; *AB*, glass-fabric unsaturated polyester.

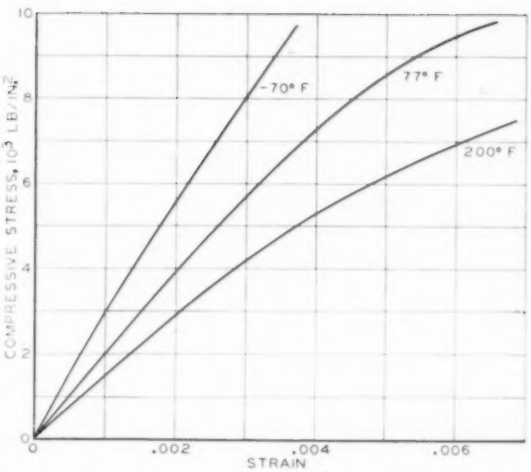

FIGURE 34. *Compressive stress-strain curves of rayon-cotton-fabric phenolic laminate, Z2.*

Lengthwise specimens.

Temperature	Secant modulus of elasticity, 0 to 2,500 lb/in.²	Compressive strength
° F	*lb/in.²*	*lb/in.²*
−70	2,970,000	46,100
77	2,030,000	24,800
200	1,460,000	22,300

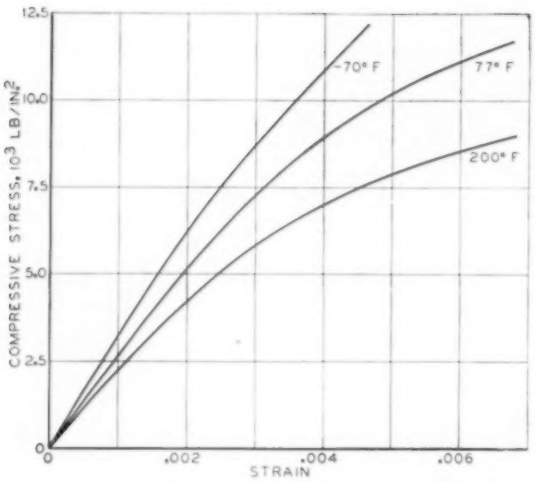

FIGURE 35. *Compressive stress-strain curves of high-strength-paper phenolic laminate, S2.*

Lengthwise specimens.

Temperature	Secant modulus of elasticity, 0 to 2,500 lb/in.^{2}	Compressive strength
° F	*lb/in.*^{2}	*lb/in.*^{2}
−70	3,270,000	35,400
77	2,680,000	19,200
200	2,220,000	14,900

The high-strength-paper, S2, and the rayon-fabric, Z2, phenolic laminates increased in compressive strength 85 percent at −70° F and decreased in compressive strength 10 to 20 percent at 200° F. The changes in compressive modulus of elasticity with temperature were less for the high-strength-paper laminate than for the other cellulose laminates, the increase at −70° F being 20 percent and the decrease at 200° F being 15 percent. The changes in compressive properties of a high-strength-paper phenolic laminate at −69° F and 200° F relative to 77° F, reported by Meyer and Erickson [4], are in good agreement with the results given in this report, except that they obtained much smaller increases in modulus of elasticity at −69° F.

The asbestos and glass laminates, K2 and AB2, in general, showed much smaller variations in compressive properties with temperature than the cellulose laminates. The changes in compressive strength and modulus of elasticity for the asbestos-fabric phenolic laminate were 30 and 15 percent, respectively, at −70° F, and −10 and −15 percent, respectively, at 200° F. The changes in the glass-fabric laminate were almost the same except for the 30-percent loss in compressive strength at 200° F.

The compressive-strength variation with temperature of the Grade AA asbestos-fabric laminate reported by Norelli and Gard [3] agrees in trend with, but differs in magnitude from, the data presented here. They obtained an increase of less than 10 percent at −67° F and a decrease of 25 percent at 167° F. No comparative data were found in the literature for a glass-fabric laminate similar to the sample, AB2.

The approximate values for the percentage changes in compressive strength and modulus of elasticity at −70° and 200° F, relative to the value at 77° F for lengthwise specimens, are as follows:

Type of laminate	Change in compressive strength		Change in compressive secant modulus of elasticity (0 to 2,500 lb/in.^{2})	
	−70° F	200° F	−70° F	200° F
	Percent	*Percent*	*Percent*	*Percent*
Grade C phenolic, low-pressure (L, V)	50	−10	60	−20
Grade C phenolic, high-pressure (W, I)	50 to 70	−15 to −30	30 to 45	−25 to −30
Rayon-cotton-fabric phenolic (Z)	85	−10	45	−30
High-strength-paper phenolic (S)	85	−20	20	−15
Asbestos-fabric phenolic (K)	30	−10	15	−15
Glass-fabric unsaturated-polyester (AB)	30	−30	10	−15

All of the cotton-fabric laminates, the asbestos-fabric and the rayon-cotton-fabric laminates failed in compression in the same manner. The break started at the top of the specimen at one edge and went downward across the machined face at an angle between 45° and 60° to the horizontal. A similar failure occurred in the low-pressure cotton-fabric laminate, except that there was splitting along a central ply. The line of failure in the high strength-paper laminate, S2, progressed from one corner to a diagonally opposite corner, partly on a 45° angle and partly by delamination. The glass-fabric laminate, AB2, failed explosively and delaminated at several places. Examples of broken compression specimens of similar laminates are shown by Findley and Worley (see fig. 50, [9]) and by Marin (see fig. 42, [10]).

5. Comparison of Temperature Dependence of Flexural, Tensile, and Compressive Properties

Figure 36 shows the percentage changes in strength and modulus of elasticity with temperature based on 77° F values for flexural, tensile, and compressive tests.

For the cellulose laminates, the percentage changes in tensile and flexural strengths with temperature for a given sample were about the same. These strength values increased 15 to 25 percent at −70° F and decreased 25 to 40 percent at 200° F. The compressive-strength behavior of the cellulose materials was different; the increases at −70° F were 50 to 85 percent, the decreases at 200° F were only 10 to 30 percent. For a given sample, the percentage increase in compressive strength at −70° F was at least double the percentage increase in flexural or tensile strength; at 200° F the percentage loss in compressive strength, in general, was half the percentage loss in flexural or tensile strength.

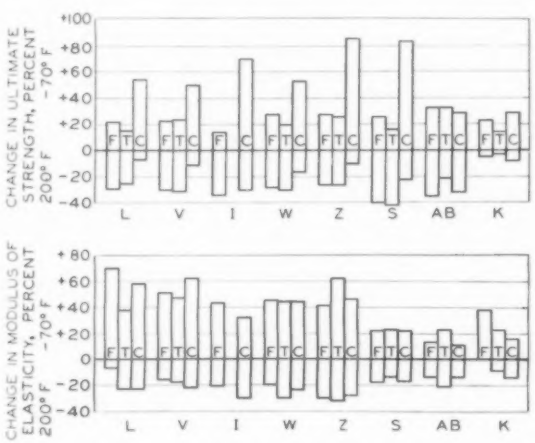

FIGURE 36. *Comparison of changes in flexural (F), tensile (T), and compressive (C) properties of laminates at −70° and 200° F based on values at 77° F.*

Types of laminates shown are: *L*, low-pressure cotton-fabric phenolic; *V*, low-pressure Grade C phenolic; *I*, Grade C phenolic; *W*, high-pressure Grade C phenolic; *Z*, rayon-cotton-fabric phenolic; *S*, high-strength-paper phenolic; *AB*, glass-fabric unsaturated-polyester; *K*, asbestos-fabric phenolic.

The increases in the three moduli of elasticity of the five cellulose-fabric laminates at −70° F were about 40 to 60 percent, and the decreases in moduli of elasticity at 200° F were from 15 to 30 percent. The high-strength-paper laminate, for which the three moduli change very similarly (fig. 36), showed smaller changes in moduli at −70° F than the other cellulose laminates.

The percentage changes in strength with temperature of the laminates with mineral reinforcement did not vary much with the type of test, in contrast to the cellulose laminates, for which the variation in compressive strength with temperature was much different from the percentage changes in flexural and tensile strength. The percentage changes in flexural, tensile, and compressive strengths of the asbestos-fabric laminate were increases of 15 to 30 percent at −70° F and decreases of about −5 percent at 200° F. The percentage changes in the three strength values for the glass-fabric laminate, AB, were nearly alike, particularly at −70° F. The respective increases in the flexural, tensile, and compressive moduli of the glass-fabric laminates at −70° F were almost equal to the decreases at 200° F. The changes in flexural and compressive moduli were about 12 percent; the tensile modulus changes were 22 percent. The over-all changes in the moduli of elasticity of the asbestos-fabric laminate for the temperature range −70° to 200° F were approximately 30 percent; there was no regularity in these changes.

6. Variation of Strength Properties of Laminates With Orientation of Specimen

Four of the nine samples tested, the two glass-fabric laminates, the asbestos-fabric laminate, and the Grade C laminate, I2, were of parallel-ply construction (table 1). The most pronounced

difference in strength properties between specimens taken from the principal directions of the sheet was observed in the asbestos-fabric laminate, K2. The other three parallel-ply samples showed differences in strength with direction of testing, but not for all types of tests as did the asbestos-fabric laminate.

In the impact tests, directional properties were observed for the parallel-ply laminates, I2 and K2. The asbestos-fabric sample, K2, for which the effect was greatest, exhibited an impact strength in the crosswise direction less than half of the corresponding value in the lengthwise direction.

For all samples the impact strength for specimens struck edgewise was lower than that of specimens of the same sample tested flatwise. For a given orientation of specimens in the sheet, the ratio of edgewise to the flatwise impact strength was very nearly constant for a given material over the range of temperature employed. These ratios are given in table 7. The mean value of this ratio was 0.5 to 0.6 for the cotton-fabric laminates, 0.2 for the paper laminate, 0.8 for the asbestos-fabric laminate, and about 0.4 for the rayon-fabric laminate. The data of Meyer and Erickson [4] for cross-ply high-strength-paper laminate give a value of 0.19 for this ratio at the various test temperatures.

The following ratios have been calculated from impact data reported by Witt, Wolfe, and Rust [6]:

Material designation	Average ratio of edgewise impact strength to flatwise impact strength
Grade C, high-pressure (11 samples)	0.57
Grade C, low-pressure (6 samples)	.53
Grade AA (5 samples)	.84
Grade L (10 samples)	.47

Each of these phenolic laminates was tested at three temperatures, −70°, 77°, and 160° F, in both the lengthwise and crosswise directions. These data agree with the data given in table 7.

The effect of orientation on the flexural stress-deflection curves is shown in figures 37 to 39 for samples that have pronounced directional behavior. The asbestos-fabric sample, K2, had a flexural strength crosswise that was of the order of 55 percent of that lengthwise (fig. 37). The two glass-fabric laminates had flexural strengths crosswise about 85 percent of those lengthwise. All of the other samples, both parallel-ply and cross-ply, had flexural strengths in the crosswise direction almost

TABLE 7. *Ratio of edgewise impact strength to flatwise impact strength for ½-in.-thick laminates at various temperatures* [a]

Material designation	Orientation of specimen	Ratio at test temperature of—				Mean ratio, all temperatures
		−70° F	0° F	77° F	200° F	
L2, Low-pressure cotton-fabric phenolic	Lengthwise	0.57	0.56	0.54	0.54	0.55
	Crosswise	.56	.58	.52	.55	
V2, Low-pressure Grade C phenolic	Lengthwise	.....	.46	.50	.50	.51
	Crosswise	.....	.51	.53	.56	
W2, High-pressure Grade C phenolic	Lengthwise	.51	.47	.48	.52	.55
	Crosswise	.63	.57	.61	.60	
I2, Grade C phenolic	Lengthwise	.62	.58	.53	.58	.59
	Crosswise	.60	.61	.58	.61	
Z2, Rayon-cotton-fabric phenolic	Lengthwise	.53	.43	.38	.38	.39
	Crosswise	.41	.36	.34	.30	
S2, High-strength-paper phenolic	Lengthwise	.17	.17	.20	.16	.18
	Crosswise	.17	.18	.21	.15	
K2, Asbestos-fabric phenolic	Lengthwise	.77	.80	.84	.82	.80
	Crosswise	.82	.73	.80	.85	
AB2, Glass-fabric unsaturated-polyester	Lengthwise	.....	.....	.32	.....	.....
	Crosswise	.....	.....	.32	.....	.....

[a] This table was computed from data in table 2.

equal to those in the lengthwise direction. The flexural properties of the Z2 rayon-fabric and AB2 glass-fabric laminates were greatly reduced for the 45° direction, as is evident from figures 38 and 39. The ratio of edgewise to flatwise flexural strength was nearly 1.0 for all of the samples except the glass-fabric laminate, AB2, for which the edgewise flexural strength was greater. The flexural modulus of elasticity of the high-strength-paper laminate, S2, was about 10 to 15 percent greater edgewise than flatwise, but in all the other samples there was little difference between the edgewise and flatwise flexural moduli of elasticity.

The variations of tensile and compressive strengths and secant moduli of elasticity for the various materials in the lengthwise, crosswise, and 45° diagonal directions are shown in figures 40 to 43. In general, the tensile strength and the tensile and compressive secant moduli of elasticity of the cotton-fabric and the high-strength-paper laminates showed small variations with the direction of test. The diagonal values were about 10 to 20 percent lower than the other values.

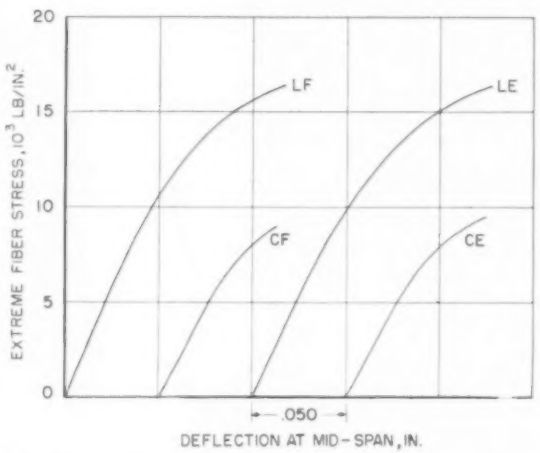

FIGURE 37. *Flexural stress-deflection curves for asbestos-fabric phenolic laminate, K2, at 77° F.*

Span-depth ratio 8:1. *LF*, Lengthwise specimens tested flatwise; *LE*, lengthwise specimens tested edgewise; *CF*, crosswise specimens tested flatwise; *CE*, crosswise specimens tested edgewise.

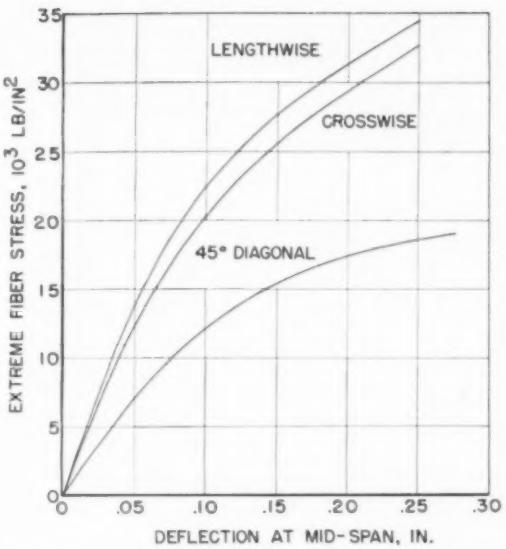

FIGURE 38. *Flexural stress-deflection curves for rayon-cotton-fabric phenolic laminate, Z2, tested flatwise at 77° F.*

Span-depth ratio 8:1. Initial flexural modulus of elasticity: lengthwise, 1,580,000 lb/in.^{2}; crosswise, 1,400,000 lb/in.^{2}; 45° diagonal, 760,000 lb/in.^{2}

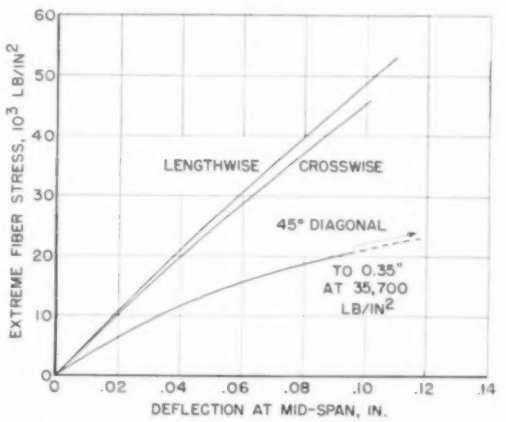

FIGURE 39. *Flexural stress-deflection curves for glass-fabric unsaturated-polyester laminate, AB2, tested flatwise at 77° F.*

Span-depth ratio 8:1. Initial flexural modulus of elasticity: lengthwise, 2,880,000 lb/in.^{2}; crosswise, 2,840,000 lb/in.^{2}; 45° diagonal, 1,810,000 lb/in.^{2}

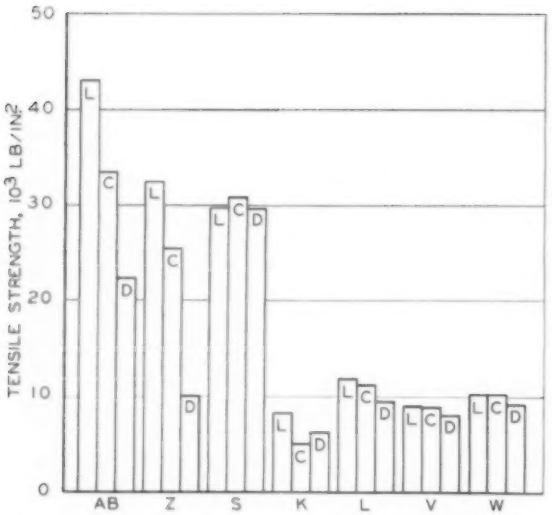

FIGURE 40. *Tensile strengths for the lengthwise (L), crosswise (C), and 45° diagonal (D) directions of ⅛-in.-thick laminates.*

Types of laminates are: *AB*, glass-fabric unsaturated-polyester; *Z*, rayon-cotton-fabric phenolic; *S*, high-strength-paper phenolic; *K*, asbestos-fabric phenolic; *L*, low-pressure cotton-fabric phenolic; *V*, low-pressure Grade C phenolic; *W*, high-pressure Grade C phenolic.

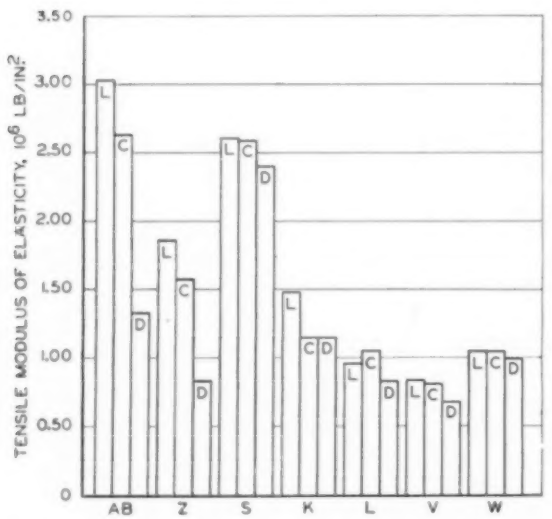

FIGURE 41. *Tensile secant moduli of elasticity for lengthwise (L), crosswise (C), and 45° diagonal (D) directions of ⅛-in.-thick laminates.*

Stress ranges: 0 to 5,000 lb/in.^{2} for *AB*, *Z*, *S*; 0 to 2,500 lb/in.^{2} for *K*, *L*, *V*, *W*. Types of laminates shown are: *AB*, glass-fabric unsaturated-polyester; *Z*, rayon-cotton-fabric phenolic; *S*, high-strength-paper phenolic; *K*, asbestos-fabric phenolic; *L*, low-pressure cotton-fabric phenolic; *V*, low-pressure Grade C phenolic; *W*, high-pressure Grade C phenolic.

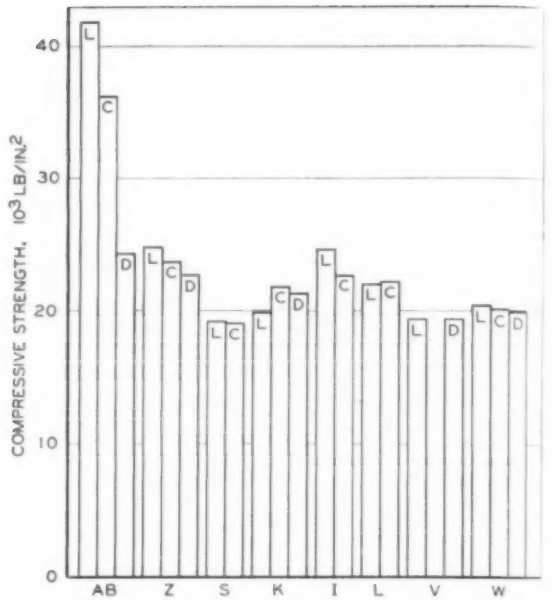

FIGURE 42. *Compressive strengths for lengthwise (L), crosswise (C), and 45° diagonal (D) directions of ⅛-in.-thick laminates.*

Types of laminates shown are: *AB*, glass-fabric unsaturated-polyester; *Z*, rayon-cotton-fabric phenolic; *S*, high-strength-paper phenolic; *K*, asbestos-fabric phenolic; *I*, Grade C phenolic; *L*, low-pressure cotton-fabric phenolic; *V*, low-pressure Grade C phenolic; *W*, high-pressure Grade C phenolic.

The rayon-fabric and the glass-fabric laminates, similarly to their behavior in flexure, showed large variations in tensile strength and tensile and compressive moduli with the direction of test. The diagonal values were as low as 30 to 50 percent of the lengthwise values. The rayon-fabric sample, although a crossed-ply laminate, showed the greatest variation between the lengthwise and crosswise values of tensile modulus of elasticity.[4]

In the asbestos-fabric sample, a parallel-ply laminate, the tensile strength and the tensile and compressive moduli were greatest in the lengthwise, least in the crosswise, and intermediate in the diagonal directions (fig. 40).

[4] This may be explained as follows: The rayon fabric, of higher strength and modulus of elasticity than the resin, was practically unidirectional in strength. In the ⅛-in. thickness there were four plies lengthwise to three crosswise. If the modulus of elasticity of the resin, small compared to the fabric, is neglected, the ratio of lengthwise to crosswise tensile modulus of elasticity should be 1.33; the measured ratio was 1.18. Application of the same idea to the compressive moduli, where the specimen has 12 lengthwise and 11 crosswise plies, indicates a corresponding ratio of 1.09; the measured ratio was 1.07.

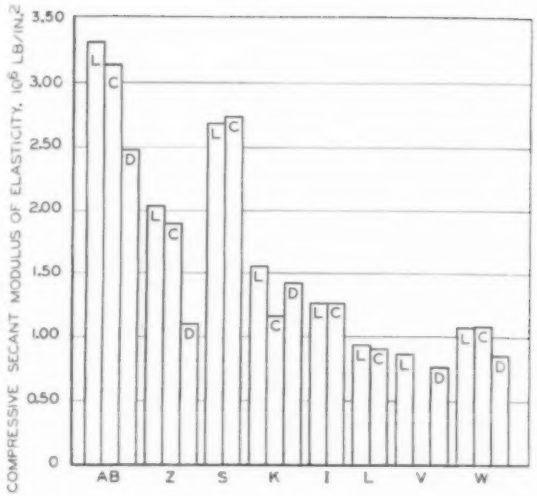

FIGURE 43. *Compressive secant moduli of elasticity (0 to 2,500 lb/in.²) for lengthwise (L), crosswise (C), and 45° diagonal (D) directions of ½-in.-thick laminates.*

Types of laminates shown are: *AB*, glass-fabric unsaturated-polyester; *Z*, rayon-cotton-fabric phenolic; *S*, high-strength-paper phenolic; *K*, asbestos-fabric phenolic; *I*, Grade C phenolic; *L*, low-pressure cotton-fabric phenolic; *V*, low-pressure Grade C phenolic; *W*, high-pressure Grade C phenolic.

In all samples, the compressive strength varied less with direction than the tensile strength. For a given sample, the compressive strengths for the three directions of test differed by 10 percent or less. The only exception was the glass-fabric laminate whose compressive strength in the 45°-diagonal direction was only 60 percent of that in the lengthwise direction. Moreover, except for the glass-fabric laminate, the compressive strengths of the laminates were within 10 percent of 21,000 lb/in.²; the tensile strengths of these same laminates (excluding the glass-fabric laminate) ranged from 5,000 to 32,000 lb/in.²

The relative constancy of compressive strength with variation of direction and reinforcement indicates that the strength of the resin is the major factor in determining the compressive strength of fabric and paper laminates. This conclusion was reached by Erickson and Mackin (see p. 268 and tables 1 and 2, [19]) in regard to a parallel-ply high-strength-paper laminate. Witt, Wolfe, and Rust [6] showed that, although the average lengthwise tensile strength for ten Grade L laminates was 50 percent greater than the average crosswise tensile strength, and for eleven Grade C laminates 15 percent greater, the difference in compressive strengths of the different directions of the two materials was less than 3 percent.

7. Strain at Failure

Except for the asbestos-fabric laminates, the elongation at failure in tension (table 8) was the same for the lengthwise and crosswise directions and greatest for the 45°-diagonal direction. The greatest elongations in tension were those of the two low-pressure cotton-fabric laminates, L1 and V1, and the glass-fabric laminate in the 45°-diagonal direction.

Table 8 also shows that, in compression, the maximum strain at failure occurred in the 45°-diagonal direction. In general, the strain at failure in compression was greater than in tension for the same sample and orientation of specimen.

The elongation in tension for the cellulose

TABLE 8. *Strain at failure in tension and compression tests* [a]

Material designation	Orientation of specimen	Total strain of failure			
		Tension			Compression at 77° F
		−70° F	77° F	200° F	
		Percent	*Percent*	*Percent*	*Percent*
L, Low-pressure cotton-fabric phenolic, cross ply.	Lengthwise	2.9	4.9	4.2	12.2
	Crosswise	3.3	4.8	3.2	11.6
	45° diagonal	.....	8.7	.....	.....
V, Low-pressure Grade C phenolic, cross ply.	Lengthwise	3.9	4.8	3.7	10.5
	Crosswise	3.9	5.0	3.6	.....
	45° diagonal	.....	8.5	.....	14.7
W, High-pressure Grade C phenolic, cross ply.	Lengthwise	3.3	3.7	2.8	8.6
	Crosswise	3.0	4.8	2.5	8.2
	45° diagonal	.....	4.7	.....	11.8
I, Grade C phenolic, parallel ply.	Lengthwise	.....	.....	.....	12.0
Z, Rayon-cotton-fabric phenolic, cross ply.	Lengthwise	2.8	4.0	3.4	5.7
	Crosswise	3.0	3.9	3.4	5.8
	45° diagonal	.....	4.9	.....	8.6
S, High-strength-paper phenolic, cross ply.	Lengthwise	1.2	1.7	1.1	4.5
	Crosswise	1.3	1.7	1.1	.....
	45° diagonal	.....	2.0	.....	.....
K, Asbestos-fabric phenolic, parallel ply.	Lengthwise	2.1	1.8	1.2	5.1
	Crosswise	0.5	0.6	0.5	6.3
	45° diagonal	.....	.6	.....	5.4
AB, Glass-fabric unsaturated polyester, parallel ply.	Lengthwise	.....	1.8	.....	1.5
	Crosswise	2.2	1.7	1.7	1.5
	45° diagonal	.....	8.2	.....	2.5

[a] The tension tests were made on ⅛-in.-thick samples, and the compression tests were made on ½-in.-thick samples.

laminates was greater at 77° F than at either −70° or 200° F. The deflection at failure in flexural testing was greater at 77° F than at either −70° or 200° F for the six cellulose laminates (figs. 14 to 17). Meyer and Erickson [4] have shown that the elongation at failure in tension of a high-strength-paper laminate increases directly with the moisture content of the laminate. Therefore, part of the increase in brittleness of the cellulose laminates at 200° F may be due to the decrease in moisture content of the laminates caused by 24-hr conditioning at 200° F.

V. Conclusions

The Izod impact strength-temperature trend of the laminated plastics is different for the various types of reinforcement. The glass-fabric laminates decrease steadily in impact strength with increasing temperature, the value of 200° F being about 70 percent of the −70° value. The asbestos-fabric, rayon-fabric, and high-strength-paper laminates show little variation in impact strength between −70° and 200° F. The cotton-fabric laminates exhibit increasing impact strength with temperature, roughly doubling their impact strength between −70° and 200° F.

The Izod impact-strength values for the rayon-fabric and the glass-fabric laminates are much greater than for the other materials.

An increase in flexural properties occurs for all the samples at low temperature, and at high temperature, a decrease occurs for all the samples except the asbestos fabric laminate, which shows no change.

The high-strength-paper and two glass-fabric laminates are outstanding in flexural properties. When the samples are compared on the basis of specific strength values, the paper and rayon-fabric laminates are superior to the others.

The low-pressure Grade C phenolic laminate, V2, compares favorably in flexural strength properties with the high-pressure laminate, W2, made with the same reinforcement, especially when the comparison is made in terms of specific strength properties.

The tensile and compressive strengths and moduli of elasticity of all laminates increase at low temperature and decrease at high temperature relative to the values at 77° F.

For all laminates, except the asbestos-fabric product, the tensile and compressive strengths at 200° F are approximately half of the corresponding values at −70° F. The changes in the strength values of the asbestos-fabric product are much smaller and less than for any other laminate.

For the cellulose laminates, the increase in compressive strength at the low temperature is much greater in magnitude than the decrease at the high temperature; the tensile strength variation, however, is less at the low temperature than at the high temperature. The tensile and flexural strengths of these samples exhibit similar temperature changes.

The tensile and compressive moduli of all samples increase more at the low temperature than they decrease at the high temperature. Except for the high-strength-paper laminate, the over-all changes are greater for the cellulose than for the mineral-type laminates. The high-strength-paper, asbestos-fabric, and glass-fabric laminates show about the same over-all variation of tensile and compressive moduli with temperature.

The tensile strengths of the high-strength-paper, rayon-fabric, and glass-fabric laminates are about three times greater than those of the cotton-fabric and asbestos-fabric phenolics.

The glass-fabric laminate is outstanding in compressive strength; at 77° F its strength is 36,000 and 42,000 lb/in.^{2}, respectively, in the crosswise and lengthwise directions. The compressive strength of the other laminates is 21,000 lb/in.^{2} within about 10 percent.

The tensile and compressive moduli of elasticity of the glass-fabric and high-strength-paper laminates are greater than for the other materials at all temperatures and are in the range 2,600,000 to 3,300,000 lb/in.^{2}

The flexural properties of plastic laminates at high temperature are not a function of temperature alone, but may be affected by further cure of the resin and loss of moisture content. The effect of high humidity in addition to an elevated temperature may be much different from the effect of the elevated temperature alone. A severe loss in strength was noted for the high-strength-paper and one low-pressure cotton-fabric laminate at 150° F and 90-percent relative humidity.

The ratio of edgewise to flatwise impact strength for the ½-in.-thick phenolic laminates tested is nearly constant over the range of temperatures, −70° to 200° F.

VI. References

[1] P. M. Field, Basic physical properties of laminates, Modern Plastics **20,** 91, 126, 128, 130 (Aug. 1943).

[2] T. T. Oberg, R. T. Schwartz, and D. A. Shinn, Mechanical properties of plastic materials at normal and subnormal temperatures, Air Corps Tech. Report No. 4648 (June 6, 1941); Modern Plastics **20,** 87, 122, 124, 126, 128 (Apr. 1943).

[3] P. Norelli and W. H. Gard, Temperature effect on strength of laminates, Ind. Eng. Chem. **37,** 580 (1945).

[4] H. R. Meyer and E. C. O. Erickson, Factors affecting the strength of papreg. Some strength properties at elevated and subnormal temperatures, Forest Products Laboratory Report No. 1521 (Jan. 1945).

[5] W. C. Renwick, Properties of plastic laminates, Part VI. Naval Air Exp. Sta. Report TED NAM 252170 (June 3, 1944).

[6] R. K. Witt, P. D. Wolfe, and D. W. Rust, Report on the NEMA laminated plastics test project at the Johns Hopkins Univ. (Nov. 1945). Also R. K. Witt, P. D. Wolfe, and D. W. Rust, Cotton fabric laminates, Modern Plastics **25,** 123, 184 (May 1948).

[7] F. B. Fuller, Engineering properties of plastics, Modern Plastics **20,** 95, 130 (June 1943).

[8] D. A. Shinn, Impact data for plastic materials at various temperatures, Air Corps Tech. Report No. 5012 (Aug. 9, 1943); Modern Plastics **22,** 145, 184 (July 1945).

[9] W. N. Findley and W. J. Worley, Mechanical properties of five laminated plastics. NACA Tech. Note No. 1560 (Aug. 1948).

[10] J. Marin, Static and dynamic properties of laminated plastics for various types of stress. NACA Tech. Note 1105 (Feb. 1947).

[11] J. J. Lamb and B. M. Axilrod, Tensile stress-strain relationships of laminated plastics for small strains. ASTM Bulletin No. 151, p. 59 to 66 (Mar. 1948).

[12] W. A. Crouse, D. C. Caudill, and F. W. Reinhart, Effect of simulated service conditions on plastics. NACA Tech. Note No. 1240 (July 1947). Effect of simulated service conditions on plastics during accelerated and 2-year weathering tests. NACA Tech. Note No. 1438 (May 1948).

[13] W. N. Findley, C. H. Adams, and W. J. Worley, The effect of temperature on the creep of two laminated plastics. Presented at the June 1948 annual meeting of the American Society for Testing Materials.

[14] Federal Specification L–P–406a, Plastics, Organic; General Specifications, Test Methods (Jan. 24, 1944). Government Printing Office, Washington 25, D. C.; price 15 cents.

[15] B. M. Axilrod, R. W. Thiebeau, and G. E. Brenner, A variable-span flexure test jig for plastic specimens. ASTM Bulletin No. 148, p. 96 to 99 (Oct. 1947).

[16] C. S. Aitchison and J. A. Miller, A subpress for compressive tests. NACA Tech. Note No. 912 (Dec. 1943).

[17] C. D. Jones, Physical properties of Fiberglas reinforced low-pressure laminated plastics. Owens-Corning Fiberglas Corporation Research Laboratories Report to Aircraft Laboraroty, Wright Field (Feb. 4, 1944).

[18] E. O. Hausmann, A. E. Parkinson, and G. H. Mains, Heat resistance of laminated plastics. Modern Plastics **22,** 151, 190, 192, 194, 196, 198 (Nov. 1944).

[19] E. C. O. Erickson and G. E. Mackin, Properties and development of papreg, a high-strength laminated paper plastic, Trans. ASME **67,** 267 (1945).

WASHINGTON, May 23, 1949.